FERRIMAGNETIC RELAXATION MEASUREMENTS AND MICROWAVE CIRCUIT PROPERTIES OF FERRITE ELLIPSOIDS

By

L. K. Anderson

Technical Note
Contract AF 49(638)-415
Project Number 47501

The research reported in this document has been sponsored by the
Air Force Office of Scientific Research
Air Research and Development Command

M.L. Report No. 880
February 1962

Microwave Laboratory
W. W. Hansen Laboratories of Physics
Stanford University
Stanford, California

No DDC limit.

AFOSR-2121

Microwave Laboratory
W. W. Hansen Laboratories of Physics
Stanford University
Stanford, California

FERRIMAGNETIC RELAXATION MEASUREMENTS AND MICROWAVE CIRCUIT PROPERTIES OF FERRITE ELLIPSOIDS

By

L. K. Anderson

Technical Note
Contract AF 49(638)-415
Project Number 47501

February 1962

The research reported in this document has been
sponsored by the
Air Force Office of Scientific Research
Air Research and Development Command

M. L. Report No. 880

ABSTRACT

The object of this paper is to describe the results of an experimental investigation of relaxation processes in microwave ferrites. The study of relaxation in ferrites has always been of paramount importance, both for the development of practical ferrite devices, and for the basic understanding of ferrimagnetism, and has proceeded virtually continuously since the discovery of the phenomenon of ferromagnetic resonance more than fifteen years ago. Recent advances toward a detailed theory of ferrimagnetic relaxation, however, have provided new impetus for its experimental study, as well as a new framework which we have utilized in the present investigation. A new experimental procedure has been developed in which the contribution of the uniform precessional mode to the relaxation may be separated from that of the other spin modes by controlling the interaction between the ferrite sample and its microwave environment.

To characterize this interaction in detail, scattering matrix and lumped-element equivalent circuit representations are developed for a section of uniform waveguide containing a small ferrite ellipsoid. The circuit representation is then used to discuss radiation damping in a variety of microwave structures. In contrast to previous theories, the results are valid even when the interaction is large, provided that the sample is not too close to a waveguide wall. This "wall effect," which takes the form of a shift, broadening and distortion of the resonance line, is discussed in some detail.

Transient solutions are obtained for the rate equations which describe the deviation of the z-component of magnetization (M_z) from its equilibrium value, in the presence of appreciable radiation damping. The results of small-signal measurements of the transient response of M_z to rectangular pulses of rf drive, made on polished single crystal spheres of yttrium iron garnet, are then fitted to the theory, yielding values of the relaxation parameters consistent with those obtained by Fletcher, et al., using a less direct technique.

The results of large signal measurements of spin mode amplitude and relaxation rate, made on the same materials using similar procedures, are correlated with information obtained from the susceptibility decline at high power levels. The principal observations are:

(i) The susceptibility starts to decline at the signal level predicted by the substitution of the observed spin mode relaxation rate into existing theories.

(ii) Complete saturation does not occur, however, at the very small precession angle predicted by theory, (1°) , but instead occurs quite abruptly when the angle reaches the relatively large value of 2.5°.

(iii) Correlation of the susceptibility decline with the observed spin mode dissipation suggests that the final saturation may be due to nonlinear spin-lattice coupling of the uniform mode, rather than the spin-spin coupling usually postulated.

Small signal relaxation measurements, using transient techniques, were also made on a number of polycrystalline samples of yttrium iron garnet having different linewidths. The spin mode relaxation rate was found to be about 30×10^{6} sec^{-1} for all samples, considerably faster than previous results based on susceptibility decline measurements had led us to believe, and just marginally within the capabilities of our equipment.

ACKNOWLEDGMENTS

This work, like most of its kind, owes much to the environment in which it was carried out, and I sincerely thank my colleagues in the Microwave Laboratory for their assistance. In particular, I would like to thank Mr. P. M. Richards for valuable advice concerning the properties of normal modes in ferrites, and Mr. B. J. Elliott for help with several aspects of the instrumentation. I also benefitted greatly from discussions with Drs. B. A. Auld, M. Sparks and D. K. Winslow, and Messrs. R. L. Comstock and C. H. Holmes. Special thanks go to Mrs. Clark S. Sturges for her careful typing from the manuscript.

Above all, I want to thank Dr. H. J. Shaw, who supervised the work, for continuous help and encouragement.

TABLE OF CONTENTS

PART III

MEASUREMENT OF FERRIMAGNETIC RELAXATION PARAMETERS

LIST OF FIGURES

PART I

INTRODUCTION AND GENERAL THEORY

PART II

LIST OF TABLES

BLANK PAGE

PART I

INTRODUCTION AND GENERAL THEORY

CHAPTER I

INTRODUCTION

The object of the investigation reported in this paper was to study experimentally the relaxation processes in various microwave ferrites,(1) particularly single crystal yttrium iron garnet, with the aim of obtaining a more detailed understanding of their fundamental properties. By "relaxation processes," we mean, in the present context, all those mechanisms whereby the energy that is delivered to the ferrite by an external microwave signal source is eventually dissipated, in the form of heat, within the material and its surroundings. In characterizing these dissipative processes, the experimental approach may be made on a number of different levels of sophistication, depending on the extent to which we understand, or think we understand, the details of the individual relaxation mechanisms. The earliest measurements of relaxation in ferrites were based on the use of a phenomenological equation of motion,[1] from which was derived an effective susceptibility tensor[2] relating the steady-state rf magnetization to the applied rf magnetic field. By measuring the elements of this tensor by standard cavity perturbation techniques,[3] as a function of frequency, dc field, and any other relevant parameters, a complete characterization of the small-signal behavior of the material is possible. Such a procedure, however, yields almost no insight into the details of the actual relaxation mechanisms, and is even of little utility for the practical design of ferrite devices, since the measured susceptibility is found to be strongly dependent on the details of the individual sample size, shape and preparation.

At the other extreme, considerable theoretical progress has been made recently in the analysis of the microscopic relaxation processes,[4-7] using a completely quantum-mechanical formulation. This approach, although valuable, has the disadvantage that many of the quantum-mechanical results are difficult to interpret in terms of experimentally observable processes.

The most successful characterization of ferrimagnetic relaxation combines, as one might expect, some elements of both of these approaches. The

---

(1) In this paper we shall use the word "ferrite" to describe all ferrimagnetic insulators.

procedure is based on what we might call the normal mode theory of ferrimagnetic resonance. In the forumlation the motion of the magnetization in a given ferrite sample is viewed, in the absence of loss, as the superposition of a large number of relatively simple normal modes, some of which are obtainable by solving the macroscopic electromagnetic boundary value problem of a magnetic sample in free space, while others require a more microscopic, quantum mechanical approach. Relaxation is then introduced into this hitherto lossless system by coupling these modes together and to the crystal lattice. This is the core of the now accepted theories of ferrimagnetic relaxation, in which the principal energy transfer is by way of those modes which can be approximated as plane spin waves. In some cases this coupling can be calculated, in others it can only be described in terms of a phenomenological parameter. The advantage of the normal mode approach in this regard, however, is that these modes can be separately characterized by physically observable quantities, which allows the individual determination of the relaxation parameters.

Although our primary goal throughout this investigation is to study those processes which are characteristic of the ferrite material itself, it is impossible to ignore the interaction between the material and its surroundings, partly because the experimental environment affects the relaxation processes themselves, but more fundamentally because it is through the "back-reaction" of the ferrite sample on the microwave circuit in which it is placed that we gain much (but not all) of our information about the relaxation processes in the ferrite. For this reason we have studied extensively the coupling between a small ferrite sample and its surrounding microwave circuitry. Because this problem is of considerable interest in its own right, we have, in fact, pursued this phase of the study beyond the immediate requirements of the relaxation investigation.

One result of the careful study of the interaction between the ferrite sample and its microwave environment has been the development of a new pulse technique for measuring relaxation parameters, in which for the first time we have been able to clearly separate the contribution of the uniform precession to the overall relaxation from that of the remaining spin modes, leading to a direct measurement of the spin mode relaxation rate. In previous CW experiments[8] the various contributions to the relaxation appear in such a way that detailed curve fitting is required for

their separate evaluation. These previous measurements were also limited to small signals, a restriction which does not apply to the present technique, and which has enabled us for the first time to carry out accurate relaxation measurements under large signal conditions.

Among the results has been the first experimental evidence for a type of mutual coupling among certain spin modes that has been predicted theoretically[9] to be of considerable importance. We have obtained other results in the large signal range which in some cases confirm, and in other cases show surprising disagreement with, existing theories. For a brief summary of the principal results, the reader may turn immediately to Section C of Chapter XVI.

The organization of the paper is as follows: In the remainder of Part I, we review those elements of the normal mode theory of ferrimagnetic resonance that are essential to the analysis of our relaxation measurements, and we obtain equations of motion for the actual physical observables. One of the prime advantages of the normal mode approach, in contrast to ones based solely on energy balance considerations,[8] or on quantum-mechanical transition probabilities,[4] is the ease with which the possible ellipticity of the modes may be included, although, as we shall show later from the general result (for the particular conditions of our experiment this ellipticity may be ignored), this is by no means as generally true as other published approaches would lead one to believe. Another useful feature of the normal mode theory of ferrimagnetic resonance is that it allows a lumped electrical circuit analog of the magnetic system to be constructed by inspection.

In Part II we take up a detailed study of the coupling between the uniform precessional mode in a small ferrite ellipsoid and its microwave environment. We do this by first finding the scattering matrix of a uniform section of waveguide containing the sample, and from this derive lumped element equivalent circuits for the ferrite-loaded waveguide. These are then specialized to several microwave configurations of interest by an appropriate choice of terminating impedances.

In Part III we present a new technique for experimentally determining the relaxation parameters of the ferrite; it involves a somewhat more sophisticated application of previously described pulse techniques,[10-12] together with careful control of the interaction between the ferrite and

the microwave circuit. The underlying principles of the technique can be understood by means of an approximate, but simple flow diagram, discussed in the Introduction to Part III, whose existence is made possible by the fact that for the conditions of our experiment we can ignore the ellipticity of the various modes of the spin system. Finally, we shall present and discuss the results of the application of the technique to both single crystal and polycrystalline samples of yttrium iron garnet.

CHAPTER II
THE NORMAL MODE THEORY OF FERRIMAGNETIC RESONANCE

A. THE NORMAL MODES OF A FERRITE ELLIPSOID

Just as for any electrical or mechanical system, the normal modes of a ferrite sample are determined by the free oscillations of the isolated system. For a ferrite, however, this implies that the sample dimensions must be much less than a free space wavelength, otherwise the sample will radiate, and can not be considered an isolated system. Although normal modes will exist for a sufficiently small sample of arbitrary geometry, explicit solutions have been obtained[14] only for ellipsoidal samples so small that retardation effects may be neglected.[(1)] Such solutions are obtained by solving the quasi-static form of Maxwell's equations, $\nabla \cdot (\vec{H} + \vec{M}) = 0$ and $\nabla \times \vec{H} = 0$, simultaneously with the equation of motion for the magnetization,

$$\frac{d\vec{M}(\vec{r})}{dt} = - \mu_0 \gamma \vec{M}(\vec{r}) \times \vec{H}(\vec{r}) \quad , \qquad (1.1)$$

subject to the continuity of normal $\vec{B}$ and tangential $\vec{H}$ at the surface of the ellipsoid. Here $\vec{M}$ is the magnetization, $\vec{H}$ the magnetic field, μ_0 the permeability of free space,[(2)] and γ the gyromagnetic ratio, here taken to be positive for electrons.

If $\vec{H}(\vec{r})$ is taken to be the sum of three fields, a uniform dc field, $\vec{H}_0$, a dipolar field, $\vec{H}_{dip}$, and an exchange field of quantum mechanical origin, $\vec{H}_{ex}$, then solutions to Eq. (1.1) can be obtained in the linear

---

(1) This, in general, is more restrictive than the requirement that the sample be small compared to a wavelength in free space.

(2) MKS units are used throughout. The reader may find it convenient, in referring to later sections in which experimental results are discussed, that 1 oersted (Gaussian units) is equivalent to about 80 amp/m (MKS units).

approximation in terms of an infinite set of magnetostatic modes in which the magnetization is space varying. As the spatial variation becomes very rapid, these magnetostatic modes approach elliptically polarized plane waves[15] having a wave vector $\vec{k}$ which can take on a quasi-continuous range of values. For sufficiently large values of k, the boundary conditions are irrelevant; but when the wavelength, $2\pi/\lambda$, becomes comparable to the size of the sample, plane waves are no longer a good approximation to the actual normal modes, which must then be obtained by proper application of the boundary conditions. These modes have been investigated by Walker[14] for the special case where exchange can be ignored, and are often called "Walker" modes or just simply "magnetostatic" modes.

B. EFFECT OF MODE COUPLING AND LOSS

The modes enumerated in the preceding paragraph are true normal modes only in a perfectly ordered crystal, and then (because of the essential nonlinearity of the equation of motion) only in the limit of vanishingly small excitation. Since any practical experiment will always involve a finite excitation of at least one mode in the system, and will be done in crystals having both spatial and temporal disorder, the former arising from lattice defects, surface imperfections, etc., and the latter from thermal agitation of the lattice, there will always exist coupling among modes of the magnetic system, and between these modes and the lattice.

In analogy with the much simpler example of paramagnetic relaxation, in the past it has been customary to divide ferrimagnetic relaxation processes into two categories, spin-spin, and spin-lattice. In the present context, spin-spin relaxation arises from coupling among the modes of the spin system, while spin-lattice relaxation results from coupling between the spin system and the lattice vibrational modes. More recently, however, it has been recognized that this division is not the most useful, particularly since in ferrites the direct spin-lattice processes are believed to be relatively of little importance.(1) Rather, it is more meaningful to speak of the relaxation processes as being either <u>intrinsic</u> or <u>direct</u>. Intrinsic relaxation processes are those which remove energy from the spin sub-system consisting of all those modes degenerate in

(1) Ultimately, of course, spin-lattice relaxation must dissipate all the energy being delivered to the sample. Provided that these processes are sufficiently strong to keep the spin system in approximate thermal equilibrium with the lattice, however, their exact nature need not concern us here.

resonant frequency with the uniform mode. (These have been called "S-modes."[5]) Direct processes are those in which energy is interchanged among S-modes, or between S-modes and the uniform precession, and thus are, by definition, a form of spin-spin relaxation. Under many practical circumstances, some of which we shall consider in Part III, intrinsic processes are equivalent (as far as the observable behavior of the spin system is concerned) to spin-lattice relaxation, so that the difference between the old nomenclature and the new becomes largely one of semantics.

In the small signal range, the process by which energy is coupled from the uniform mode to the S-modes is commonly called "inhomogeneity scattering," since it arises from a spatial disorder of the crystal lattice. Although these coupling coefficients can be evaluated specifically only for rather unrealistically simplified cases[4,9,17,18] a very important general result has been obtained,[19] namely that the cumulative effect of scattering to many modes is to add a single loss term to the uniform mode, corresponding, in effect, to a simple spin-lattice relaxation.

In most present theories, the intrinsic relaxation is accounted for by the addition to the equation of motion for each mode of a phenomenological loss term, which is to be experimentally determined.

In addition to the relaxation processes discussed above, the fact that the equation of motion [Eq. (1.1)] is essentially nonlinear results in nonlinear coupling between the magnetic modes which in turn gives rise to a number of "high power effects" which have been the subject of extensive theoretical[13,19,21] and experimental investigation. Their discussion will be deferred until Section B of Chapter XVI, where the results of large-signal relaxation measurements are presented. All of the intervening sections will be concerned only with the linear, small signal behavior of the magnetic system.

C. MATHEMATICAL FORMULATION OF NORMAL MODE THEORY

A detailed normal mode theory of ferrimagnetic resonance has been developed by Suhl[13] and Schloemann[21] for the special case of an ellipsoid magnetized along one of its principal axes. In their treatment they assume that the motion of the magnetization can be adequately described in terms of the uniform precession together with a set of plane spin waves.

They show that a spin wave pair with spatial dependences $e^{j\vec{k}\cdot\vec{r}}$ and $e^{-j\vec{k}\cdot\vec{r}}$ can be represented by a "state vector"(1) whose complex normal components, designated b_k and b^*_{-k}, satisfy the differential equations

$$\dot{b}_k = j[(\omega_k + j\eta_k)b_k + p^*_{0k}b_0]$$

and (1.2)

$$\dot{b}^*_{-k} = -j[(\omega_k - j\eta_k)b^*_{-k} + p^*_{0k}b^*_0] \quad ,$$

where ω_k, the spin wave resonant frequency, is given by[16]

$$\omega_k = \sqrt{(\omega_H + \omega_{ex}a^2k^2)(\omega_H + \omega_{ex}a^2k^2 + \omega_M \sin^2\theta_k)} \quad , \qquad (1.3)$$

in which ω_H, $\omega_{ex}a^2k^2$ and ω_M are just $\mu_0\gamma$ times the internal dc field, exchange field, and saturation magnetization respectively, and θ_k is the polar angle of the spin wave, referred to the direction of the dc field. The quantity η_k is a phenomenological constant, added, as mentioned in Section B, to account for the intrinsic relaxation of the k^{th} spin wave, while p_{0k} is the inhomogeneity coupling parameter connecting the uniform precession, b_0, to the k^{th} spin wave.(2) In this approach, the differential equation describing the free motion of the uniform precession is

$$\dot{b}_0 = j\left[(\omega_0 + j\eta_0)b_0 + \sum_{k\neq 0} p_{0k}b_k\right] \quad , \qquad (1.4)$$

---

(1) The quantities b_k and b^*_{-k} are obtained by carrying out a well known linear transformation (see reference 22) on the Fourier components obtained by expanding the transverse magnetization in terms of plane waves. The utility of the transformation lies in the fact that, in a free oscillation of the system, each b_k has a simple $e^{j\omega_k t}$ time dependence, whereas in terms of the actual Fourier components, the motion is more complicated.

(2) In general, there will be additional terms coupling b_k to the other spin waves. These have been ignored by Fletcher, et al., (see reference 8) and by Suhl and Fletcher, (reference 18) and in the treatment given here, we shall do likewise. Recent calculations by Sparks, Loudon and Kittel, (reference 9) however, have shown that there can, under certain circumstances, exist coupling between all those modes degenerate in frequency with the uniform mode (the so-called S-modes) which is strong enough to profoundly affect the relaxation. These results, however, do not affect the final form of the equations of motion which we go on to derive, but only their interpretation, as we shall discuss later.

where η_0 is the phenomenological spin-lattice loss term, and ω_0 is given by the Kittel formula,[23]

$$\omega_0 = \sqrt{(\omega_H + N_x\omega_M)(\omega_H + N_y\omega_M)} \quad , \tag{1.5}$$

N_x and N_y being the transverse demagnetizing factors[24] of the ellipsoidal sample. The term

$$\sum_{k\neq 0} p_{0k} b_k$$

appearing in Eq. (1.4) represents the "back-reaction" of the spin modes on the uniform precession. Suhl and Fletcher[19] have established the form of this term when it can be assumed that the summation extends over a large number of modes, forming a quasi-continuous spectrum. They then obtain[(1)]

$$\sum_{k\neq 0} p_{0k} b_k = j\eta_0' b_0 \quad , \tag{1.6}$$

with

$$\eta_0' = \pi \int_{S\omega_0} |p_{0k}|^2 n(\omega_0, S\omega_0) dS\omega_0 \quad , \tag{1.7}$$

the integration extending over the surface of constant frequency in k-space for which $\omega_k = \omega_0$, and on which the density of spin modes per unit frequency, per unit area is $n(\omega_0, S\omega_0)$. Equation (1.4) then takes the simple form

$$b_0 = j[\omega_0 + j(\eta_0 + \eta_0')]b_0 \quad . \tag{1.8}$$

D. PHYSICAL OBSERVABLES IN TERMS OF THE NORMAL MODE AMPLITUDES

In order to apply the normal mode theory of ferrimagnetic resonance to practical situations, it is necessary to express the complex normal mode amplitudes in terms of physical observables. In particular, we may

---

(1) In their derivation, Suhl and Fletcher assume η_k to be independent of k for those modes excited. The result is probably more general than this.

associate with each normal mode a certain fraction of the total energy, W, together with a certain fraction of the total departure of the time and space averaged longitudinal or z-component of magnetization[1] from its equilibrium value, M_s. This deviation we might call its "differential z-component of magnetization."

1. Total Energy

If W_k is the energy of the k^{th} spin mode, the total energy of the magnetic system, per unit volume, is given by[21]

$$W = \sum_k W_k = \sum_k \frac{\omega_k M_S}{2\gamma} b_k b_k^* \quad . \tag{1.9}$$

In terms of energy, the equations of motion for the spin modes may be combined to give

$$\sum_{k\neq 0} \frac{dW_k}{dt} = -2 \sum_{k\neq 0} \eta_k W_k + 2\eta_0' W_0 \quad , \tag{1.10}$$

while for the uniform precession one obtains

$$\frac{dW_0}{dt} = -2(\eta_0 + \eta_0')W_0 \quad . \tag{1.11}$$

This simple result allows us to characterize the uniform precession by an unloaded Q, which we denote by Q_f. In terms of the free decay of the natural oscillations of the uniform mode, we have, by definition,

$$Q_f = \frac{\omega_0 W_0}{-\frac{dW_0}{dt}} \quad ,$$

so that it follows at once that

$$Q_f = \frac{\omega_0}{2(\eta_0 + \eta_0')} \quad . \tag{1.12}$$

---

[1] The external field is assumed to be applied along the z-direction.

By combining the usual definition of Q in terms of frequency bandwidth with the Kittel resonance formula, we can also write the Q in terms of the linewidth,[1] ΔH, of the uniform mode,

$$Q_f = \frac{\omega_0^2}{\mu_0 \gamma \Delta H} \frac{1}{\omega_H + \frac{\omega_M}{2}(N_x + N_y)} \quad . \tag{1.13}$$

2. Z-Component of Magnetization

If ΔM_{zk} is the decrease in the time and space averaged z-component of magnetization associated with the k^{th} mode, it can be shown[2] that the total departure of M_z from its equilibrium value is given by

$$\Delta M_z = \sum_k \Delta M_{zk} = \sum_k \frac{1}{2} \frac{A_k}{\omega_k} M_S b_k b_k^* \quad . \tag{1.14}$$

Here the ratio ω_k/A_k is a measure[3] of the ellipticity of the mode, being unity for modes that are circularly polarized. It can be shown that, for plane spin waves, we have

$$A_k = \omega_H + \omega_{ex} a^2 k^2 + \frac{\omega_M}{2} \sin^2 \theta_k \quad , \tag{1.15}$$

while for the uniform precession we have

$$A_0 = \omega_H + \frac{1}{2} \omega_M (N_x + N_y) \quad . \tag{1.16}$$

---

[1] The linewidth is the dc field increment between points where the power absorbed by the sample is half of that absorbed at resonance, the rf driving field remaining constant.

[2] P. M. Richards[24] has demonstrated the validity of Eqs. (1.9) and (1.14) for any representation in which the energy is diagonal.

[3] In terms of the eccentricity, e, of the orbit, the ratio is

$$\frac{\omega_k}{A_k} = \sqrt{1 - \frac{e^2}{(2 - e^2)^2}} \quad .$$

By expressing the energy of each mode in terms of its contribution to ΔM_z , a coupled set of equations describing the free motion of the differential z-components of magnetization may be obtained:

$$\frac{d\Delta M_{z0}}{dt} = - 2(\eta_0 + \eta_0')\Delta M_{z0} \quad , \tag{1.17}$$

and

$$\sum_{k\neq 0} \frac{\omega_k^2}{A_k} \frac{d\Delta M_{zk}}{dt} = - 2 \sum_{k\neq 0} \eta_k \frac{\omega_k^2}{A_k} \Delta M_{zk} + 2\eta_0' \frac{\omega_0^2}{A_0} \Delta M_{z0} \quad . \tag{1.18}$$

In the approach adopted here, we are considering in detail only the energy transfers among the various S-modes, i.e., among those modes degenerate in resonant frequency with the uniform mode. All the other processes which transfer energy within the spin system we have lumped into the intrinsic relaxation parameters, η_k . This procedure, which we justify in some detail in Part III, then allows us to assume that in effect only those modes having $\omega_k \approx \omega_0$ are appreciably excited, so that Eq. (1.18) simplifies to

$$\sum_{k\neq 0} \frac{1}{A_k} \frac{d\Delta M_{zk}}{dt} = - 2 \sum_{k\neq 0} \frac{\eta_k}{A_k} \Delta M_{zk} + \frac{2\eta_0'}{A_0} \Delta M_{z0} \quad . \tag{1.19}$$

In the experiments described in subsequent sections, the actual observables are the amplitude of the uniform precession, which can be inferred from the measured susceptibility and rf driving field, and which is proportional to $\sqrt{\Delta M_{z0}}$, together with the total differential z-component of magnetization, ΔM_z . In order to write Eqs. (1.17) and (1.18) in terms of these quantities alone, it is necessary to make some additional approximations. One of these is to assume that A_k is independent of k . This will certainly be true in the plane spin wave approximation whenever the excited spin waves have low values of k ,[1] and will be approximately true, in our experiments, as we shall discuss in Part III, for any value of k . Further progress then requires some

[1] This is evident from the form of Eqs. (1.3) and (1.15) for the case where $k \to 0$.

assumptions about the nature of the scattering processes. There are two cases in which simple results can be obtained:

(i) The term η_k is independent of k for those modes excited by inhomogeneity scattering. This is the approach taken in references 8 and 19, and since it is known that η_k depends explicitly on k,[7] it is equivalent to assuming that the scattering is such as to preferentially excite spin waves having a narrow range of k.

(ii) There exists sufficiently strong coupling between the individual S-modes that their populations tend to remain equal, so that ΔM_{zk} is independent of k. Sparks, et al.,[9] have shown that such a situation can exist when the inhomogeneity is due mainly to surface pits having a moderate (a few microns) size.

With either of these assumptions, Eqs. (1.17) and (1.18) may be combined to give

$$\frac{d\Delta M}{dt} = -2\left[\eta_0 - \eta_k + \eta_0'\left(1 - \frac{A_k}{A_0}\right)\right]\Delta M_{z0} - 2\eta_k \Delta M_z \quad , \qquad (1.20)$$

where now the interpretation of η_k depends on which of the assumptions (i) or (ii) has been made. In case (i), η_k is the average over a narrow range of values of η_k appropriate to the spin modes excited. In the second case η_k is a simple average over <u>all</u> the S-modes.[(1)]

A third possible assumption, one that we have not investigated in detail, is that the inhomogeneity scattering is "white," i.e., energy is scattered uniformly from the uniform precession to all other S-modes, but that the individual spin modes are uncoupled. In this case the equations of motion are fundamentally different, and it is not immediately evident that a single effective intrinsic spin mode relaxation rate can be uniquely defined. Nonetheless, in the balance of this paper, we shall assume the validity of Eq. (1.20), a procedure justified by the experimental results to which, as we shall show in Part III, Eq. (1.20) provides an excellent fit. It must be borne in mind, however, that the physical significance of the measured quantity η_k is not completely unambiguous, although the experimental evidence favors the second of the two possibilities described above.

---

(1) M. Sparks, private communication.

Equations (1.20) and (1.17) describe the free "motion" of the physical observables in a ferrimagnetic resonance experiment, and as such will form the basis for the measurement techniques to be discussed in Part III. They differ from the equations first derived by Fletcher, LeCraw and Spencer[8] in that the ellipticity of the modes is specifically taken into account, although, for the conditions of our experiment, it will turn out that this ellipticity may be ignored.

E. CIRCUIT ANALOG OF THE FERRIMAGNETIC SYSTEM

The form of Eqs. (1.2) and (1.4) for the amplitude of the magnetic normal modes suggests a representation of the spin system in terms of an electrical network of coupled resonant circuits. Such an analog can be placed on a reasonably rigorous basis for the quasi steady-state, i.e., when the system is driven at a fixed frequency, and all changes are assumed to occur adiabatically. For this case it can be shown that Eqs. (1.2) and (1.4) describe the behavior of the circuit of Fig. 1.1, provided that we identify the normal mode amplitudes with the complex current, spin-lattice loss with resistance, and spin-spin coupling with mutual inductance. In this equivalent circuit, to be consistent with the assumptions that led to Eqs. (1.2) and (1.4), we have shown explicitly only one tank circuit, that which is the analog of the uniform precession, to be coupled to the signal source. The general case, where a large number of modes can be excited directly by the external drive, or where there is appreciable coupling between individual spin modes, can also, of course, be readily represented.

The main utility of the equivalent circuit representation lies in the intuitive insight it can provide into the behavior of the spin system. For example, it is a trivial problem to show that the effect of coupling the primary (uniform precession) to a large number of secondaries (spin modes) whose resonant frequencies form a quasi-continuum is to introduce into the primary only a frequency independent[(1)] resistance, R_0' (equivalent to η_0'), that is independent of the secondary resistance, R_k (equivalent to η_k). The reactive terms effectively sum to zero. This leads to either of the circuit representations of Fig. 1.2, corresponding to a

---

[(1)] It is frequency independent in the sense that R_0' does not vary appreciably over the bandwidth of the uniform mode.

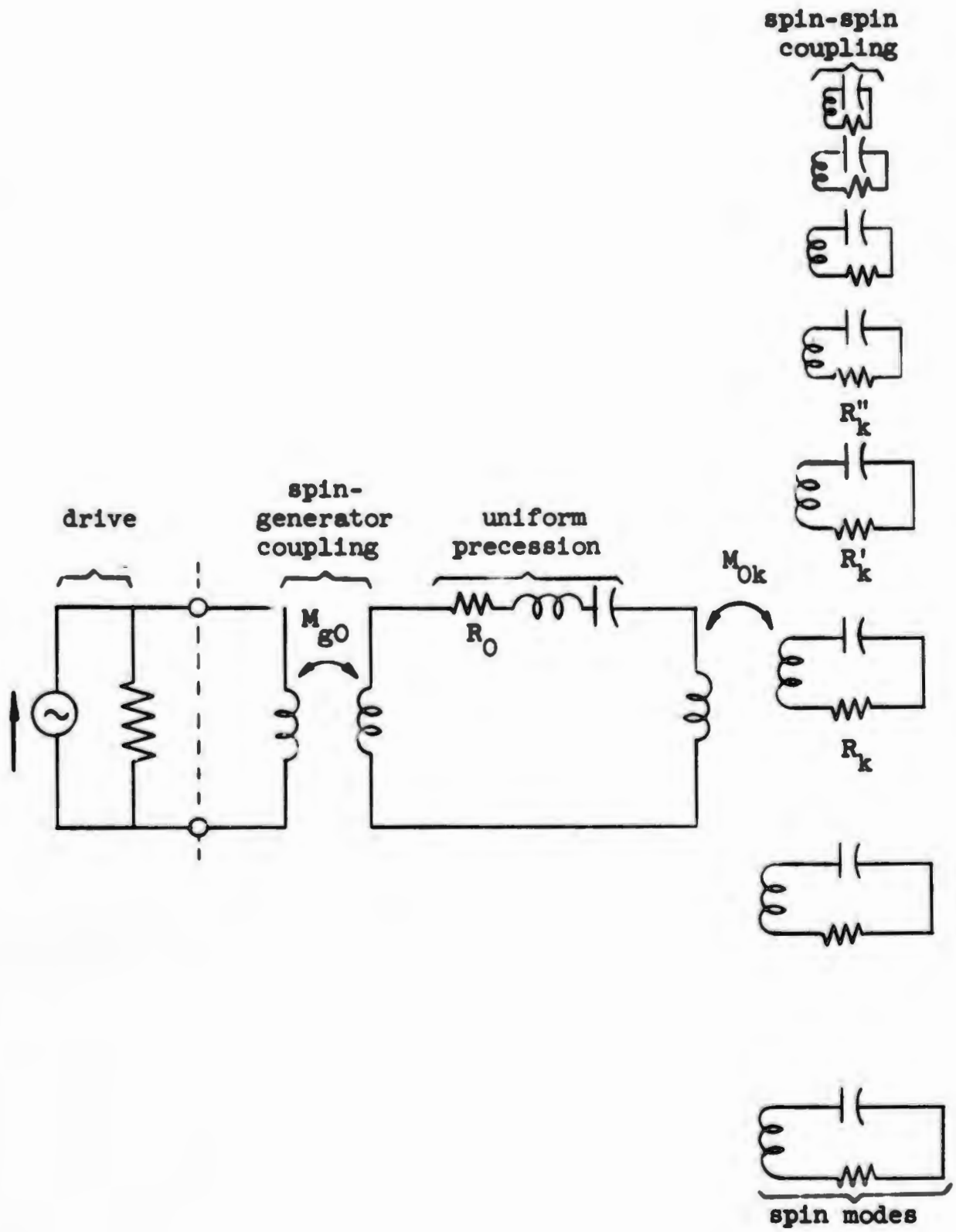

FIG. 1.1--Circuit representation of spin system.

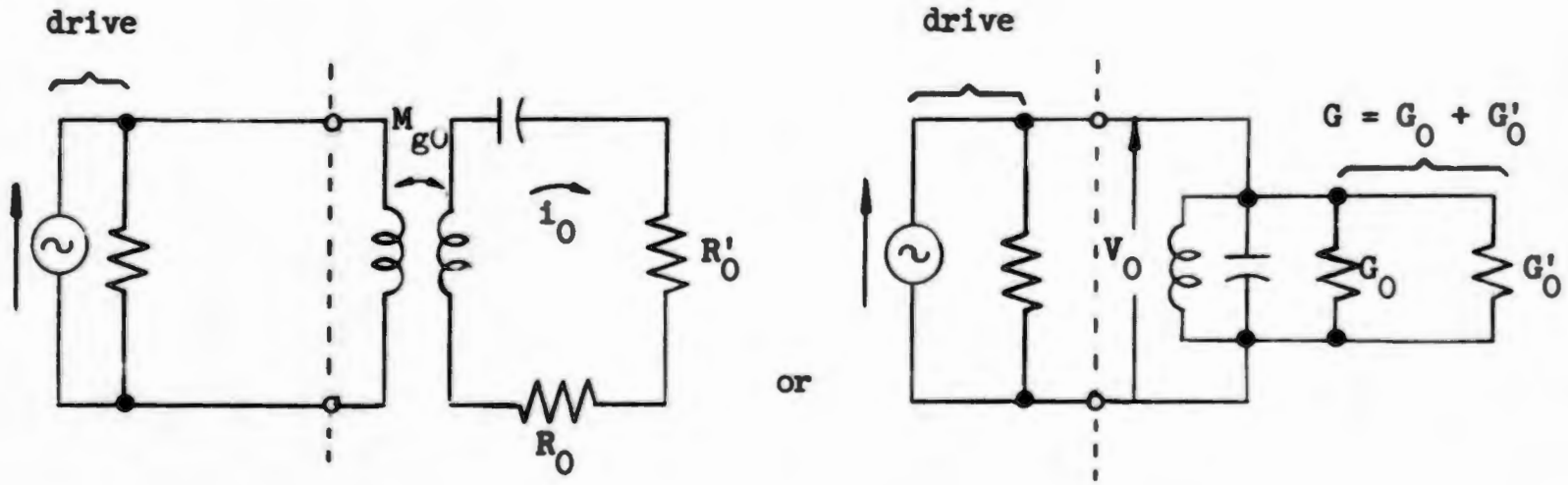

FIG. 1.2--Circuit representations of uniform precessional mode including inhomogeneity scattering.

system with but a single degree of freedom, and hence a Lorentzian-shaped resonance line. The equivalent circuit may also be used to predict qualitatively what will happen when there is appreciable coupling between the uniform mode and those low order magnetostatic modes for which the spin-mode spectrum is no longer quasi-continuous. Such coupling can occur whenever there is what we might call "large-scale disorder" in the sample, such as, for example, a nonellipsoidal shape, or a polycrystalline sample with extraordinarily large single-crystal grains, or -- and this is often important in practice -- when the sample is placed too close to a conducting wall. Some experimental manifestations of this latter effect will be described in Part II.

The most important use that we shall make of the equivalent circuit representation in the present paper is in the consideration of radiation damping in Part II, and in the description of various experimental procedures for determining the linewidth, given in Appendix B. In both of these applications considerable simplicity and unity of approach result from the use of the network representation.

PART II

COUPLING OF SMALL FERRIMAGNETIC ELLIPSOIDS TO MICROWAVE CIRCUITS

CHAPTER III

INTRODUCTION

In Part I we saw that the expansion of the magnetization of a small ferrite ellipsoid into a set of normal modes led naturally to the representation of the spin system in terms of lumped equivalent electrical circuits. Such an approach, of course, tells us nothing about the nature of the coupling between the magnetic modes and the microwave circuit. In the present section we shall consider this coupling problem in detail. The approach adopted is to obtain an impedance matrix for a uniform section of waveguide containing a ferrite ellipsoid, and from this impedance matrix construct, by inspection, a lumped equivalent circuit.

The first step in such a program is to solve the general problem of the scattering of electromagnetic waves from a small ferrite ellipsoid in a uniform waveguide. Such a problem has been considered by a number of authors[26-30] using approaches which are superficially quite different, but which reduce to the application of first-order perturbation theory. Epztein and Berk[26] consider the problem of an axially magnetized thin ferrite post located parallel to the narrow wall of a rectangular waveguide propagating only the TE_{10} mode. Their method is to reduce the problem to a two-dimensional one by assuming no field variation along the axis of the post. A scattered wave, $\vec{H}_s$, is obtained by matching tangential components of $\vec{E}$ and $\vec{H}$ on the boundary of the post, ignoring the boundary conditions at the waveguide walls, but assuming the post to be illuminated by the fundamental mode of the waveguide. The actual scattered wave in the guide is obtained as a superposition of $\vec{H}_s$ and a "mirrored" wave $\vec{H}_m$ which, taken together, satisfy the boundary conditions of the waveguide (but not of the post).

Pistolkors and Shen[27,28] have analyzed the scattering from both a transversely and a longitudinally magnetized ferrite sphere in rectangular waveguide. Their approach is basically that of Epztein and Berk. They solve the boundary problem of a sphere illuminated by a uniform plane wave whose propagation vector makes an arbitrary angle with the dc magnetic field. This is done in terms of the magnetostatic modes of Walker.[14]

By expanding the incident waveguide mode in plane waves, the scattering of each of which is known, and resumming the results, a total scattered wave, $\vec{H}_s$, is obtained. The actual scattered wave in the guide is obtained by expanding $\vec{H}_s$ in waveguide normal modes and picking out the propagating part.

Nikol'skii,[29] on the other hand, uses a somewhat different approach. He derives exact expressions for the scattering coefficients of a section of waveguide containing a ferrite sample in terms of two sets of fields, one appropriate to the empty guide, and the other to the same guide containing the sample. In these expressions the important quantity has the form

$$\int_{\substack{\text{Volume}\\ \text{of Sample}}} \vec{H}_0 \cdot \overleftrightarrow{\chi}\, \vec{H} d\tau \quad , \tag{2.1}$$

where $\vec{H}_0$ is the field in the empty waveguide, $\vec{H}$ is the field with the sample present, and $\overleftrightarrow{\chi}$ is the susceptibility tensor. Nikol'skii then obtains a first-order perturbation solution by substituting for the exact field $\vec{H}$, the field obtained as the lowest order magnetostatic solution of the boundary value problem appropriate to the sample geometry. This is equivalent to replacing $\overleftrightarrow{\chi}\vec{H}$ by $\overleftrightarrow{\tilde{\chi}}\vec{H}_0$ where $\overleftrightarrow{\tilde{\chi}}$ is an equivalent tensor susceptibility.

Two limitations are characteristic of all these methods. First, in order to obtain numerical results, it is necessary to assume that the significant dimensions of the sample are small compared with a wavelength in the medium, and second, higher order scatterings are neglected. In physical terms this means that the reaction back on the sample of fields which scatter first on the sphere and then on the waveguide wall is neglected. This restricts the analysis to samples from which the scattering is small, and which are not too close to the waveguide walls.

Hauser[30] also starts from the exact expression [Eq. (2.1)], but uses it to obtain an amplitude independent variational expression for the scattering coefficients into which various trial fields with variable parameters may be inserted. In principle, this technique may be carried out numerically, for individual cases to any arbitrary degree of accuracy, although Hauser has not done so.

In an effort to develop a simple approximate theory that is valid for samples which, although small physically, represent large electrical discontinuities in the waveguide, we have used a different approach, which may be broken up into a number of distinct steps, as follows:

(1) The uniform rf magnetization produced by a given uniform external rf driving field is determined in terms of an external or effective[31,32] tensor susceptibility derived from the transverse part of the equation of motion for the magnetization.

(2) Maxwell's equations are solved, subject to the usual boundary conditions for a perfectly conducting waveguide, treating the rf magnetization as a known point source. This is done using the method of Marcuvitz and Schwinger,[33] in which the waveguide is replaced by a set of uncoupled transmission lines, one for each mode of the waveguide, and the sources by current and voltage generators.

(3) From such an active network representation the magnitudes of the forward and backward scattered waves are obtained.

(4) The external field assumed in step (1) is then determined by the requirement of conservation of energy. This procedure leads to a self-consistent scattering matrix, which, although approximate, is nonetheless a considerable improvement over the first-order perturbation result.

(5) Finally, from the scattering matrix, impedance and admittance matrices are derived which are separated into symmetric and antisymmetric parts. The symmetric parts of the matrices are represented by π and T networks, the antisymmetric parts by gyrators.[34]

The advantage of this network formulation lies in the ease with which a great variety of ferrite problems may be solved by a suitable choice of the terminating impedances for the network.

CHAPTER IV

EXCITATION OF A WAVEGUIDE BY A MAGNETIC DIPOLE

As discussed in Part I, one of the normal modes of a small ferrimagnetic ellipsoid is a uniform precession. If the sample is in free space, illuminated by a uniform drive field,(1) the uniform precession

(1) This can be achieved approximately by illuminating the sample with a plane wave whose wavelength is much greater than a transverse sample dimension.

is the only mode that is excited, and as far as small-signal interaction with the applied field is concerned, the sample may be replaced by a macroscopic dipole, or rather, by two dipoles, one for each transverse component of magnetization. The external dipolar fields satisfy all the boundary conditions of the "microwave circuit," in this case, the trivial condition that the fields drop to zero at infinity.

If the sample is now placed in a waveguide or cavity, surrounded by metal walls, these external dipolar fields can no longer satisfy the boundary conditions of the circuit, but we may think of the original dipolar fields as being mirrored, in some fashion, in the waveguide walls, resulting in an additional nonuniform driving field at the sample which alters the motion of the magnetization in such a way as to produce a total field that does satisfy the boundary conditions of the waveguide. Thus, in the general case, the waveguide fields must be expressed as a summation of all the normal modes of the empty guide, and the magnetization as a summation of all the normal modes of the isolated sample. If, however, the microwave structure is resonant in, or can propagate, only a single mode at the operating frequency, and if none of the magnetostatic modes excited in the sample is degenerate with the uniform precession, these higher modes do not take part in the energy transfer within the ferrite-microwave system. Their main effect is a shift of the resonant frequency of the ferrite, the microwave structure, or both. Under most circumstances, then, one need consider only dominant mode interactions, although an exception occurs when the sample is placed too close to a waveguide wall.[42-44] Since some of our experiments required that the sample be placed near a wall, a reasonably exact characterization of "too close" is required, and this question will be discussed later.

For the present, then, we assume that in some way, as yet unspecified, we excite a uniform rf magnetization $\vec{m}$ in the sample. This uniform magnetization can then be replaced by a macroscopic dipole $\vec{m}V_s$, where V_s is the volume of the sample. The excitation of the waveguide by this dipole is then obtained by solving Maxwell's equations in the form

$$\nabla \times \vec{E} = - j\omega\mu_0 \vec{H} - j\omega\mu_0 \vec{m} V_s \delta^3(\vec{r} - \vec{r}_0)$$

$$\nabla \times \vec{H} = j\omega\epsilon \vec{E} \quad , \tag{2.2}$$

subject to the usual boundary conditions at the waveguide walls. Here $\delta^3(\vec{r} - \vec{r}_0)$ is a three-dimensional delta function, the sample being located at $\vec{r} = \vec{r}_0$. In this formulation we neglect the dielectric properties of the sample, and take ϵ to be the permittivity of the material filling the waveguide. Because we are using the magnetostatic approximation for the fields in the ferrite, in which we neglect the electric field associated with the precessing magnetization, the scattering due to the dielectric properties of the sample may be treated independently of that arising from the magnetic properties, and will not be considered here.

The solution of Eqs. (2.2) appropriate to waveguides with perfectly conducting walls is most conveniently effected by expanding the actual waveguide fields in terms of a set of normal modes of the guide. Thus, assuming propagation in the y-direction, we write

$$\vec{E}(x,y,z) = \sum_n V_n(y)\vec{e}_n(x,z)$$

$$\vec{H}(x,y,z) = \sum_n I_n(y)\vec{h}_n(x,z) \quad . \tag{2.3}$$

The y dependence for the n^{th} mode is assumed to be of the form $e^{j\beta_n y}$, and is included explicitly in the coefficients V_n and I_n, which may be considered as the voltage and current, respectively, on an equivalent uniform TEM transmission line. The eigenvectors $\vec{e}_n$ and $\vec{h}_n$ then depend only on the transverse coordinates x and z. As usual, we choose the normal modes in such a way that they may be divided into two sets, one with no y-component of electric field (TE modes) and the other with no y-component of magnetic field (TM modes).

Thus, we can write

$$\left.\begin{aligned} \vec{e}_n &= \vec{e}_{tn} \\ \vec{h}_n &= \vec{h}_{tn} + h_{yn}\hat{a}_y \end{aligned}\right\} \text{TE modes}$$

$$\left.\begin{aligned} \vec{e}_n &= \vec{e}_{tn} + \vec{e}_{yn}\hat{a}_y \\ \vec{h}_n &= \vec{h}_{tn} \end{aligned}\right\} \text{TM modes} \tag{2.4}$$

where $\vec{e}_{tn}$ and $\vec{h}_{tn}$ are the transverse components of $\vec{e}_n$ and $\vec{h}_n$, $\vec{e}_{yn}$ and $\vec{h}_{yn}$ the longitudinal components, and $\hat{a}_y$ is a unit vector in the longitudinal (y) direction. It is usual to choose the transverse component of the eigenvector corresponding to the electric field to be real, and to be normalized so that

$$\int_S \vec{e}_{tn} \cdot \vec{e}_{tn} ds = 1 \quad ,$$

with the integration extending over the waveguide cross section. The other components are then

$$\vec{h}_{tn} = \hat{a}_y \times \vec{e}_{tn} \tag{2.5a}$$

$$e_{yn} = \frac{\nabla_t \cdot \vec{e}_{tn}}{j\beta_n} \quad \text{(TM modes)}$$

and

$$h_{yn} = \frac{\nabla_t \cdot \vec{h}_{tn}}{j\beta_n} \quad \text{(TE modes)} \quad , \tag{2.5b}$$

where ∇_t is the transverse gradient operator. With this normalization, the ratio (V_n/I_n) is just Z_n, the wave impedance of the n^{th} mode, and the integral $\int_S 1/2 R_e V_m I^*_n ds$ is the power carried by the n^{th} mode.

The point source of excitation described by the delta-function term in Eqs. (2.2) can be represented by voltage and current generators in the modal transmission lines, as shown by Marcuvitz and Schwinger.[33] Thus, the waveguide containing the sample is replaced by a set of transmission lines, one for each mode of the waveguide, in which the effect of the rf magnetization of the sample is represented by voltage and current generators, located in the transverse plane of the sample, as shown in Fig. 2.1. If we assume that the equilibrium orientation of the magnetization, $\vec{M}$, is along the z-axis, the rf magnetization will have only x and y components,[(1)] in terms of which the strengths of the generators are

$$Y_n V_n = j\beta_n V_s m_x h_{xn}(x_0, y_0) \quad ,$$

[(1)] Throughout this part, we consider only the linear approximation.

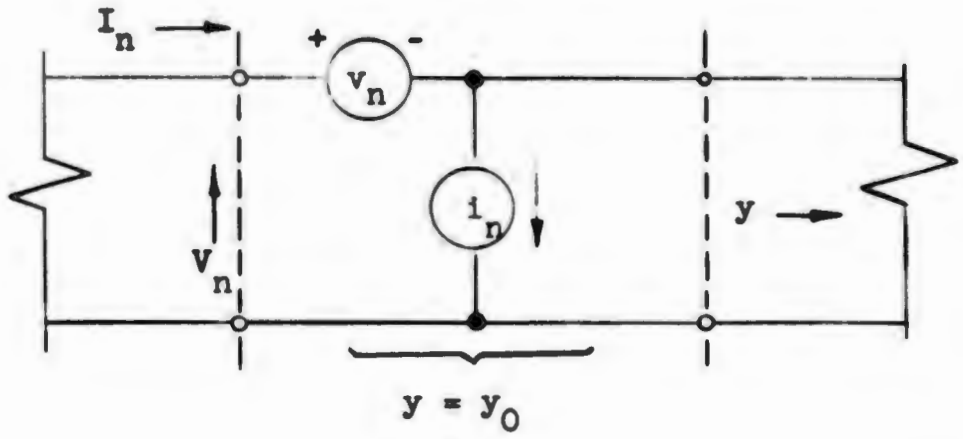

FIG. 2.1--Equivalent circuit for point-source excitation of n^{th} waveguide mode.

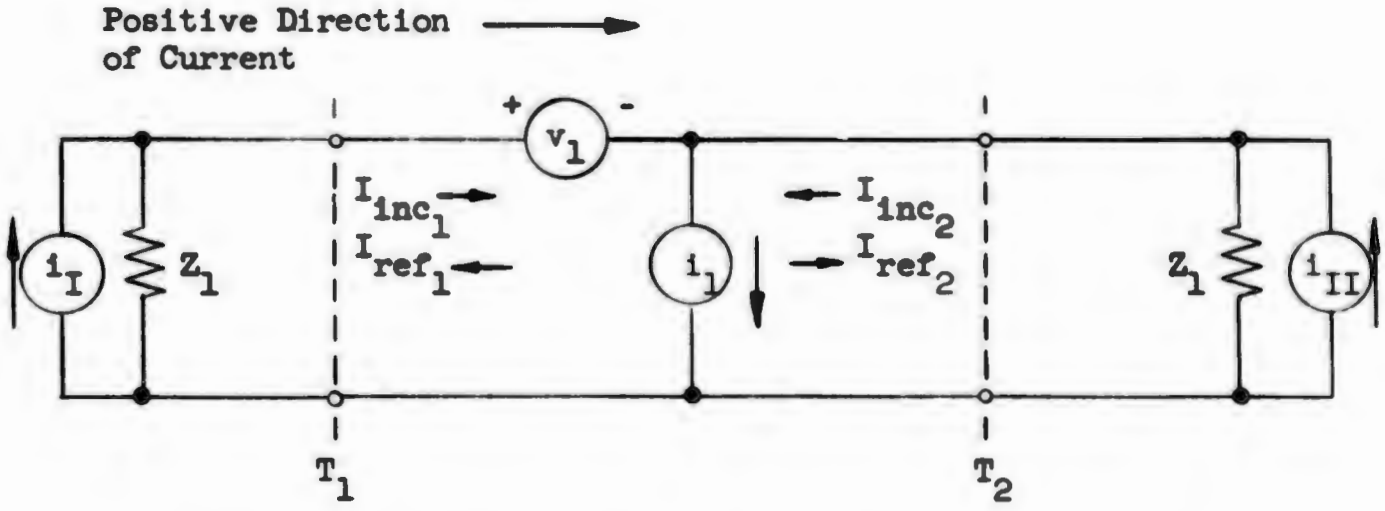

FIG. 2.2--Circuit used to calculate scattering matrix.

and

$$i_n = - j\beta_n V_s m_y h_{yn}(x_0,y_0) \quad , \tag{2.6}$$

where Y_n is the wave admittance of the n^{th} mode, β_n its propagation constant, and V_s is the volume of the sample.

CHAPTER V
THE SCATTERING MATRIX

A. DERIVATION OF GENERAL SCATTERING MATRIX

For any passive, linear two-port network, the relations between the incident and reflected waves at the two ports can be written in terms of a scattering matrix:[34]

$$\begin{pmatrix} b_1 \\ b_2 \end{pmatrix} = \begin{pmatrix} S_{11} & S_{12} \\ S_{21} & S_{22} \end{pmatrix} \begin{pmatrix} a_1 \\ a_2 \end{pmatrix} \quad , \tag{2.7}$$

where a_1 and a_2 are the incident waves at ports 1 and 2, respectively, and b_1 and b_2 are the reflected waves.

The results of Chapter IV may be used to obtain the reflected waves, if we assume that the sample is placed in a guide propagating only one mode and reflectionlessly terminated at both ends. The equivalent circuit for this arrangement is shown in Fig. 2.2. The reference planes T_1 and T_2 are coincident at the plane of the ferrite. From Fig. 2.2 we have, by superposition,

$$I_{ref_1} = - \frac{1}{2}\left(\frac{v_1}{Z_1} - i_1\right) + I_{inc_2} \quad ,$$

$$I_{ref_2} = - \frac{1}{2}\left(\frac{v_1}{Z_1} + i_1\right) + I_{inc_1} \quad . \tag{2.8}$$

To obtain the scattering coefficients, the voltage and current generators v_1 and i_1 must be related to the drive. This may be done

by defining an equivalent susceptibility tensor, $\overleftrightarrow{\chi}$, so that[1]

$$\vec{m} = \overleftrightarrow{\chi}\vec{H}_{ext} \quad , \tag{2.9}$$

where $\vec{H}_{ext}$ is the externally applied rf driving field. In a first-order theory, $\vec{H}_{ext}$ would be the sum of two fields, one due to a wave incident from the left, the other to a wave incident from the right. Thus, we would write

$$\vec{H}_{ext} = I_{inc_1}\vec{h}_1 + I_{inc_2}\vec{h}_{-1} \quad , \tag{2.10}$$

where $\vec{h}_1$ is the eigenvector of the dominant mode propagating to the right, and $\vec{h}_{-1}$ of that propagating to the left. In terms of their components, if we write

$$\vec{h}_1 = \begin{pmatrix} h_x \\ h_y \\ h_z \end{pmatrix} \quad , \text{ then } \vec{h}_{-1} = \begin{pmatrix} h_x \\ -h_y \\ h_z \end{pmatrix} \quad . \tag{2.11}$$

A better approximation can be obtained by taking for $\vec{H}_{ext}$ the average of the <u>total</u> dominant mode field at the reference planes T_1 and T_2.[2] Thus, we assume that

$$\vec{H}_{ext} = \left(\frac{I_{inc_1} + I_{ref_2}}{2}\right)\vec{h}_1 + \frac{\left(I_{inc_2} + I_{ref_1}\right)}{2}\vec{h}_{-1} \quad . \tag{2.12}$$

By combining Eqs. (2.6), (2.8), (2.9), (2.11) and (2.12) with the definition[3]

---

(1) See Appendix A.

(2) This seemingly arbitrary assumption can be justified, <u>post facto</u>, by showing that it leads [in contrast to the assumption of Eq. (2.10)] to the conservation of energy.

(3) The minus sign arises because scattering coefficients are customarily defined with regard to the electric fields or voltages of the incident and reflected waves. We are using <u>currents</u>, which have an additional 180° phase shift upon reflection, relative to the reflected <u>voltages</u>.

of the scattering coefficients,

$$S_{11} = \left.\frac{-I_{ref_1}}{I_{inc_1}}\right|_{I_{inc_2}=0} \quad ; \quad S_{22} = \left.\frac{-I_{ref_2}}{I_{inc_2}}\right|_{I_{inc_1}=0} \quad ;$$

$$S_{12} = \left.\frac{I_{ref_2}}{I_{inc_1}}\right|_{I_{inc_2}=0} \quad ; \quad S_{21} = \left.\frac{I_{ref_1}}{I_{inc_2}}\right|_{I_{inc_1}=0} \quad ,$$

and assuming that the effective susceptibility tensor has the general form

$$\overleftrightarrow{\chi} = \begin{pmatrix} \chi_{11} & \chi_{12} \\ \chi_{21} & \chi_{22} \end{pmatrix} \quad ,$$

we obtain a scattering matrix of the form

$$\overleftrightarrow{S} = \frac{1}{E}\begin{pmatrix} A + B & C - D \\ C + D & A - B \end{pmatrix} \qquad (2.13a)$$

where

$$A = \chi_{11}h_x^2 + \chi_{22}h_y^2 \quad , \qquad (2.13b)$$

$$B = h_x h_y(\chi_{12} + \chi_{21}) \quad , \qquad (2.13c)$$

$$C = \frac{2}{j\beta_1 V_s} \quad , \qquad (2.13d)$$

$$D = h_x h_y(\chi_{12} - \chi_{21}) \quad , \qquad (2.13e)$$

and

$$E = \frac{2}{j\beta_1 V_s} + \chi_{11}h_x^2 - \chi_{22}h_y^2 - \frac{j\beta_1 V_s}{2} h_x^2 h_y^2(\chi_{11}\chi_{22} - \chi_{12}\chi_{21}) \quad . \qquad (2.13f)$$

This general result may be considerably simplified if we restrict ourselves here, as in Part I, to a small ellipsoid whose principal axes coincide with the coordinate axes. The dc field is then applied in the z-direction and the effective susceptibility tensor is antisymmetric, i.e., $\chi_{21} = -\chi_{12}$. Furthermore, it can be shown [1] from the form of the effective susceptibility tensor that the last term in Eq. (2.13f) is less than either the second or third by a factor of order (sample dimension/free-space wavelength),[3] so that for the small samples to which this analysis is restricted, this term may be dropped. The scattering matrix then becomes simply

$$\overleftrightarrow{S} = F\begin{pmatrix} \frac{j\beta_1 V_s}{2}(\chi_{11}h_x^2 + \chi_{22}h_y^2) & 1 - j\beta_1 V_s \chi_{12} h_x h_y \\ 1 + j\beta_1 V_s \chi_{12} h_x h_y & \frac{j\beta_1 V_s}{2}(\chi_{11}h_x^2 + \chi_{22}h_y^2) \end{pmatrix} \tag{2.14a}$$

where

$$F = \frac{1}{1 + \frac{j\beta_1 V_s}{2}(\chi_{11}h_x^2 - \chi_{22}h_y^2)} \quad . \tag{2.14b}$$

Any matrix can be written as the sum of a symmetric and an antisymmetric part. In the case of Eq. (2.14) this division is obvious, and by writing

$$\overleftrightarrow{S} = \overleftrightarrow{S}_{sym} + \overleftrightarrow{S}_{antisym} \quad ,$$

we obtain

$$\overleftrightarrow{S}_{sym} = F\begin{pmatrix} \frac{j\beta_1 V_s}{2}(\chi_{11}h_x^2 + \chi_{22}h_y^2) & 1 \\ 1 & \frac{j\beta_1 V_s}{2}(\chi_{11}h_x^2 + \chi_{22}h_y^2) \end{pmatrix} \tag{2.15a}$$

and

$$\overleftrightarrow{S}_{antisym} = j\beta_1 V_s \chi_{12} h_x h_y F \begin{pmatrix} 0 & -1 \\ 1 & 0 \end{pmatrix} \quad . \tag{2.15b}$$

As we might expect, the symmetric part of the scattering matrix depends only on the diagonal components, χ_{11} and χ_{22}, of the susceptibility tensor, whereas the antisymmetric part depends only on the off-diagonal component. Furthermore, the antisymmetric part vanishes whenever either h_x or h_y is zero, i.e., whenever the driving field is linearly polarized.

B. APPLICATION TO AN AXIALLY SYMMETRIC SAMPLE IN RECTANGULAR WAVEGUIDE

Of special interest to us is the form taken by Eq. (2.14) for a rectangular waveguide propagating the TE_{10} mode. For this mode, the components of the eigenvector in the coordinate system of Fig. 2.3 are given by[36]

$$h_x(x,z) = \sqrt{\frac{2}{ab}} \sin k_c x$$

$$h_y(x,z) = -j \sqrt{\frac{2}{ab}} \frac{k_c}{\beta_1} \cos k_c x \quad , \tag{2.16}$$

where a and b are the width and height of the guide, respectively, and $k_c = \pi/a$ is the cut-off wave number. If the sample is assumed to be an ellipsoid of revolution, with axial symmetry about the direction of the applied field so that $\chi_{11} = \chi_{22}$, and located a distance x_0 from the side of the waveguide, the scattering matrix becomes

$$\overleftrightarrow{S} = F \begin{pmatrix} j\eta \frac{\beta_1}{k_c} \chi_{11} \left[\sin^2 k_c x_0 - \left(\frac{k_c}{\beta_1} \right)^2 \cos^2 k_c x_0 \right] & 1 - \eta \chi_{12} \sin 2k_c x_0 \\ 1 + \eta \chi_{12} \sin 2k_c x_0 & j\eta \frac{\beta_1}{k_c} \chi_{11} \left[\sin^2 k_c x_0 - \left(\frac{k_c}{\beta_1} \right)^2 \cos^2 k_c x_0 \right] \end{pmatrix}$$

where

$$F = \frac{1}{1 + j\eta\chi_{11} \left[\sin^2 k_c x_0 + \left(\frac{k_c}{\beta_1} \right)^2 \cos^2 k_c x_0 \right]} \quad , \tag{2.17}$$

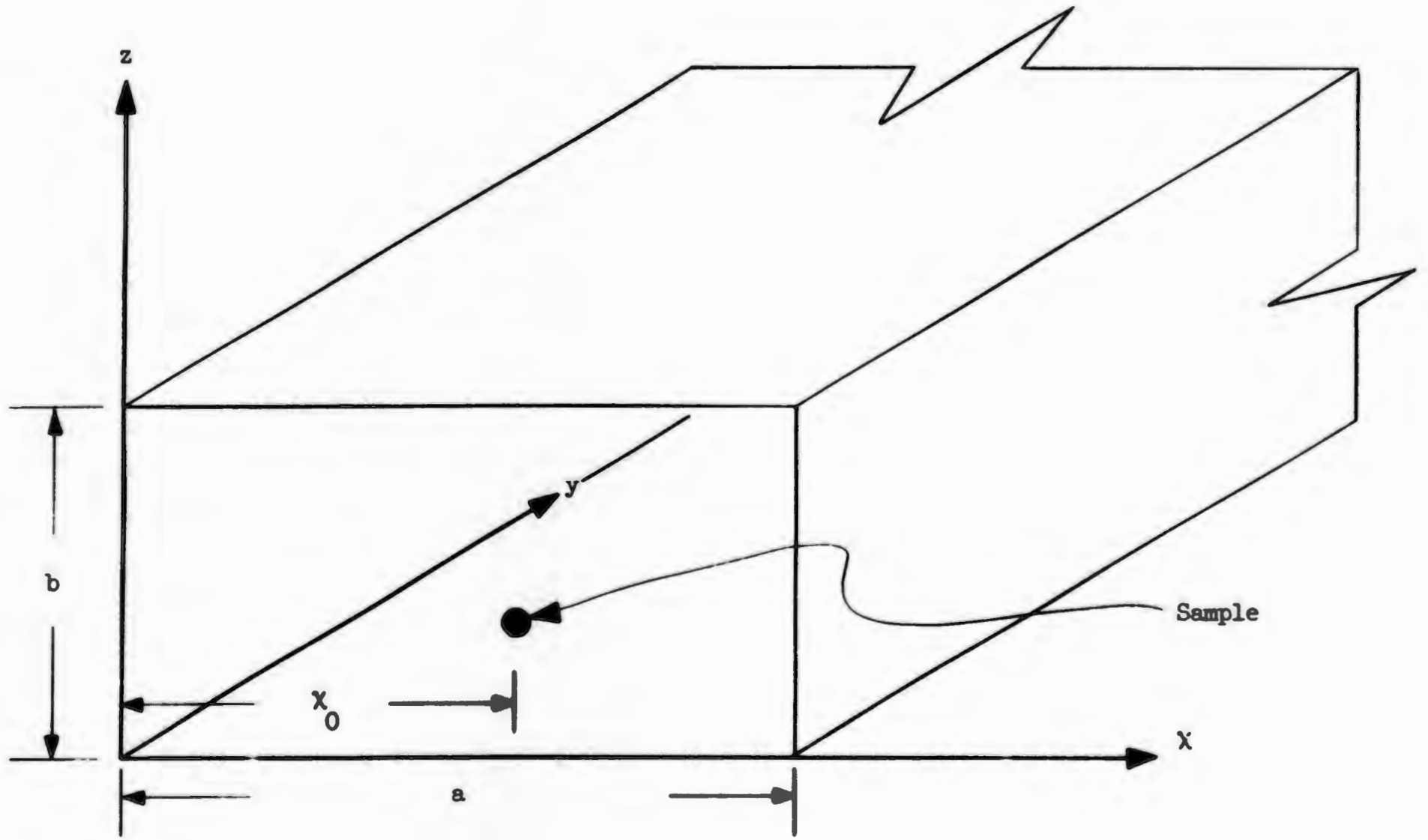

FIG. 2.3--Coordinate system for rectangular waveguide.

where $\eta \equiv k_c V_s/ab$ plays the role of a filling factor.

We can obtain some idea of how the scattering coefficients depend on the position of the sample in the waveguide by considering the special case of a low-loss sample at resonance. For this case we can make the approximation that $\chi_{12} \approx j\chi_{11} = \chi_0''$, where χ_0'' is the usual resonance susceptibility for a linearly polarized driving field.[1] The variation in reflection coefficient (S_{11}) and insertion loss $(1 - |S_{12}|^2)$ with sample position is shown in Fig. 2.4, with the ratio k_c/β_1 (and hence frequency) as a parameter. Two sets of curves are shown, one for $\eta\chi_0'' \to 0$, valid when the sample is electrically small, and hence the scattering is also small, and the other for $\eta\chi_0'' = 1$, corresponding to a sample that is critically coupled to the waveguide. To give additional insight into how the scattering depends on the sample size, we have also plotted in Fig. 2.5 the reflection and transmission coefficients versus sample position, with $\eta\chi_0''$ as a parameter, for the particular frequency at which $k_c/\beta_1 = 1$.

The behavior of the reflection coefficient as a function of sample position and size is just what one would expect on the basis of intuition. The reflection coefficient goes to zero at those points where the driving field is circularly polarized, independently of the sample size, and elsewhere increases monotonically with increasing sample size. The insertion loss (or equivalently, the transmission coefficient), however, does not behave in so simple a fashion. Although the insertion loss is zero when the sample is at the point where the driving field is circularly polarized in a sense <u>opposite</u> to that of the free precession, it is <u>not</u> a <u>maximum</u> at the point where it is circularly polarized in the <u>same</u> sense as the free precession, even when the sample is small, except at the special

---

[1] By setting $\chi_{12} = j\chi_{11}$, we neglect the interaction between the magnetization and the circularly polarized component of drive field that rotates in the opposite sense to the free precession. Actually, if we assume axial symmetry, we have

$$\frac{\chi_{12}}{j\chi_{11}} = 1 + \frac{\eta_0 + \eta_0'}{j\omega_0}$$

at resonance. For low-loss samples, however, we find $\eta_0 + \eta_0' \ll \omega_0$, so that $\chi_{12} \approx j\chi_{11}$.

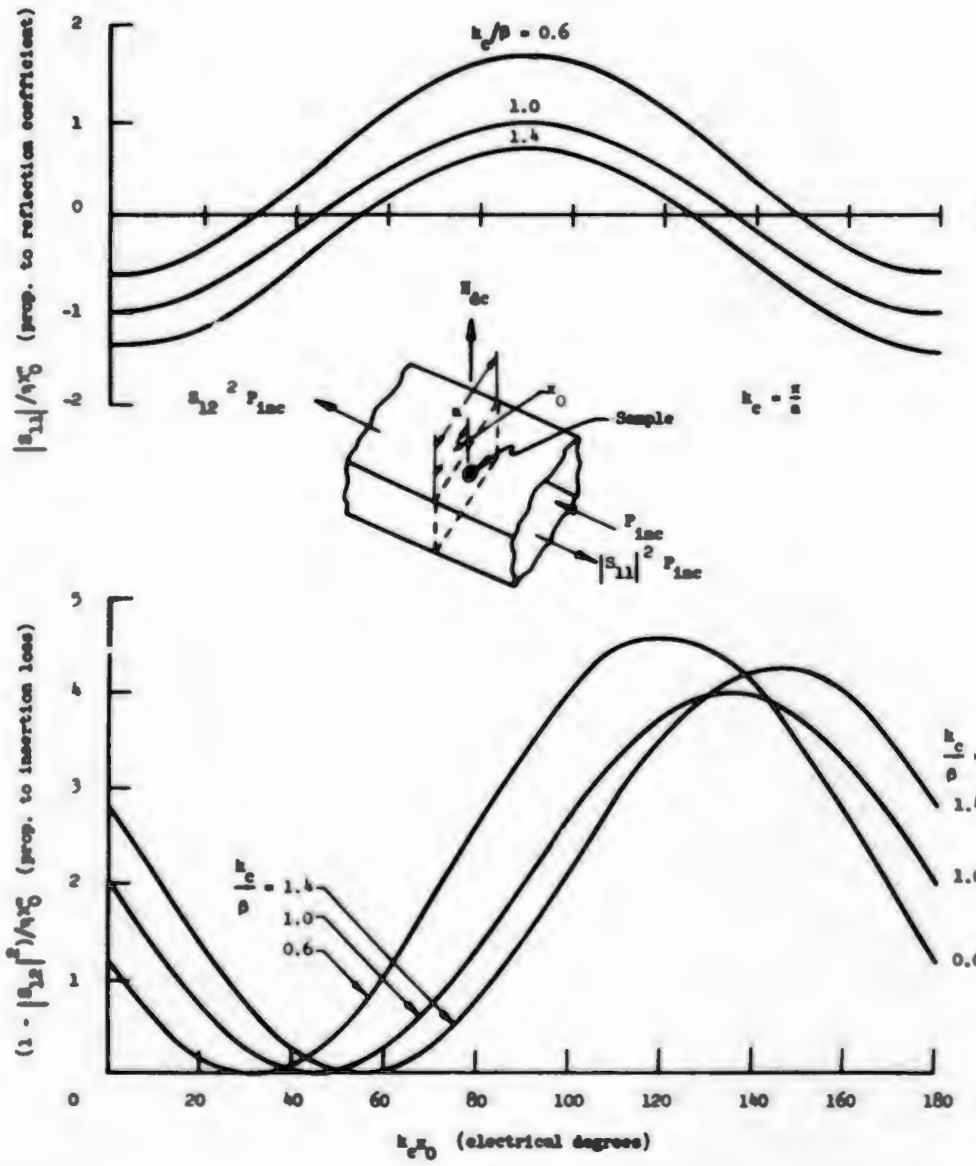

FIG. 2.4a--Reflection coefficient and insertion loss of a ferrite ellipsoid in rectangular waveguide. Case $1 - \eta\chi_0'' \rightarrow 0$.

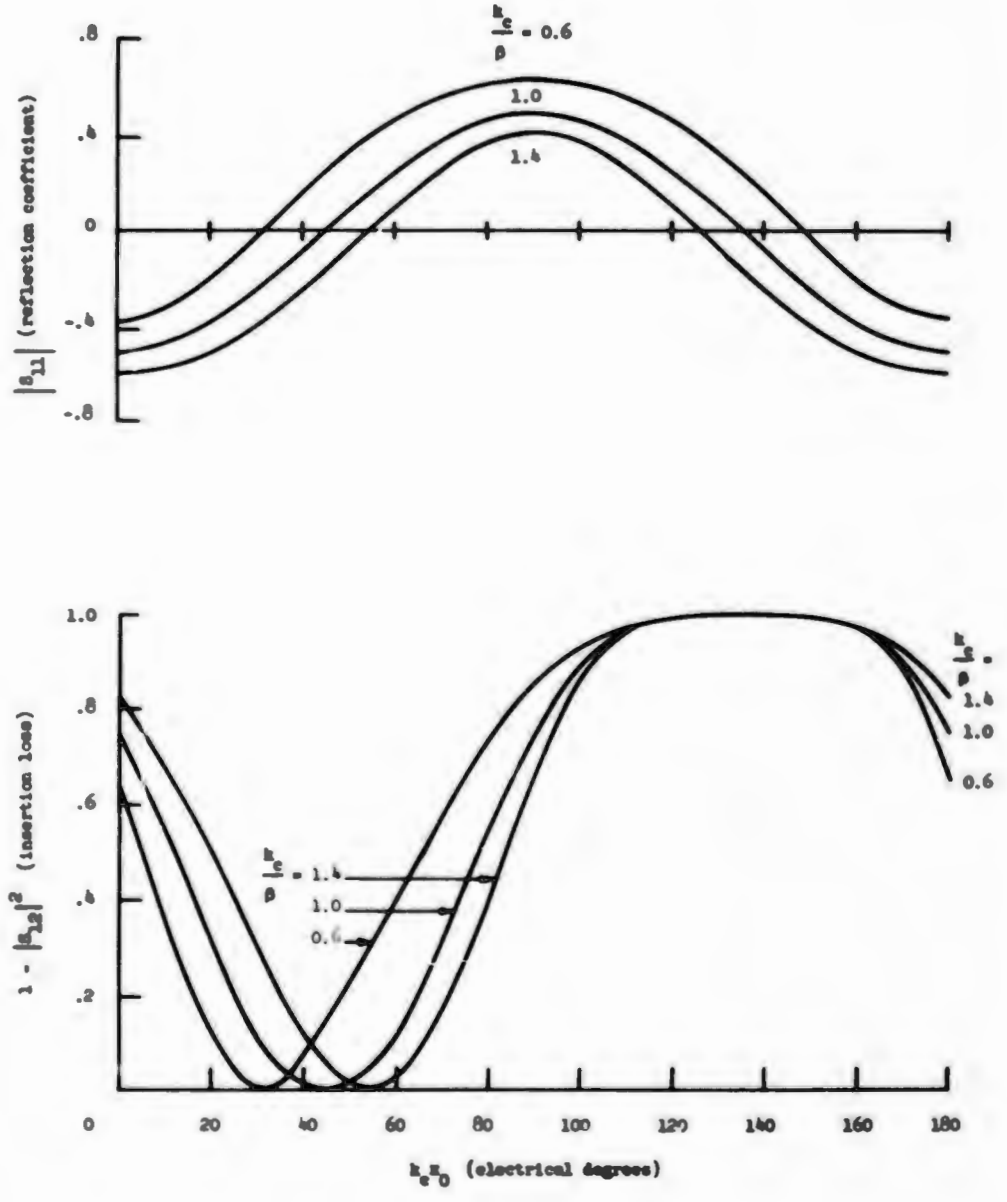

FIG. 2.4b--Reflection coefficient and insertion loss of a ferrite ellipsoid in rectangular waveguide. Case $2 - \eta\chi_0'' = \chi_1$.

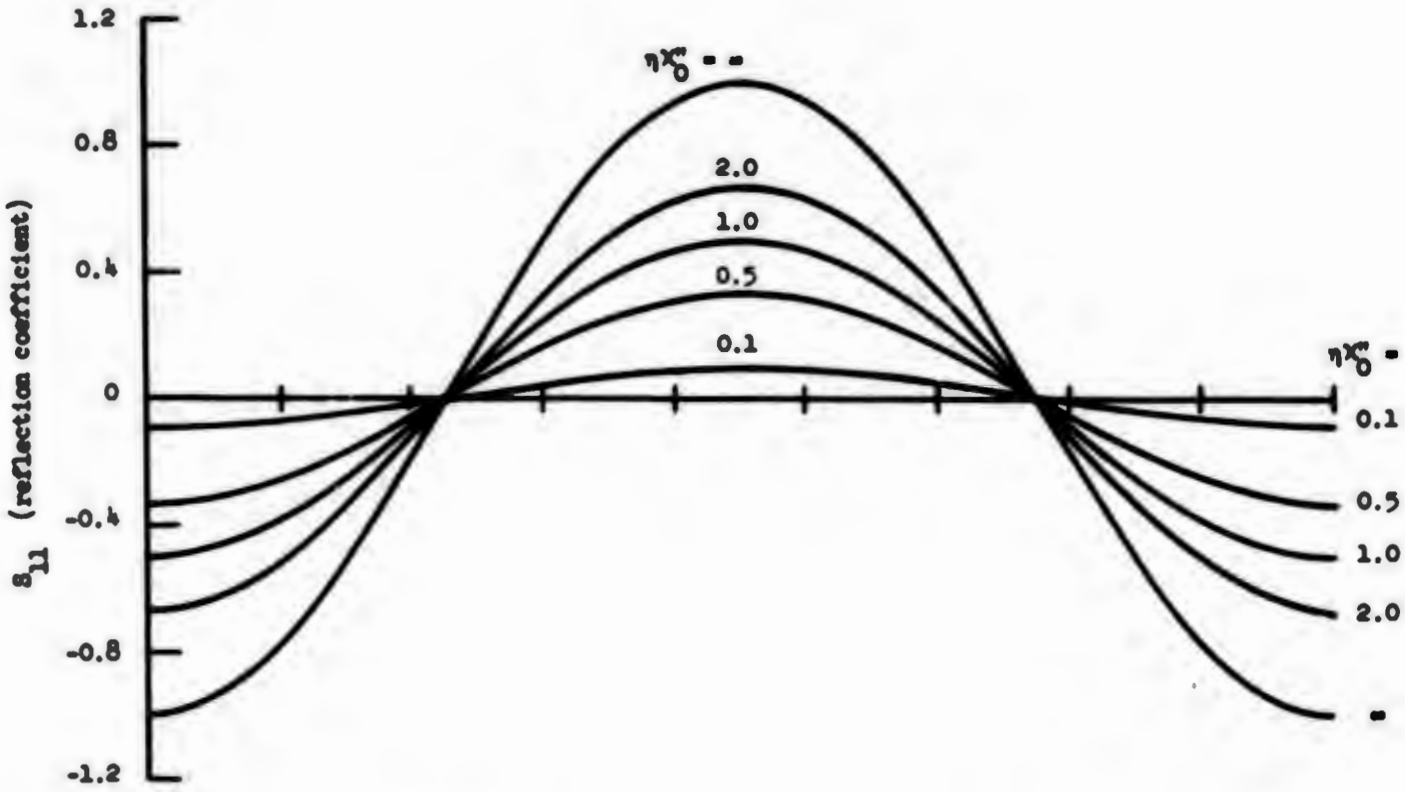

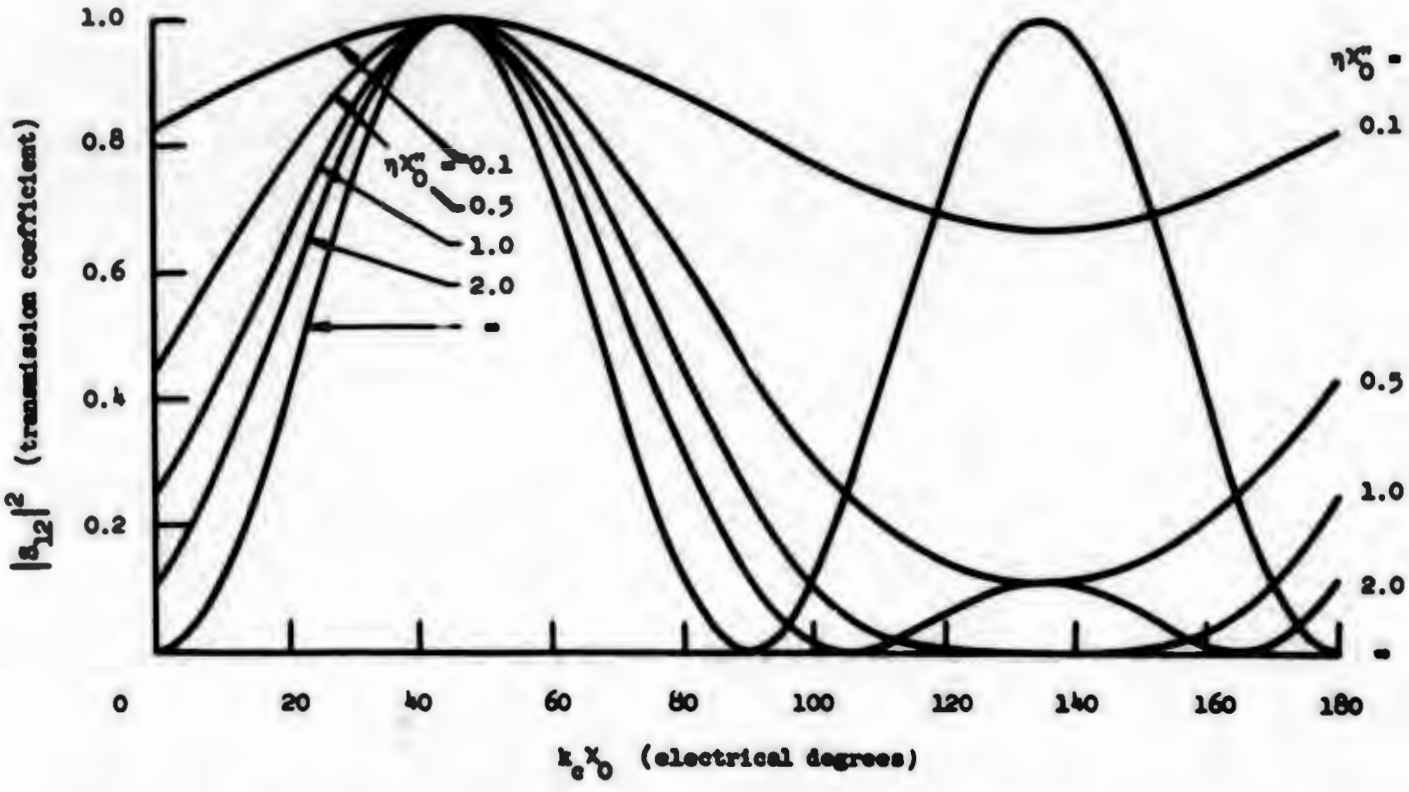

FIG. 2.5--The effect of sample size on the reflection and transmission coefficients of a rectangular waveguide containing a ferrite ellipsoid.

frequency for which $k_c/\beta_1 = 1$. When the sample is electrically small, the position of maximum insertion loss ranges over some 25 to 30 electrical degrees as the frequency is varied over the waveguide bandwidth. As the sample is made larger, however, the range diminishes, and the maximum insertion loss increases, until for a sample critically coupled to the waveguide ($\eta\chi''_0 = 1$) , the insertion loss is unity (no power transmitted) when the sample is placed at 135° (3/4 of the way across the waveguide) independently of frequency. As can be seen from Fig. 2.5b, when $\eta\chi''_0 = 1$, the position for maximum insertion loss is quite broad.

These results have important implications for the design of such devices as filters. For example, they predict that it should be possible to build, in rectangular waveguide, a magnetically tunable band-rejection filter at whose center frequency perfect rejection[1] could be obtained over the entire waveguide bandwidth. This would require a sample large enough that $\eta\chi''_0 = 1$, a value readily attained, however, with polished single crystal samples of yttrium iron garnet -- for example, in standard X-band rectangular waveguide, this condition is met by a spherical sample 0.0384 inches in diameter, having a linewidth of 80 amps/m , (1 oersted).

CHAPTER VI

ADMITTANCE AND IMPEDANCE REPRESENTATIONS

A. ADMITTANCE MATRIX

The normalized admittance matrix of any linear passive system is related to its scattering matrix by the identity[37,(2)]

$$\frac{\overleftrightarrow{Y}}{Y_1} = (1 + \overleftrightarrow{S})^{-1}(1 - \overleftrightarrow{S}) \quad .$$

---

(1) This assumes the intrinsic ferrite parameters, and hence $\eta\chi''_0$, to be independent of frequency. In practice, χ''_0 is roughly inversely proportional to frequency, so that perfect rejection could not be maintained over a finite frequency range.

(2) It is related when the input and output waveguides have the same wave admittance, Y_1 .

Applying this result to Eq. (2.14) yields the admittance matrix[1]

$$\frac{\overleftrightarrow{Y}}{Y_1} = \begin{pmatrix} \dfrac{1}{j\beta_1 V_s \chi_{11} h_x^2} & \dfrac{-1}{j\beta_1 V_s \chi_{11} h_x^2} + \dfrac{\chi_{12}}{\chi_{11}} \dfrac{h_y}{h_x} \\ \dfrac{-1}{j\beta_1 V_s \chi_{11} h_x^2} - \dfrac{\chi_{12}}{\chi_{11}} \dfrac{h_y}{h_x} & \dfrac{1}{j\beta_1 V_s \chi_{11} h_x^2} \end{pmatrix} . \quad (2.18)$$

Just as in the case of the scattering matrix, the admittance matrix may be separated into a symmetric and an antisymmetric part:

$$\left(\frac{\overleftrightarrow{Y}}{Y_1}\right)_{sym} = \frac{1}{j\beta_1 V_s \chi_{11} h_x^2} \begin{pmatrix} 1 & -1 \\ -1 & 1 \end{pmatrix} , \quad (2.19a)$$

and

$$\left(\frac{\overleftrightarrow{Y}}{Y_1}\right)_{antisym} = \frac{-\chi_{12}}{\chi_{11}} \frac{h_y}{h_x} \begin{pmatrix} 0 & -1 \\ 1 & 0 \end{pmatrix} . \quad (2.19b)$$

Equation (2.19a) will be recognized as the admittance matrix of a single series impedance, $Z/Z_1 = j\beta_1 V_s \chi_{11} h_x^2$. Equation (2.19b) describes a gyrator[34] with transfer ad ittance $Y_g/Y_1 = -(\chi_{12}/\chi_{11})(h_y/h_x)$. The complete matrix then describes the two in parallel leading to the circuit of Fig. 2.6. For low loss ferrites near resonance, the gyrator admittance $Y_g/Y_1 = -(\chi_{12}/\chi_{11})(h_y/h_x)$ will be real, and essentially independent of the ferrimagnetic properties of the sample -- to see this, we need only recall that h_y and h_x are in time quadrature [Eq. (2.5b)], and that for circumstances under which the negatively rotating component of magnetization may be ignored, we can set $\chi_{12} \approx j\chi_{11}$.

The reader may be puzzled as to why the component χ_{22} of the susceptibility does not appear in the admittance matrix. It disappears, in fact, as soon as we make the approximation that $V_s \ll \lambda^3$, (i.e., that

---

[1] In going from Eq. (2.14) to Eq. (2.18) we have dropped terms of order (sample dimension/free-space wavelength)^3 as was done in deriving Eq. (2.14).

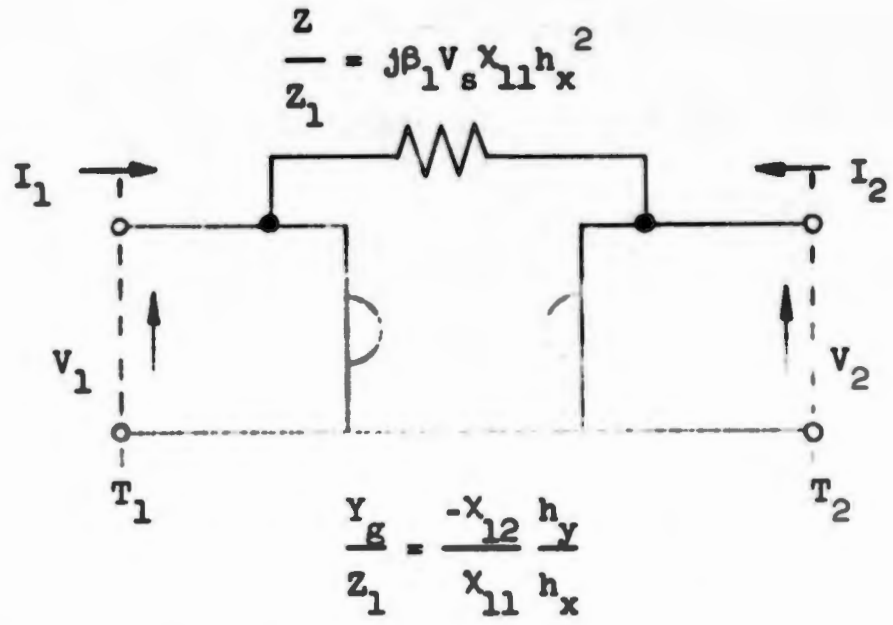

FIG. 2.6--Network representation of the admittance matrix of a ferrite ellipsoid in a waveguide.

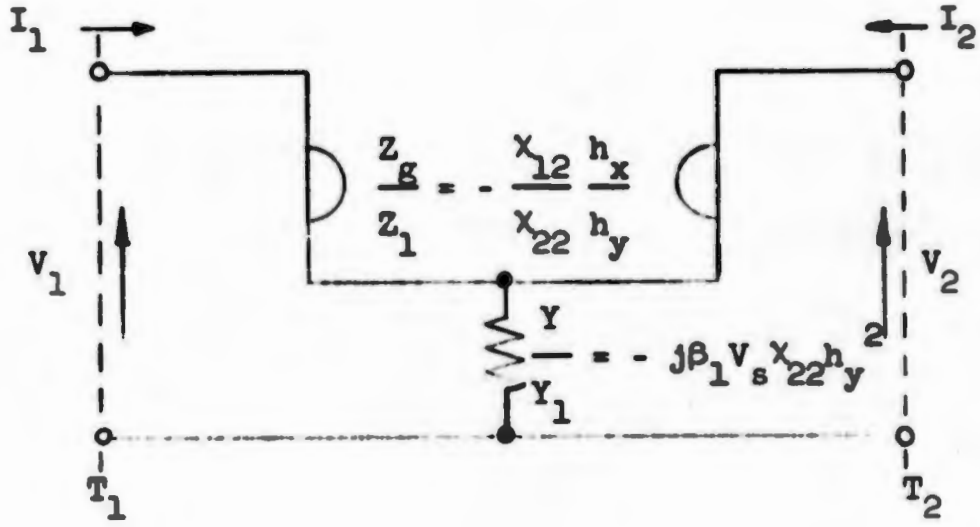

FIG. 2.7--Network representation of the impedance matrix of a ferrite ellipsoid in a waveguide.

the sample is much smaller than a wavelength), provided that the tensor susceptibility components have the explicit form given in Appendix A. Thus Eq. (2.18) has incorporated in it implicitly the fact that the susceptibility components are not all independent.

B. IMPEDANCE MATRIX

The representation of Fig. 2.6 is inappropriate at points where the transverse field, h_x, is small, but the longitudinal field, h_y, remains finite. In this range, by using the identity[37]

$$\frac{\overleftrightarrow{Z}}{Z_1} = (1 - \overleftrightarrow{S})^{-1}(1 + \overleftrightarrow{S}) \quad ,$$

we obtain an impedance matrix

$$\frac{\overleftrightarrow{Z}}{Z_1} = \begin{pmatrix} \dfrac{-1}{j\beta_1 V_s \chi_{22} h_y^2} & \dfrac{-1}{j\beta_1 V_s \chi_{22} h_y^2} + \dfrac{\chi_{12}}{\chi_{22}} \dfrac{h_x}{h_y} \\ \dfrac{-1}{j\beta_1 V_s \chi_{22} h_y^2} - \dfrac{\chi_{12}}{\chi_{22}} \dfrac{h_x}{h_y} & \dfrac{-1}{j\beta_1 V_s \chi_{22} h_y^2} \end{pmatrix} \quad , \qquad (2.20)$$

which, upon being broken up into symmetric and antisymmetric parts,

$$\left(\frac{\overleftrightarrow{Z}}{Z_1}\right)_{sym} = \frac{-1}{j\beta_1 V_s \chi_{22} h_y^2} \begin{pmatrix} 1 & 1 \\ 1 & 1 \end{pmatrix} \quad , \qquad (2.21a)$$

and

$$\left(\frac{\overleftrightarrow{Z}}{Z_1}\right)_{antisym} = \frac{-\chi_{12}}{\chi_{22}} \frac{h_x}{h_y} \begin{pmatrix} 0 & -1 \\ 1 & 0 \end{pmatrix} \quad , \qquad (2.21b)$$

leads to the network of Fig 2.7, consisting of an admittance $Y/Y_1 = - j\beta_1 V_s \chi_{22} h_y^2$ in series with a gyrator having a transfer impedance $Z_g/Z_1 = -(\chi_{12}/\chi_{22})(h_x/h_y)$.

C. EQUIVALENT CIRCUITS FOR SPECIFIC TRANSMISSION SYSTEMS

1. Structures Propagating Only a TEM Mode

For any system which supports only a TEM mode, the longitudinal field, h_y, is zero by definition, and the representation of Fig. 2.6 reduces to a reciprocal network consisting of a single series impedance. Since for TEM waves, $Z_1 = \sqrt{\mu_0/\epsilon}$, and $\beta_1 = \omega\sqrt{\mu_0\epsilon}$, the series impedance has the value $Z = j\omega\mu_0 V_s \chi_{11} h_x^2$. Specific values for several geometries are given in Table I.

2. Rectangular Waveguide

Another important structure is a rectangular waveguide operated in the TE_{10} mode. From the components of the eigenvector for this mode, given in Eq. (2.16), we obtain the element values

$$\frac{Z}{Z_1} = 2j\eta\chi_{11}\frac{\beta_1}{k_c}\sin^2 k_c x_0$$

and (2.22)

$$\frac{Y_g}{Y_1} = \frac{j\chi_{12}}{\chi_{11}}\frac{k_c}{\beta_1}\cot k_c x_0$$

for the circuit of Fig. 2.6, and the element values

$$\frac{Y}{Y_1} = 2j\eta\chi_{22}\frac{k_c}{\beta_1}\cos^2 k_c x_0$$

and (2.23)

$$\frac{Z_g}{Z_1} = j\frac{\chi_{12}}{\chi_{22}}\frac{\beta_1}{k_c}\tan k_c x_0$$

for the circuit of Fig. 2.7.

D. EQUIVALENT CIRCUITS FOR SPECIFIC SAMPLE POSITIONS

The preceding representations may be simplified when the sample is placed in either a linearly or circularly polarized field. In the case of

TABLE I

Series Impedance Reflected into a TEM Transmission Line Coupled to a Ferrite Ellipsoid

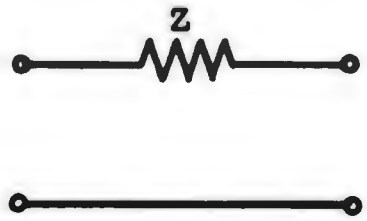

CONFIGURATION	Z
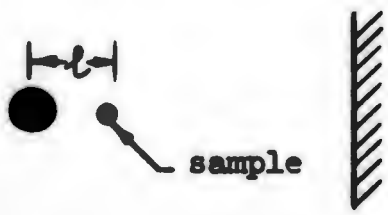	$\frac{j\omega\mu_0 V_s \chi_{11}}{(2\pi\ell)^2}$
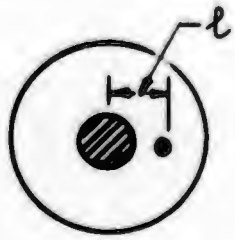	$\frac{j\omega\mu_0 V_s \chi_{11}}{(2\pi\ell)^2}$
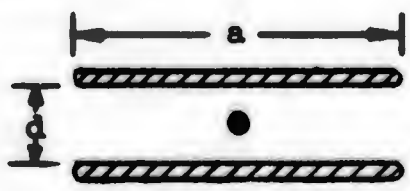 (d ≪ a)	$\frac{j\omega\mu_0 V_s \chi_{11}}{a^2}$
parallel-wire line 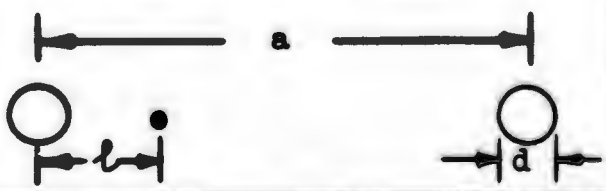	$\frac{j\omega\mu_0 V_s \chi_{11}\left[1 - \left(\frac{d}{a}\right)^2\right]}{(2\pi\ell)^2\left[1 - \frac{\ell}{a} - \left(\frac{d^2}{4\ell a}\right)^2\right]}$

linearly polarized drive, the gyrator disappears (since the network must then be reciprocal), and we are left with a single series element (transverse driving field) or a single shunt element (longitudinal driving field).

A circularly polarized driving field will exist where $h_x = \pm jh_y$, leading to a gyrator transfer admittance $Y_g/Y_1 = \pm j\chi_{12}/\chi_{11}$ in Fig. 2.6. Thus, for low loss ferrites near resonance, where, as we have pointed out before, $\chi_{12} \approx j\chi_{11}$, we have

$$\frac{Y_g}{Y_1} \approx \mp 1 \quad .$$

The gyrator can then be replaced by a unidirectional phase shifter, having π phase shift in one direction, and none in the other. An interesting feature of such a circuit is that a wave in one direction is attenuated without reflection in passing through the section containing the ferrite, while a wave in the opposite direction is neither attenuated nor reflected, behavior that is also predicted by the scattering matrix for this case. These results are summarized in Table II.

CHAPTER VII

DETERMINATION OF LUMPED CIRCUIT PARAMETERS

To complete our network representation of a waveguide containing a small ferrite sample, it is necessary to synthesize the impedance and admittance functions appearing in Figs. 2.6 and 2.7 in terms of lumped elements. This may be done by expressing the effective susceptibility as a function of frequency, and then carrying out a formal synthesis procedure on the resulting impedance and admittance functions. A simpler approach, however, is to make the circuits of Figs. 2.6 and 2.7 consistent with that of Fig. 1.2, which was derived in Part I on the basis of very general considerations concerning energy storage and dissipation in the spin system, and in which the ferrite is represented by a single tuned circuit coupled, in some unspecified way, to the signal generator.

To illustrate the procedure, consider the circuit of Fig. 2.6. Here the gyrator serves as a coupling network for the impedance, $Z/Z_1 = j\beta_1 V_s \chi_{11} h_x^2$, which characterizes energy storage and dissipation in the ferrite, and which must therefore correspond to the resonant

TABLE II

EQUIVALENT CIRCUITS FOR SPECIAL FIELD CONFIGURATIONS	
FIELD CONFIGURATION	CIRCUIT
Linear Polarization, Transverse Field Only $(h_y = 0)$	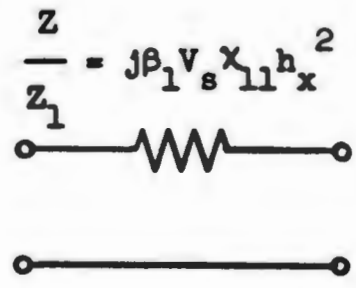
Linear Polarization, Longitudinal Field Only $(h_x = 0)$	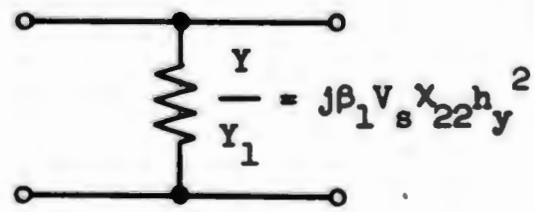
Circular Polarization, Positive Sense $(h_x = + jh_y)$	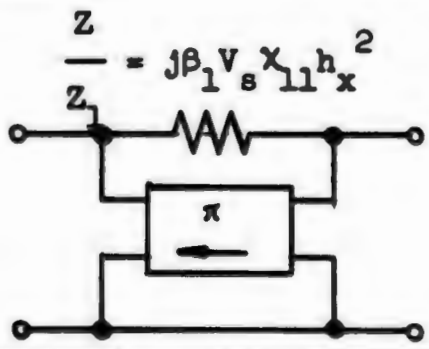
Circular Polarization, Negative Sense $(h_x = - jh_y)$	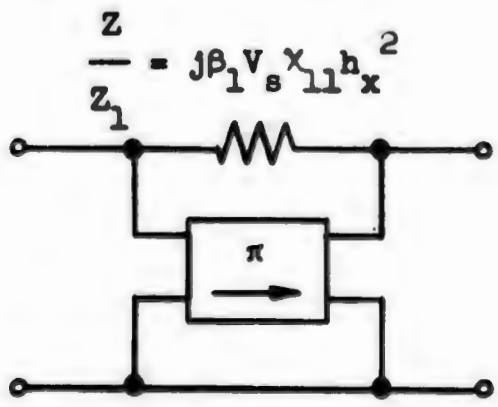

circuit of Fig. 1.2. At ferrimagnetic resonance, this impedance is real

$$\left(\frac{Z}{Z_1}\right)_{res} = \frac{R}{Z_1} = j\beta_1 V_s (\chi_{11})_{res} h_x^2 = \frac{\beta_1 h_x^2 V_s \omega_M (\omega_H + N_y \omega_M)}{2\omega_0(\eta_0 + \eta_0')} ,$$

so that the R/Q ratio[35] for the resonator is given by

$$\frac{R}{Z_1 Q_f} = \beta_1 h_x^2 \frac{V_s \omega_M (\omega_H + N_y \omega_M)}{\omega_0^2} , \qquad (2.24)$$

where Q_f is the unloaded Q of the ferrite resonator, [Eq. (1.12)]. To completely characterize the coupling, an expression for the gyrator transfer admittance, $Y_g/Y_1 = -(\chi_{12}/\chi_{11})(h_y/h_x)$ is also required. Using the effective susceptibility tensor discussed in Appendix A, together with Eq. (2.5b), we find that

$$\frac{Y_g}{Y_1} = \frac{-\omega}{\omega_H + N_y \omega_M} \frac{|h_y|}{h_x} , \qquad (2.25)$$

provided that the damping is small enough that $\eta_0 + \eta_0' \ll \omega$. The gyrator transfer admittance is then real (since h_t is real), and free of any resonant behavior.

The lumped-element networks obtained by the procedure outlined above are summarized in Table III.

CHAPTER VIII

EQUIVALENT CIRCUITS FOR FERRITE SAMPLES IN RESONANT CAVITIES

The results of the preceding section could be applied to ferrites in resonant cavities by an appropriate choice of the terminating impedances at the reference planes T_1 and T_2. Although in certain simple cases, e.g., cavities formed from short-circuited sections of uniform waveguide, such a procedure is useful, we may arrive at a much more general result by using a simple intuitive argument.

Since the fields in a microwave cavity resonant at a given frequency in a single, nondegenerate mode are linearly polarized, it must be possible to represent the coupled ferrite-cavity system, in a suitably restricted

TABLE III

LUMPED ELEMENT NETWORKS FOR FERRITES IN WAVEGUIDES		
CIRCUIT	MODE TYPES FOR WHICH CIRCUIT IS VALID	CIRCUIT CONSTANTS
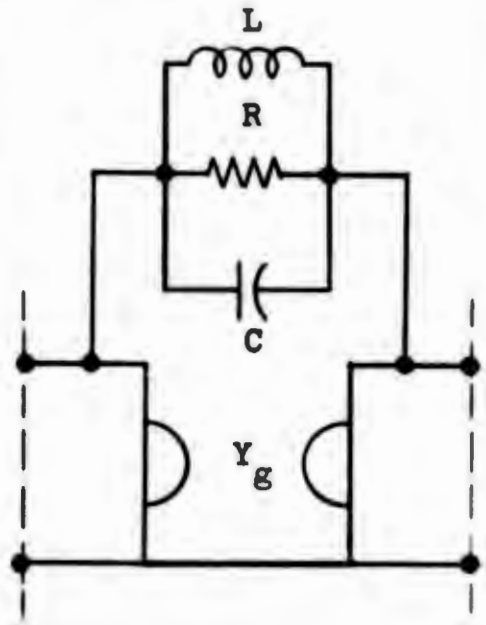	TEM TM TE (provided $h_x \neq 0$)	$\omega_0^2 = \frac{1}{LC} = (\omega_H + N_x\omega_M)(\omega_H + N_y\omega_M)$ $Q_f = \omega_0 RC = \frac{\omega_0^2}{\mu_0 \gamma \Delta H} \frac{1}{\omega_H + \frac{\omega_M}{2}(N_x + N_y)}$ $\frac{R}{Z_1 Q_f} = \frac{\beta_1 h_x^2 V_s \omega_M}{\omega_H + N_x\omega_M}$ $\frac{Y_g}{Y_1} = -\frac{\omega}{\omega_H + N_y\omega_M} \frac{\lvert h_y \rvert}{h_x}$
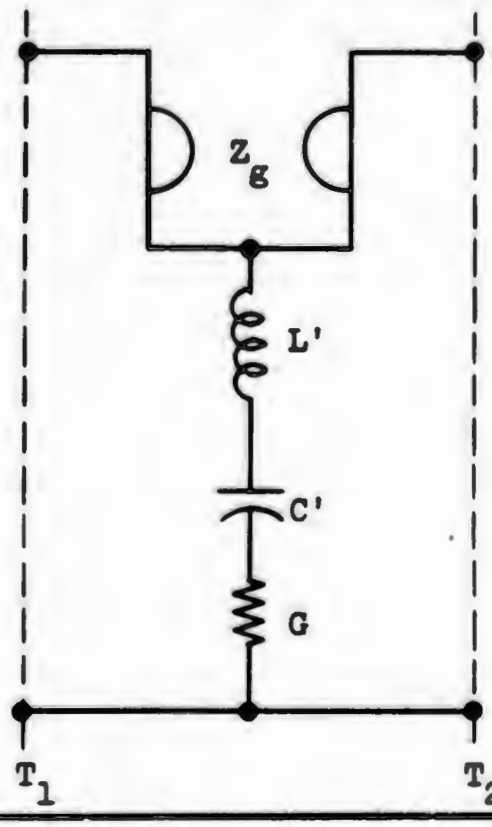	TE (provided $h_y \neq 0$)	$\omega_0^2 = \frac{1}{L'C'} = (\omega_H + N_x\omega_M)(\omega_H + N_y\omega_M)$ $Q_f = \omega_0 GL' = \frac{\omega_0^2}{\mu_0 \gamma \Delta H} \frac{1}{\omega_H + \frac{\omega_M}{2}(N_x + N_y)}$ $\frac{G}{Y_1 Q_f} = \beta_1 \lvert h_y \rvert^2 \frac{V_s \omega_M}{\omega_H + N_y\omega_M}$ $\frac{Z_g}{Z_1} = \frac{\omega}{\omega_H + N_x\omega_M} \frac{h_x}{\lvert h_y \rvert}$

frequency range, by means of the simple circuit of Fig. 2.8. In this circuit R_c accounts for the internal losses of the microwave cavity, while R accounts for the internal losses of the ferrite. The ratio R to R_c, which we shall denote by β_c, then determines the coupling between the ferrite and the cavity. Once this ratio has been found, the representation, as far as the ferrite is concerned, is essentially complete. From elementary circuit theory, we know that

$$\beta_c \equiv \frac{R}{R_c} = \frac{Q_0}{Q_f}\frac{W_f}{W_c} \quad , \tag{2.26}$$

where Q_0/Q_f is the ratio of the unloaded Q of the cavity to that of the ferrite, and W_f/W_c is the ratio of the steady-state energy stored in the ferrite to that in the cavity, assuming that both are at resonance.

The ratio W_f/W_c may be determined by the usual cavity "perturbation" theory approach, where it is assumed that the sample is sufficiently small, electrically speaking, and that the microwave fields can be assumed to have the same distribution as in the empty cavity.[3,38] To make the problem definite, we suppose that the rf magnetic field in the cavity at the sample position is in the x-direction, which is also assumed to be a principal axis of the ellipsoidal sample, and has a peak amplitude h_s. In terms of a filling factor, F, defined as

$$F \equiv \frac{h_s^2 V_s}{\int_{V_c} |h(x,y,z)|^2 dV_c} \quad , \tag{2.27}$$

where $|h(x,y,z)|$ is the peak amplitude of the rf magnetic field at the point x,y,z within a cavity of volume V_c, the energy stored in the cavity at resonance is $1/2\mu_0(h_s^2 V_s/F)$. The energy stored in the ferrite at resonance is $\omega_0\mu_0 V_s|\chi_{11}|_{res} h_s^2/4(\eta_0 + \eta_0')$, so that the coupling coefficient is given simply by

$$\beta_c = FQ_0|\chi_{11}|_{res} \quad . \tag{2.28}$$

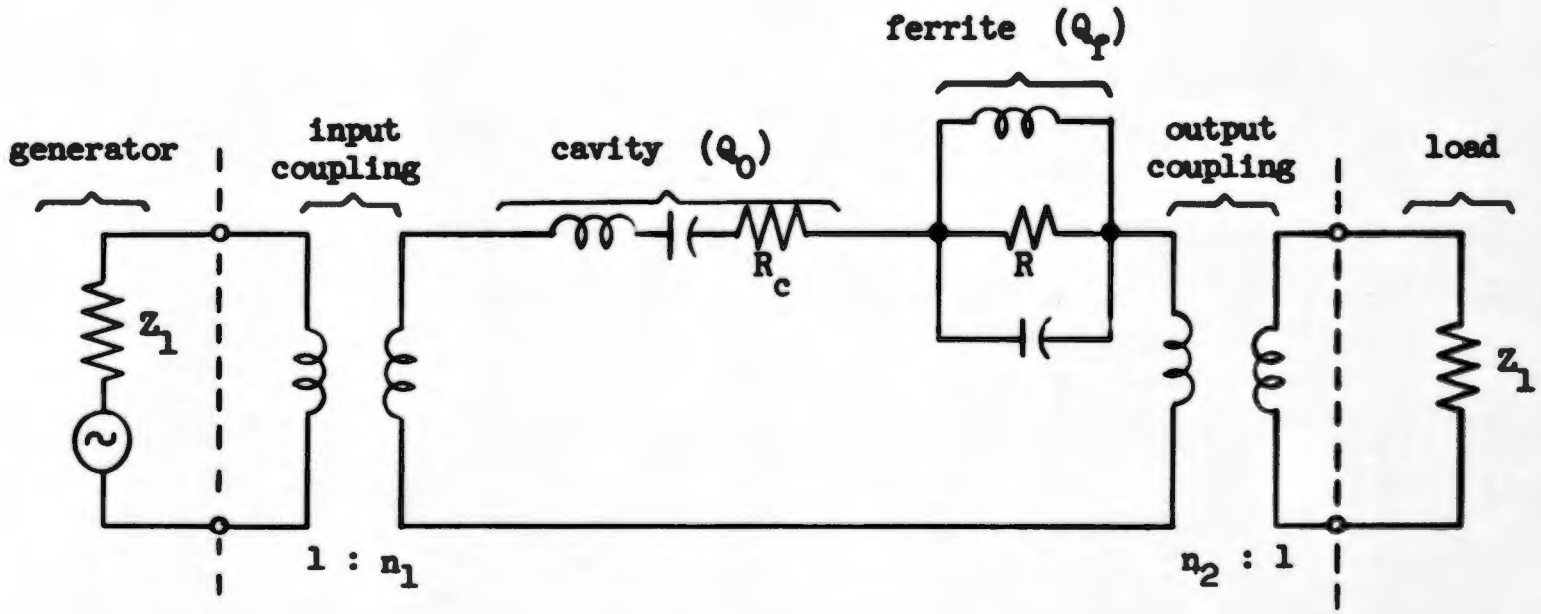

FIG. 2.8--Equivalent circuit for a ferrite ellipsoid in a cavity resonant in a single mode.

BLANK PAGE

If we insert the explicit form[1] for $|\chi_{11}|_{res}$, this becomes

$$\beta_c = \frac{FQ_0\omega_M K}{2(\eta_0 + \eta_0')} \quad , \tag{2.29}$$

where $K^2 \equiv (\omega_H + N_y\omega_M)/(\omega_H + N_y\omega_M)$ is a form-factor, depending on frequency and the shape of the sample. For ellipsoids of revolution about the direction of the dc field (z-direction), K is unity, since then $N_x = N_y$.

A special case of the preceding result, important for the relaxation measurements to be discussed in Part III, is that of a low-loss sample placed in a lossless reflection cavity of low external Q, and resonant at the operating frequency. In a suitably restricted frequency range near ferrimagnetic resonance, the cavity then acts simply as an impedance transformer whose turns ratio depends on the geometry of the cavity and the coupling between cavity and waveguide. The simple circuit of Fig. 2.9 then applies.

One of the questions that naturally arises is how the results obtained in this section are related to those obtained, by much more formal arguments, in the preceding sections. Since the two approaches are based on the same assumptions of dominant-mode interaction and conservation of energy, they must be equivalent. To show this, we may consider a special case to which both techniques are applicable, to wit, a sample placed an integral number of lengths from the end of a short-circuited waveguide. The representation of Table III then reduces to a simple shunt resonant circuit having a resonant impedance of

$$\frac{R}{Z_1} = \frac{\beta_1 V_s \omega_M K}{2(\eta_0 + \eta_0')} \quad . \tag{2.30}$$

To apply the results of the present section to this problem, we may rewrite Eq. (2.29) in terms of the loaded Q of the cavity, obtaining

$$\frac{R}{Z_1} = \frac{F\eta_1^2 Q_L \omega_M K}{2(\eta_0 + \eta_0')} \quad , \tag{2.31}$$

---

[1] See Appendix A.

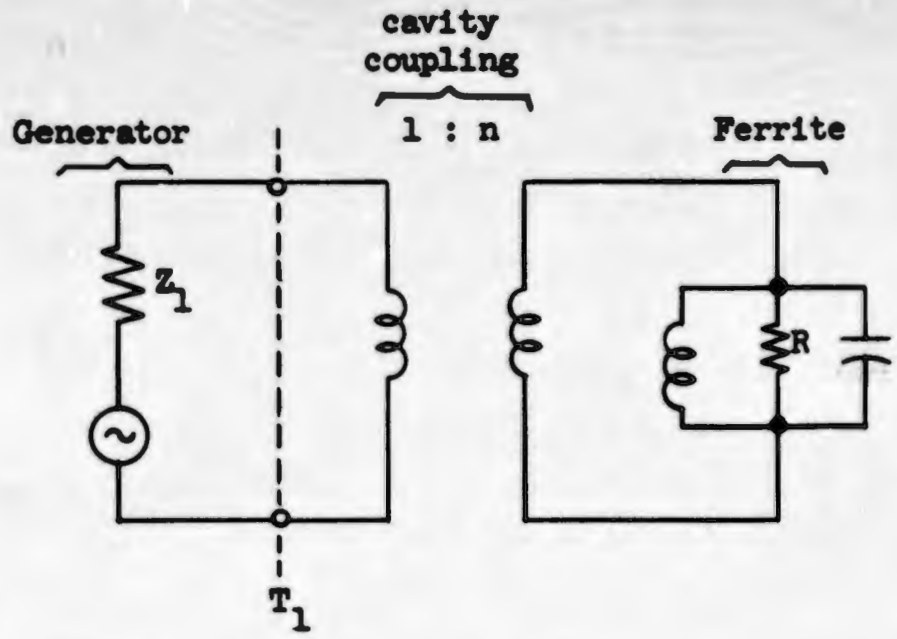

FIG. 2.9--Equivalent circuit for a ferrite sample in a resonant cavity having a low external Q .

where we have assumed a reflection cavity with an input transformer turns ratio of n_1 . A shorted section of lossless waveguide may be looked on as forming such a cavity, with a loaded Q per unit length of $\pi\lambda_t/\lambda_0^2$, and a transformer ratio of unity. The filling factor, per unit length, for this "cavity" is $2(\lambda_0/\lambda_t)^2 V_s h_x^2$, where h_x is the x-component of the field eigenvector defined in Chapter IV, so that Eq. (2.31) does in fact reduce to Eq. (2.30).

We have thus shown that for the case of a linearly polarized driving field, the results of Chapter VII are identical to those obtained by an intuitive application of the usual perturbation theory arguments. The advantage of the more formal procedure lies in its applicability to cases where the driving field is arbitrarily polarized, so that the non-reciprocal properties of the medium are important.

CHAPTER IX

RADIATION DAMPING

If a ferrite sample in which the uniform precession has been excited to some finite amplitude is placed in an initially unexcited microwave circuit, the amplitude of the mode will decay, even in the absence of

internal losses, as energy is dissipated in the circuit, a process which we may describe as "radiation damping."[39-41] In analogy with the ferrite relaxation parameters defined in Part I, under suitable circumstances we may define a radiation damping rate, η_R, or a radiation damping time constant $\tau_R = 1/\eta_R$ such that the amplitude $|b_0|$ of the uniform mode decays at the rate $\eta_R|b_0|$. An alternative way of characterizing the radiation damping is by means of a coupling coefficient β, defined as the ratio of the power dissipated in the microwave circuitry to that dissipated in the sample, in a free decay of the uniform mode. Since the power dissipated in the sample is proportional to $2(\eta_0 + \eta_0')\ |b_0|^2$ [Eq. (1.11)], the coupling coefficient and the radiation damping rate are related by[(1)]

$$\beta = \frac{\eta_R}{\eta_0 + \eta_0'} \quad . \tag{2.32}$$

A. RADIATION DAMPING IN WAVEGUIDES

The coupling coefficient for a ferrite sample placed in an arbitrarily terminated section of uniform waveguide may be determined with the help of the equivalent circuits given in Table III. If arbitrary impedances Z_L and Z_R are placed at reference planes T_1 and T_2, respectively, these circuits reduce to those shown in Fig. 2.10. The radiation damping is then determined by the complex free-oscillation frequencies of these circuits. The damping admittance of Fig. 2.10a, or damping impedance of Fig. 2.10b may be separated into a real and imaginary part. If the imaginary part is free of resonance behavior, remaining essentially constant over a frequency range comparable to the bandwidth of the ferrite, the free oscillation of the system will be a simple damped sinusoid. Otherwise, the free oscillation will be complicated, involving a periodic interchange of energy between the ferrite and the microwave circuit which cannot be characterized by a single radiation damping rate. In practice, then, the concept of radiation damping, as applied to a freely decaying system, is a useful one only when the energy stored in the ferrite is at every instant

---

(1) A third way of characterizing the radiation damping is by means of an external Q, defined as $Q_{ext} = Q_f/\beta$, where Q_f is the unloaded Q of the ferrite. In terms of the damping rate η_R, we find $Q_{ext} = \omega_0/2\eta_R$.

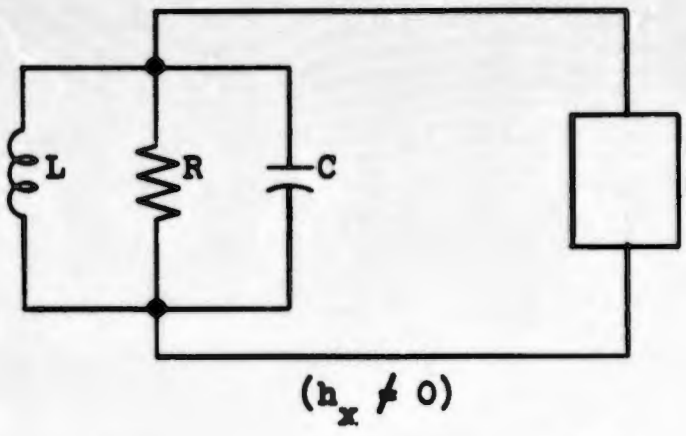

$(h_x \neq 0)$

(a)

$$Y_D = \frac{1 + Z_L Z_R Y_g^2}{Z_L + Z_R} \approx G_D + jB_D$$

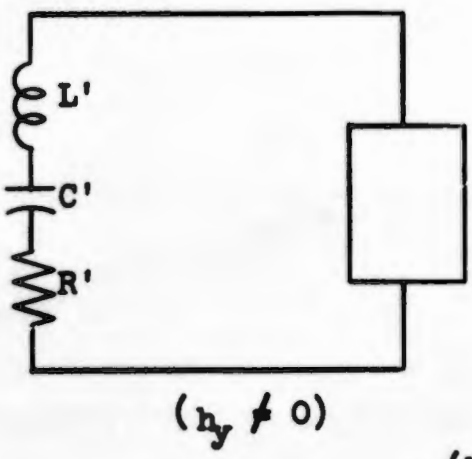

$(h_y \neq 0)$

(b)

$$Z_D' = \frac{Z_g^2 + Z_L Z_R}{Z_L + Z_R} = R_D' + jX_D'$$

FIG. 2.10--Circuits for the calculation of radiation damping.

during the decay much greater than that stored in the remainder of the microwave circuit. When this condition is met, the coupling coefficient for the circuit of Fig. 2.10a is given simply by

$$\beta = RG_D \quad , \tag{2.33}$$

while for that of Fig. 2.10b it is

$$\beta = \frac{R'_D}{R'} \quad . \tag{2.34}$$

In terms of the ferrite and microwave circuit parameters we obtain, from Eq. (2.33) or Eq. (2.34),

$$\eta_R = (\eta_0 + \eta'_0)\beta = \mathrm{Re}\left[\frac{1 + \frac{Z_L}{Z_1}\frac{Z_R}{Z_1}\left(\frac{|h_y|}{Kh_x}\right)^2}{\frac{Z_L}{Z_1} + \frac{Z_R}{Z_1}}\right]\beta_1 \frac{Kh_x^2 V_s \omega_M}{2} \quad , \tag{2.35}$$

where $K^2 = (\omega_H + N_y\omega_M)/(\omega_H + N_x\omega_M)$ is the form-factor introduced in Chapter VIII.

Two special cases of Eq. (2.35) are of particular importance:

(a) $Z_R = 0$, $Z_L = Z_1$, or equivalently, $Z_R = Z_1$, $Z_L = 0$. These terminating impedances occur when the sample is placed in a short-circuited waveguide, in the electrical plane of the short circuit, with the other end of the guide matched. For this case we obtain

$$\eta_R = \frac{\beta_1 Kh_x^2 V_s \omega_M}{2} \quad . \tag{2.36}$$

(b) $Z_R = Z_L = Z_1$. In this case the waveguide is reflectionlessly terminated at both ends, and we obtain

$$\eta_R = \left[1 + \left(\frac{|h_y|}{Kh_x}\right)^2\right]\frac{\beta_1 Kh_x^2 V_s \omega_M}{4} \quad . \tag{2.37}$$

For a transmission line propagating only a TEM mode, the radiation damping produced in case (b) is just half that produced in case (a). In more complicated structures this need no longer be true.

B. RADIATION DAMPING IN RESONANT CAVITIES

From the discussion given at the beginning of this chapter, it is evident that the concept of radiation damping can be applied to ferrites in resonant cavities only when the loaded Q of the empty cavity is much less than the unloaded Q of the ferrite. In such a case the radiation damping rate may be determined from Eq. (2.35) upon introduction of suitable values for the terminating impedances. Such a procedure is unnecessarily complicated, however, and it is simpler to use the results of Chapter VIII.

For a free decay of the system, the equivalent circuit of Fig. 2.8 reduces that shown in Fig. 2.11. The total coupling coefficient, β, as defined earlier, is then

$$\beta = \frac{R}{R_C + (\eta_1^2 + \eta_2^2)Z_1} = \frac{\beta_c Q_L}{Q_0} ,$$

so that from Eq. (2.29) we obtain

$$\beta = \frac{FQ_L\omega_M K}{2(\eta_0 + \eta_0')} , \tag{2.38}$$

or

$$\eta_R = \frac{FQ_L\omega_M K}{2} . \tag{2.39}$$

Once again we should stress the fact that Eq. (2.39), first derived in a different context by Bloembergen and Pound,[39] is valid <u>only</u> when $Q_L \ll Q_f$. When this inequality does not hold, the complete circuit of Fig. 2.8 must be analyzed as a coupled resonant system with two degrees of freedom.

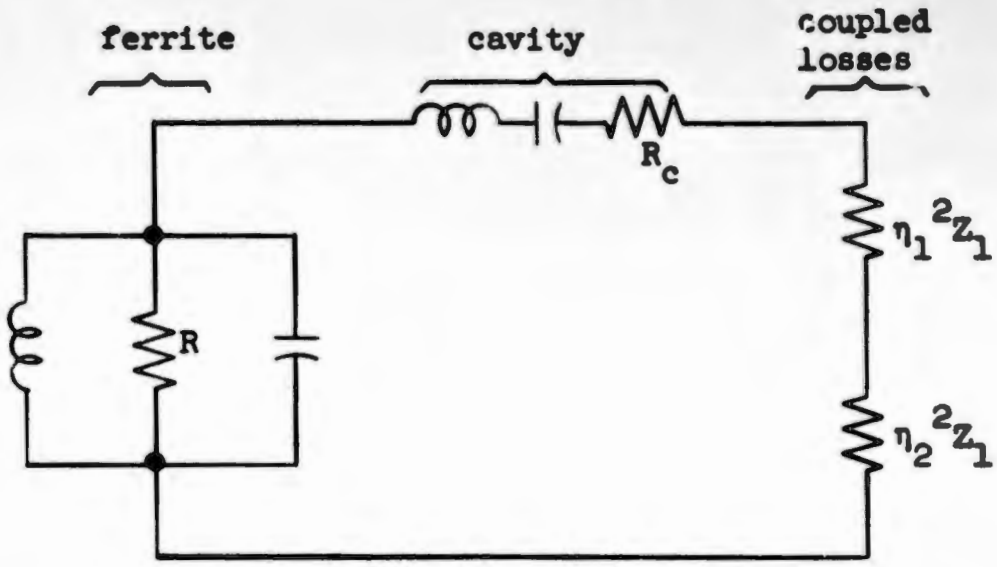

FIG. 2.11--Circuit for determining radiation damping of a ferrite ellipsoid by a low-Q microwave cavity.

CHAPTER X

EXPERIMENTAL VERIFICATION OF THE THEORY

Although no systematic attempt has been made to verify experimentally all aspects of the theory presented in the preceding sections, most of the important predictions have been experimentally established. The measurements were all made at X-band on polished single crystal spheres of yttrium iron garnet ($M_s = 1.40 \times 10^5$ amps/m) placed in rectangular waveguide.

The spin mode theory of ferrimagnetic resonance predicts that the cumulative back-reaction of the spin modes on the uniform precession takes the form of an addition to the loss parameter of the uniform mode, leading directly to a Lorentzian-shaped resonance line and a lumped-element electrical circuit representation whose basic element is a single tuned circuit. Such a representation seems so natural that one tends to forget that it is a consequence of some rather restrictive assumptions concerning the nature of the spin system, and so subject to experimental verification.

In the course of our experiments, the shapes of several lines were examined in detail, and found, in fact, to be Lorentzian. Such a procedure is subject to many experimental uncertainties, however, and a rather more convincing demonstration was afforded by measuring the input impedance of a shorted section of waveguide containing the sample, as a function of the dc field. The data, plotted in Fig. 2.12, are seen to define an almost perfect "Q-circle," appreciable deviations occurring only for very large VSWR's, where the finite loss of the microwave circuitry becomes apparent. Shown in Fig. 2.13 is a frequency scale for Fig. 2.12, constructed according to the procedure described in Ginzton.[35] The excellent linearity is evident. Figures 2.12 and 2.13, taken together, demonstrate unequivocally the validity of the representation of the interaction between the uniform mode and the microwave fields in terms of a simple tuned circuit. With this fundamental assumption established, the remaining experiments were undertaken to verify certain predictions about the coupling between the ferrite resonator and various microwave circuits.

A. VARIATION OF REFLECTION COEFFICIENT WITH POSITION

In Figs. 2.14 and 2.15 are shown the results of measurement of the reflection coefficient of a YIG sphere in rectangular waveguide as a function of the position of the sample. The data of Fig. 2.14 were obtained by placing the sample in a reflectionlessly terminated waveguide, and measuring the reflection coefficient at resonance as a function of the transverse position of the sample, The data of Fig. 2.15 were obtained in a short-circuited section of waveguide by measuring the power absorbed at resonance by a sample placed in the center of the waveguide cross-section, as a function of the distance of the sample from the shorting plane. Appreciable deviation from the theory is seen to occur only when the sample is within two or three diameters of the waveguide wall. This "wall effect"[42-44] will be discussed in Chapter XI.

B. VARIATION OF COUPLING WITH WAVEGUIDE CROSS-SECTIONAL AREA

To investigate the dependence of the coupling on the cross-sectional area of the waveguide, a shorted waveguide section containing a step $2\lambda_t$ long and of variable height, shown in longitudinal cross-section in

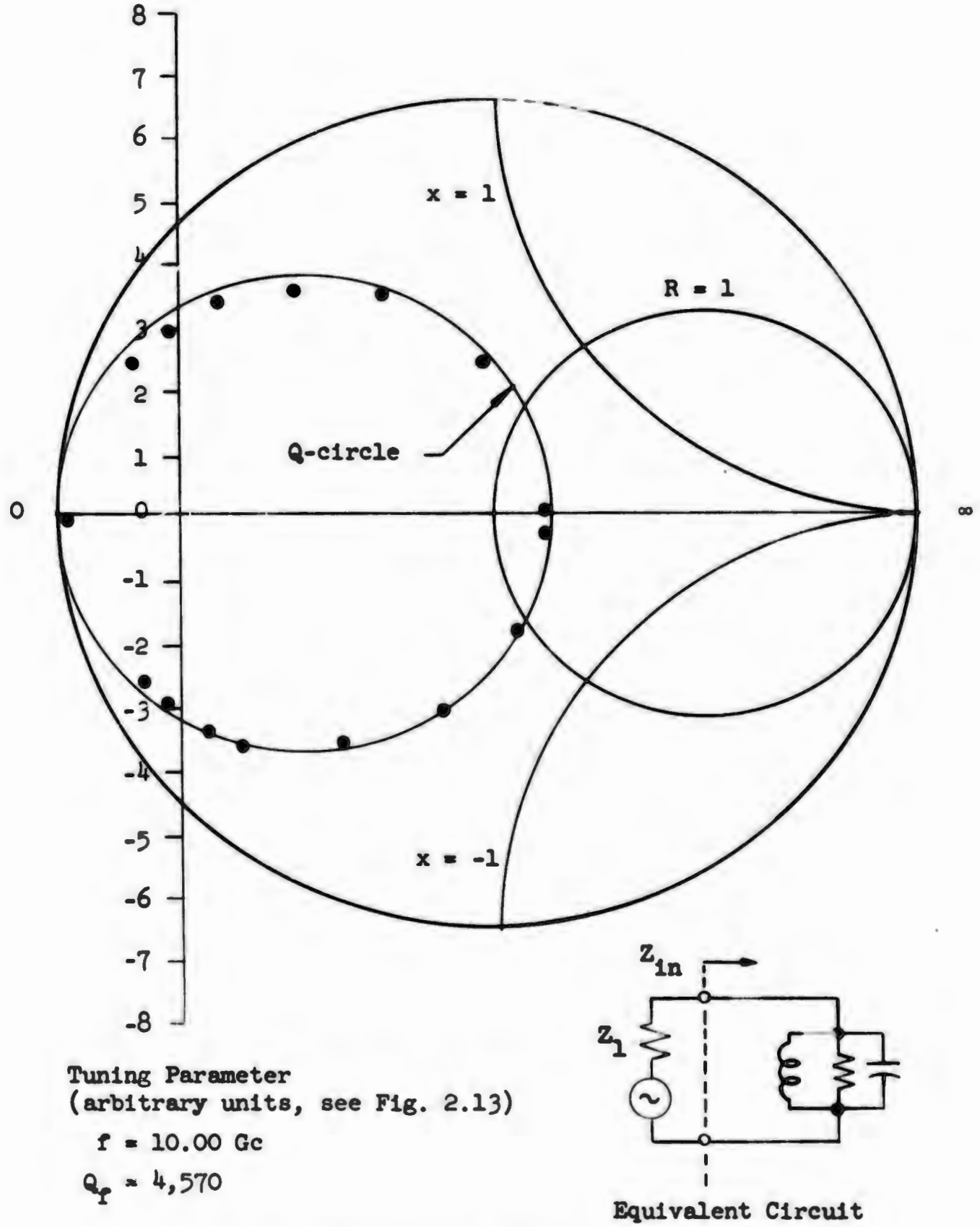

FIG. 2.12--Impedance of ferrite sphere in a shorted waveguide as a function of the dc field.

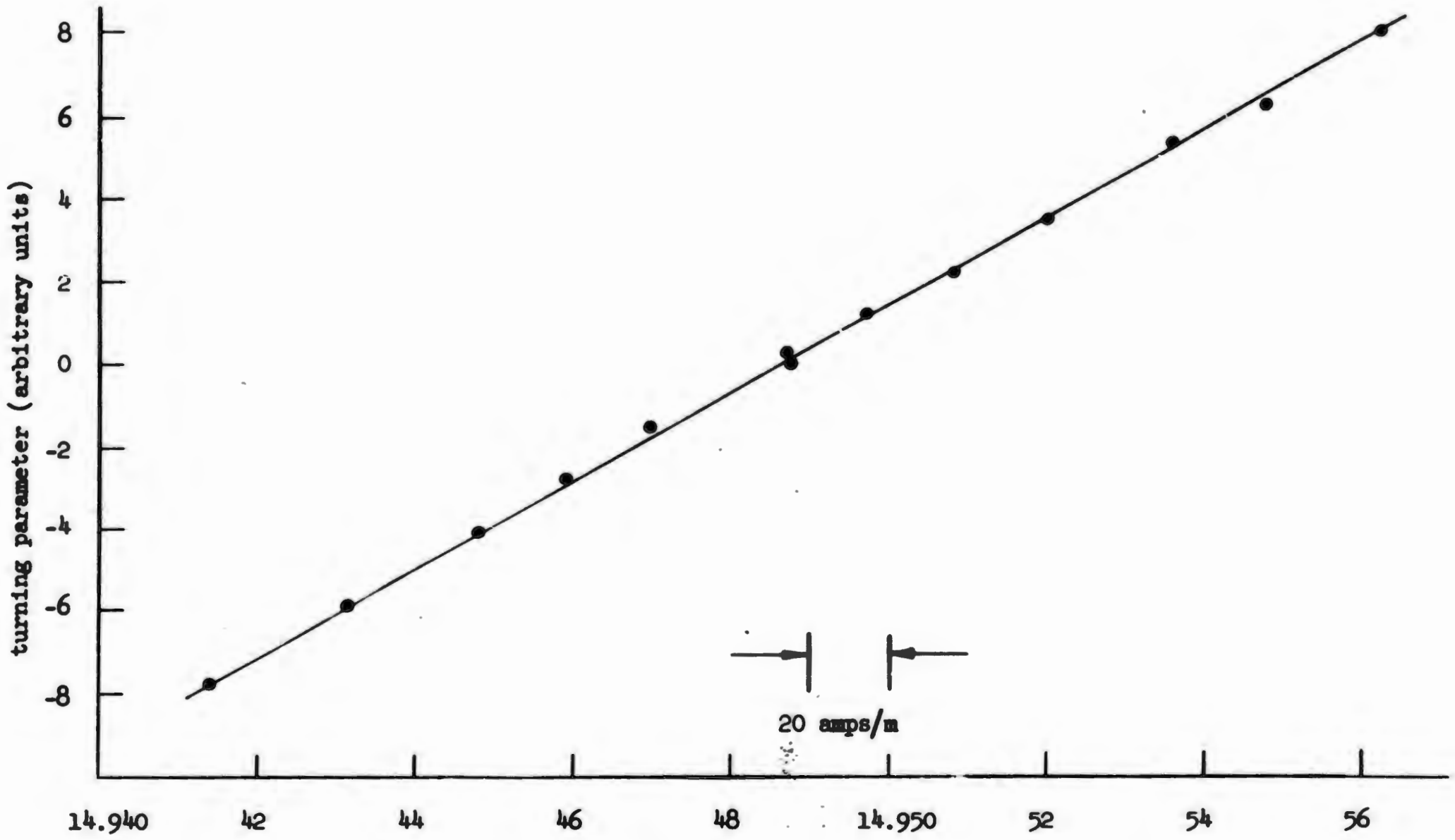

FIG. 2.13--Field calibration for Fig. 2.12.

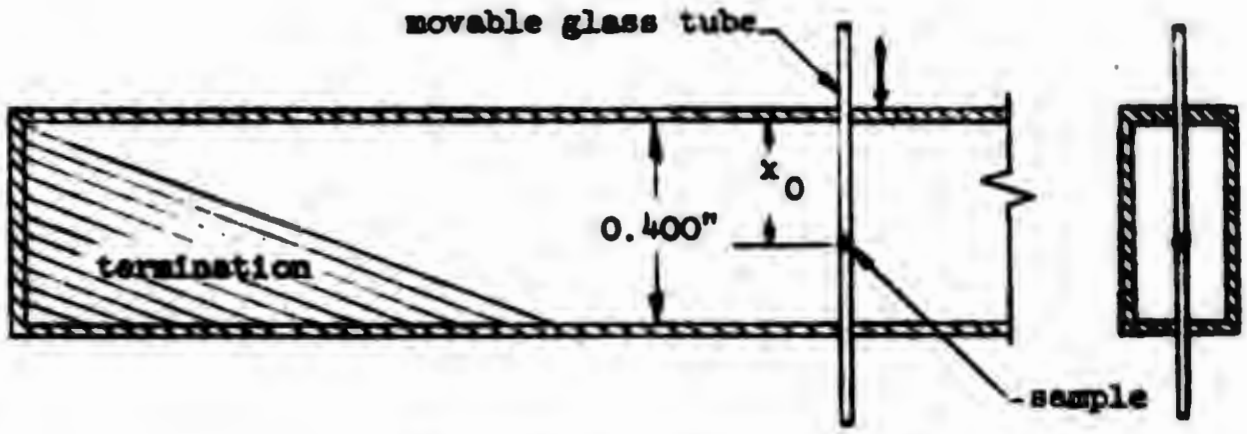

(a) Experimental Configuration

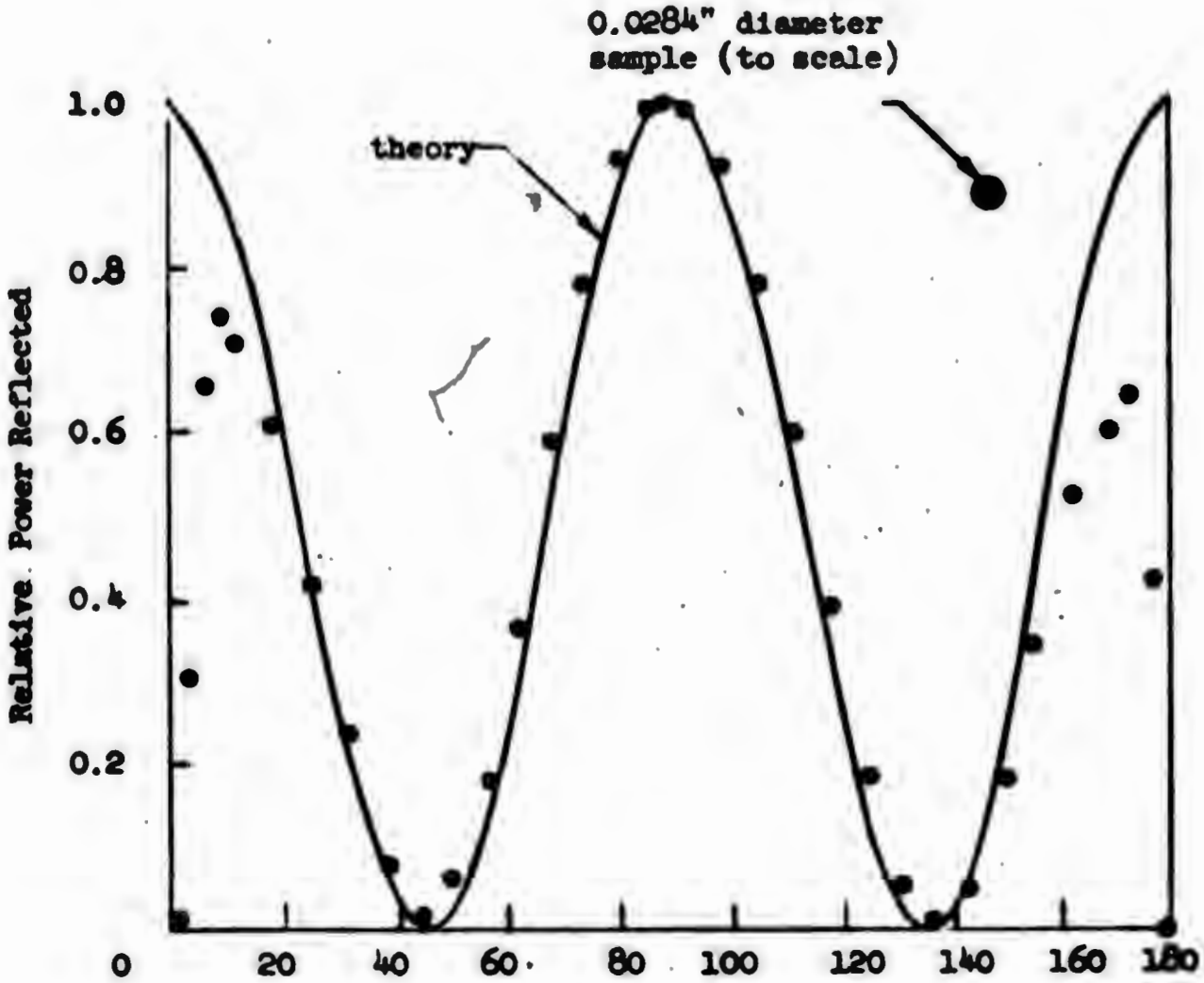

(b) Results

FIG. 2.14--Measurement of power reflected from a ferrite sphere in a terminated waveguide as a function of cross-sectional position.

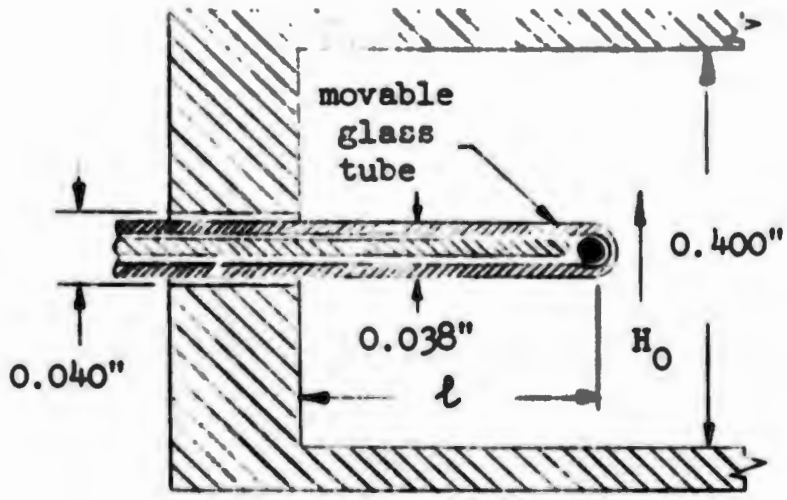

(a) Experimental Configuration

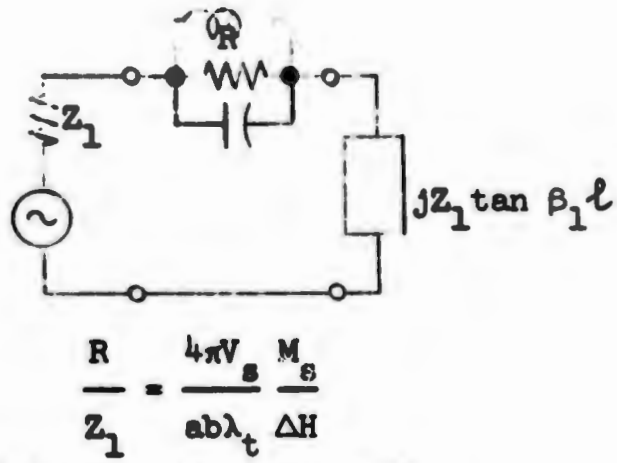

(b) Equivalent Circuit

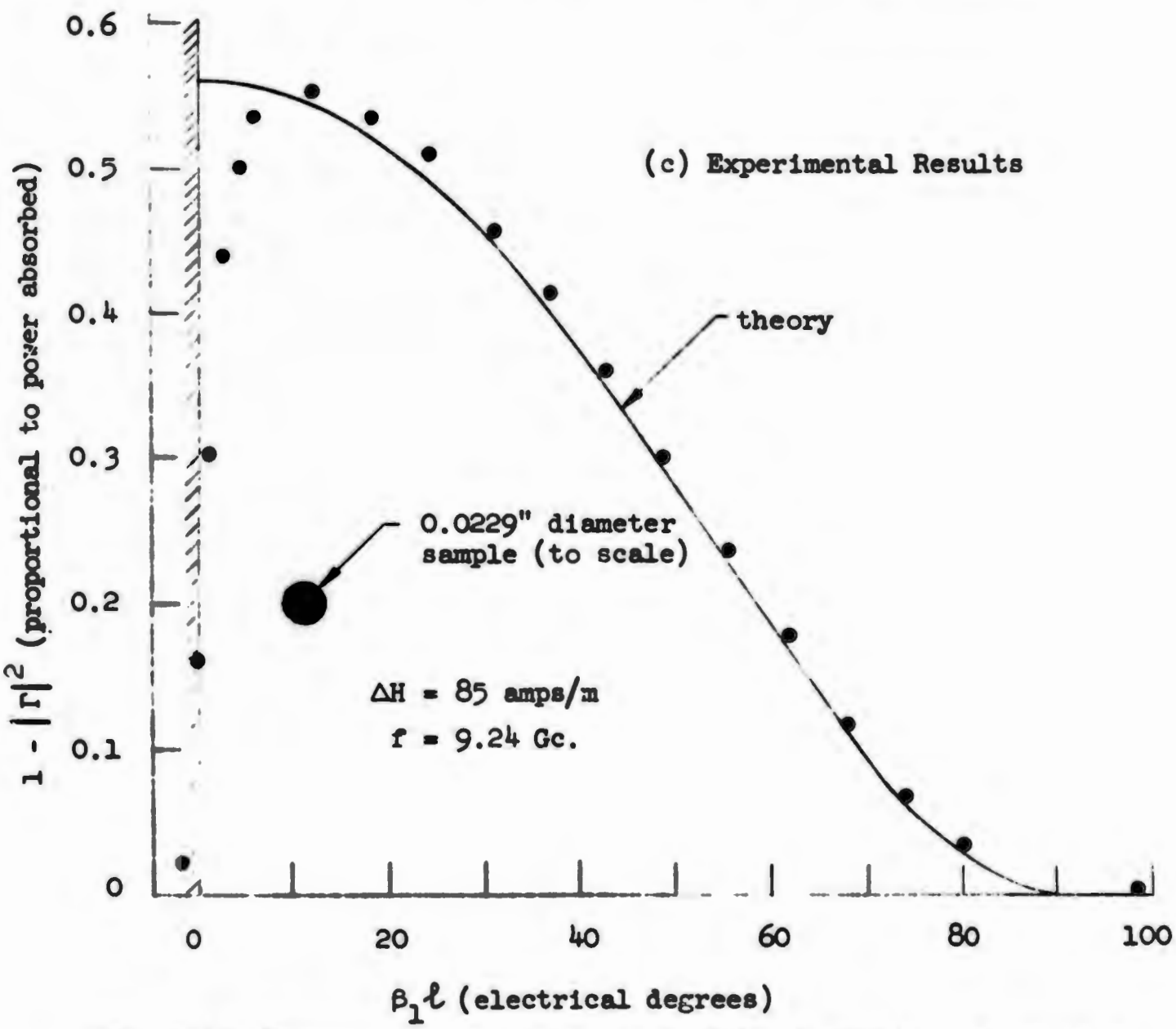

(c) Experimental Results

FIG. 2.15--Measurement of power absorbed by a ferrite sphere in a shorted waveguide as a function of the longitudinal position.

Fig. 2.16a, was constructed. By varying the height of the step, the coupling to the sample, which was located in the center of the variable section, could be changed. If the discontinuity capacitance at the step is not too large, the equivalent circuit of Fig. 2.16b is valid. This circuit predicts that the reflection coefficient at ferrimagnetic resonance of the overall configuration will be independent of the height of the step. The measured reflection coefficient, together with a value calculated from the material parameters, is shown in Fig. 2.16c. The square of the reflection coefficient is seen to vary by less than 6% over a 5:1 range in waveguide height. The fact that the measured values are almost 10% higher than calculated may be partly due to uncertainty in the sample parameters, particularly the volume of the sample, and partly due to a real increase in coupling produced by the polystyrene tube, about 0.075" in diameter, in which the sample was mounted.

C. VARIATION OF COUPLING WITH FREQUENCY

Variation of coupling with frequency was investigated for a spherical sample in a short-circuited rectangular waveguide. The sample, 0.90 mm in diameter, was supported in a polyfoam plug with its center about 2 mm from the end wall of the waveguide. For this configuration, the quantity $\beta\Delta H\lambda_t$ should be a constant, independent of frequency. These quantities were determined separately by impedance measurements, as discussed in Appendix B, for the frequency range 8 to 11 Gc. The computed product, together with the theoretical value, is shown in Fig. 2.17c. Although there is a slight tendency for the observed coupling to increase rather more slowly with increasing frequency than the theory predicts, as evidenced by a slight decrease in the quantity $\beta\Delta H\lambda_t$, the deviation of this product from the predicted constant value is actually never more than the uncertainties in the experimental values and the sample parameters would allow.

It should be pointed out that the sample used in this measurement was electrically large enough to be anything but a small perturbation in the waveguide. In fact, at a frequency of about 8.4 Gc, the sample was "critically coupled" to the waveguide, i.e., it absorbed all of the power incident upon it. That a simple theory should be able to account correctly for so large a discontinuity produced by so small an object seems rather remarkable.

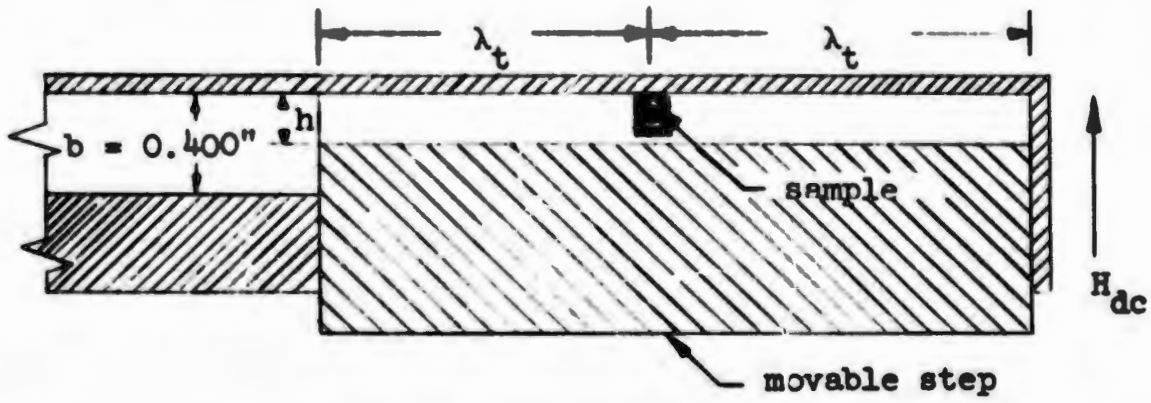

(a) Experimental Configuration

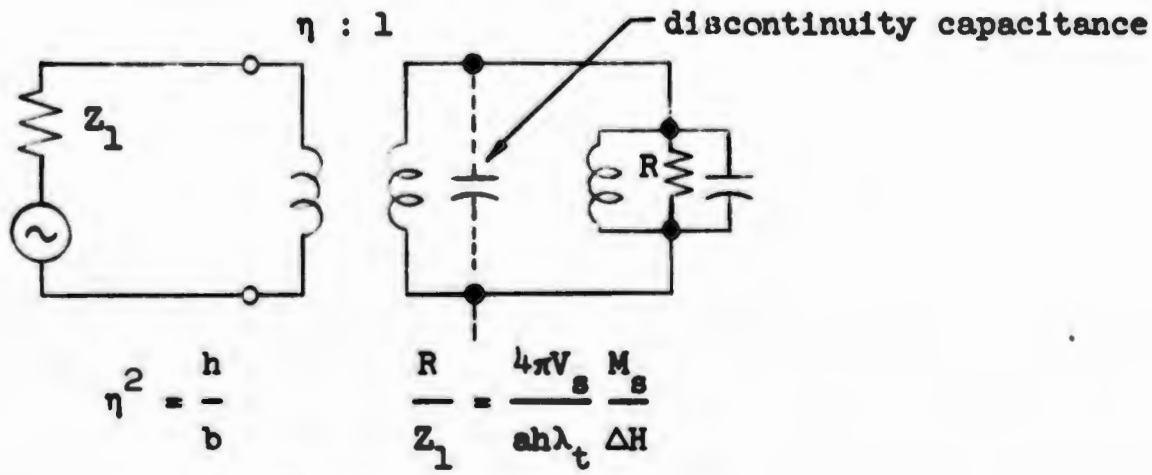

(b) Equivalent Circuit

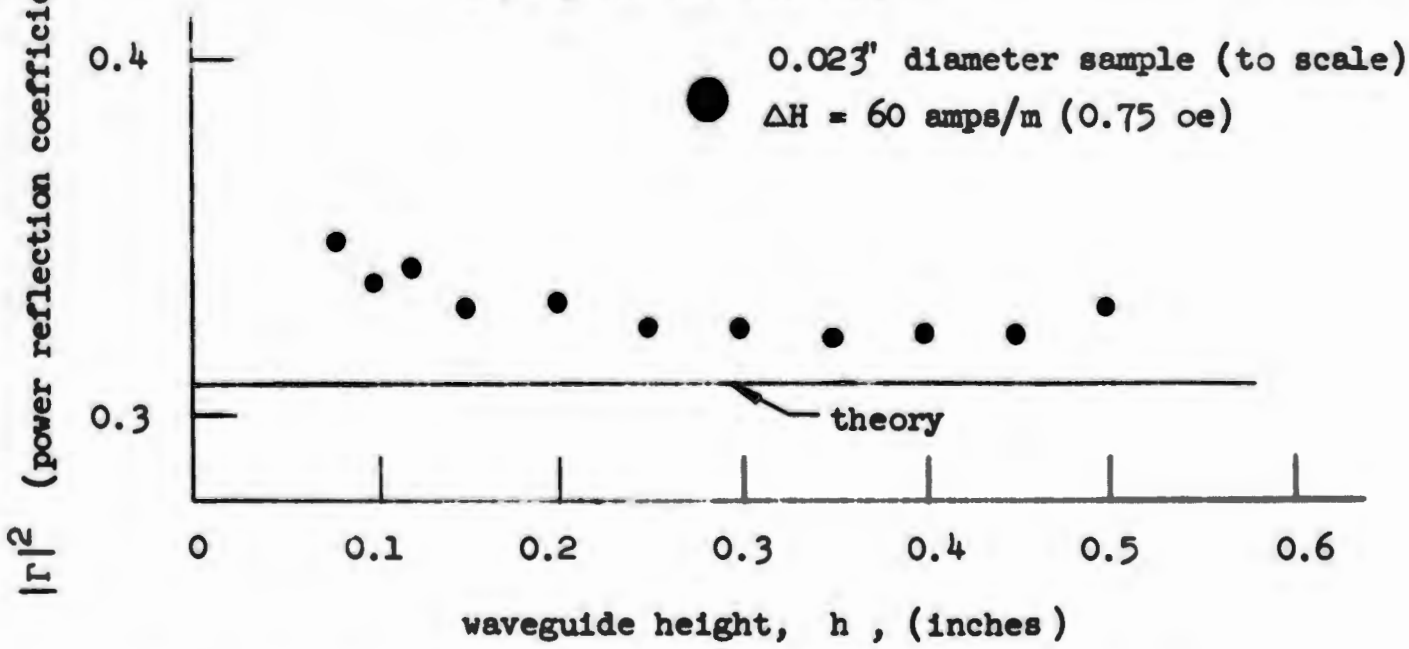

(c) Experimental Results

FIG. 2.16--Measurement of the reflection coefficient of a stepped waveguide containing a ferrite sphere.

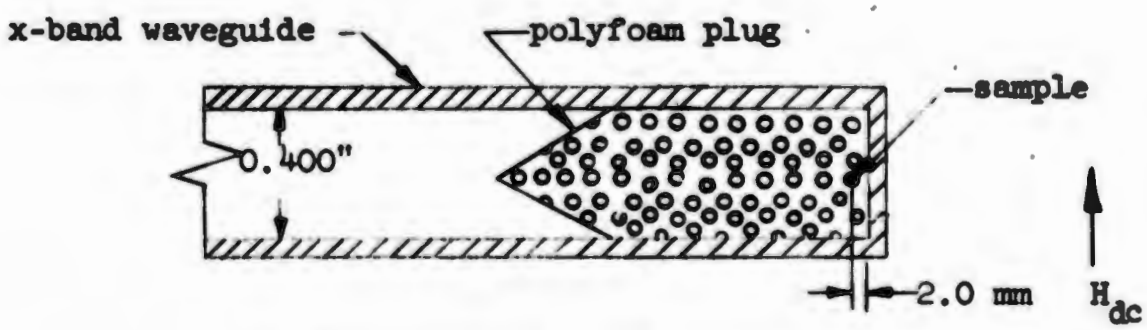

(a) Experimental Configuration

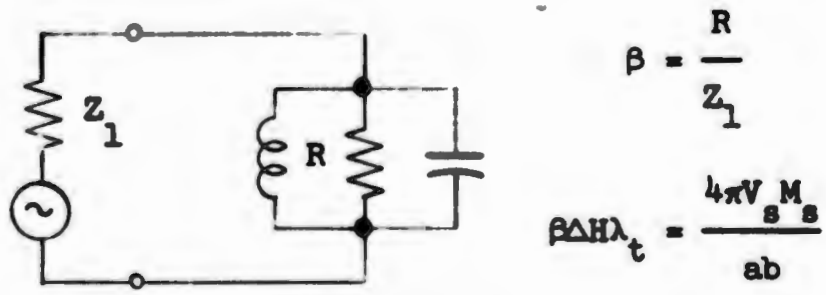

(b) Equivalent Circuit

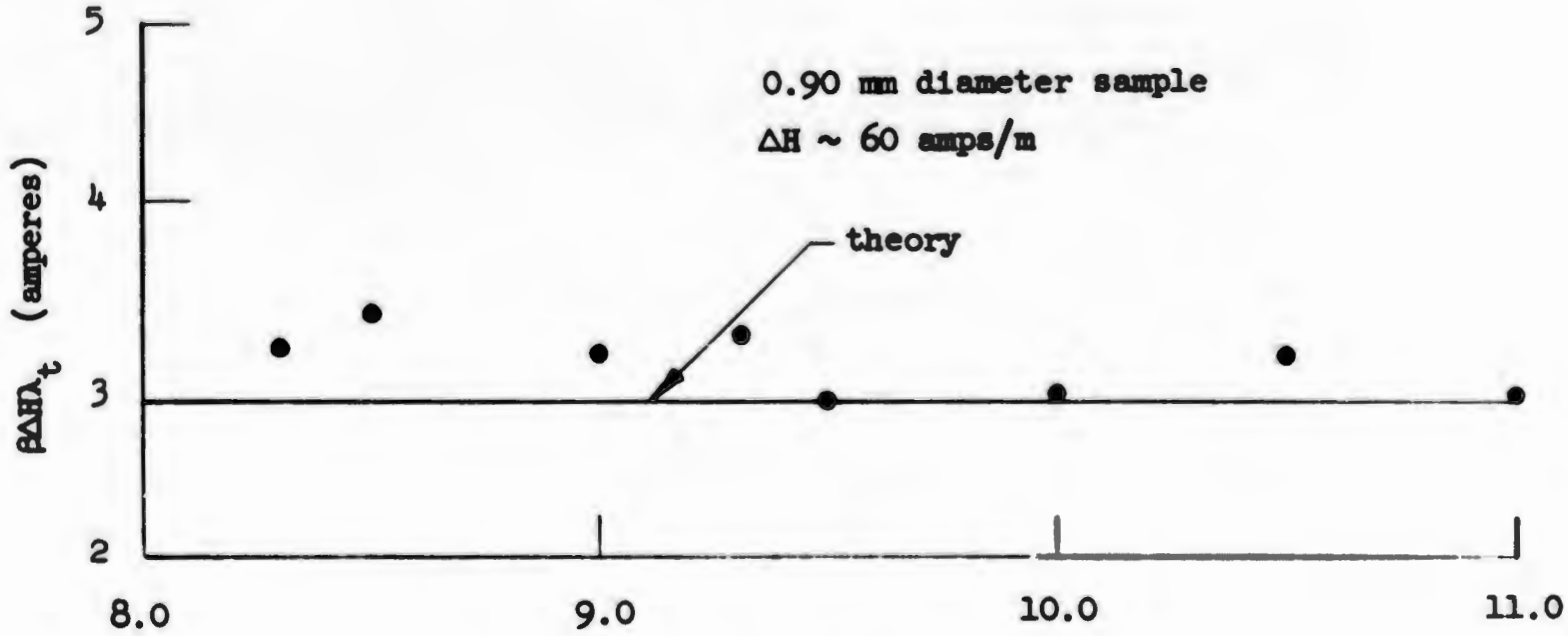

(c) Experimental Results

FIG. 2.17--Measurement of coupling between a ferrite sphere and rectangular waveguide as a function of frequency.

D. RADIATION DAMPING IN A RESONANT CAVITY

Measurements were made of the coupling between a YIG sphere 0.58 mm in diameter with a linewidth of 85 amps/m and a rectangular cavity, resonant in the $TE_{1,0,2}$ mode and iris coupled to rectangular X-band waveguide. The sample was placed in the center of the cavity. For this configuration the circuit of Fig. 2.9 applies, with a turns ratio given by $n^2 = (Q_{ext}/\pi)(\lambda_0/\lambda_t)^2$, with Q_{ext} being the external Q of the empty cavity. With a measured value for Q_{ext} of 163, the impedance transformation ratio, n^2, is then 26.0 at a frequency of 9.3 Gc. The coupling coefficient, obtained from impedance measurements at the reference plane T_1 of Fig. 2.9 was 5.35. The coupling coefficient for this same sample placed in a shorted waveguide was also measured, and found to be 0.206, or a factor of 26 less than that obtained in the cavity. For a shorted waveguide, the transformation ratio, n^2, is unity, so that this result is just what the theory predicts.

CHAPTER XI

WALL EFFECTS

From the experimental results discussed in the preceding section, it is evident that the simple representations we have discussed are no longer valid if the sample is placed too close to a conducting wall of the waveguide. Experimentally, it is found that as the distance between sample and wall is decreased, the resonance shifts in frequency, the line broadens, and the line shape becomes distorted. Because in our relaxation experiments it was necessary to put the sample rather close to the waveguide wall, in order to provide access to a loop placed about the sample, these effects were investigated in some detail.

A. EXPERIMENTAL INVESTIGATION

Experiments were carried out on a spherical sample placed in a shorted rectangular waveguide, one wavelength from the shorted end, as shown, together with an equivalent circuit for the configuration, in Fig. 2.18. Provision was made for moving the sample across the narrow dimension of the waveguide, without allowing it to turn, so that its orientation remained fixed. The dc field required for resonance, the linewidth, and the coupling coefficient were then measured as a function of d, the

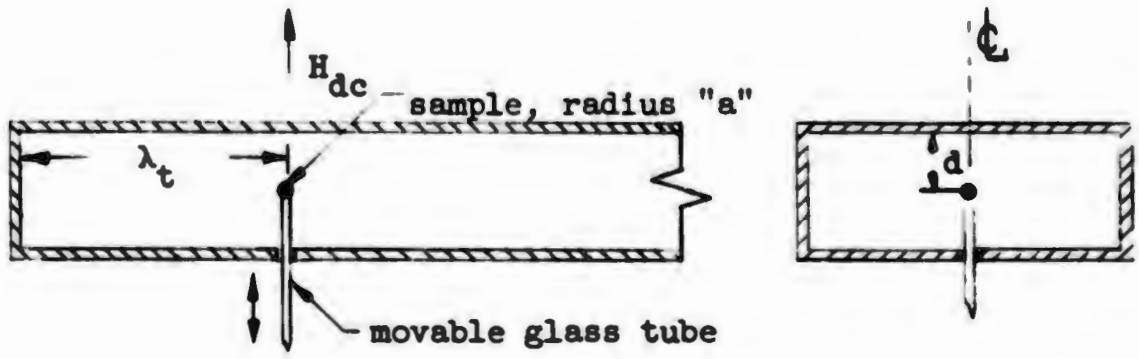

(a) Experimental Configuration

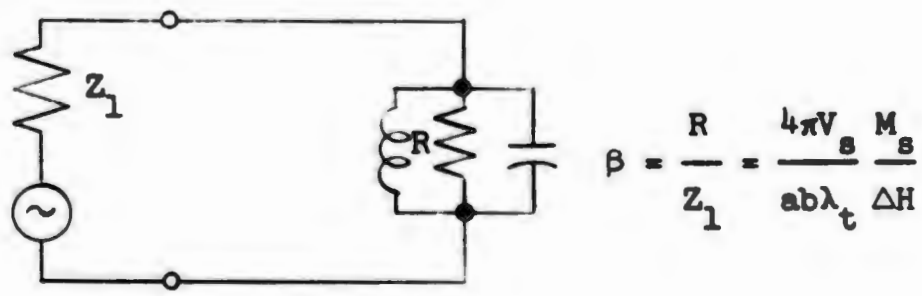

(b) Equivalent Circuit

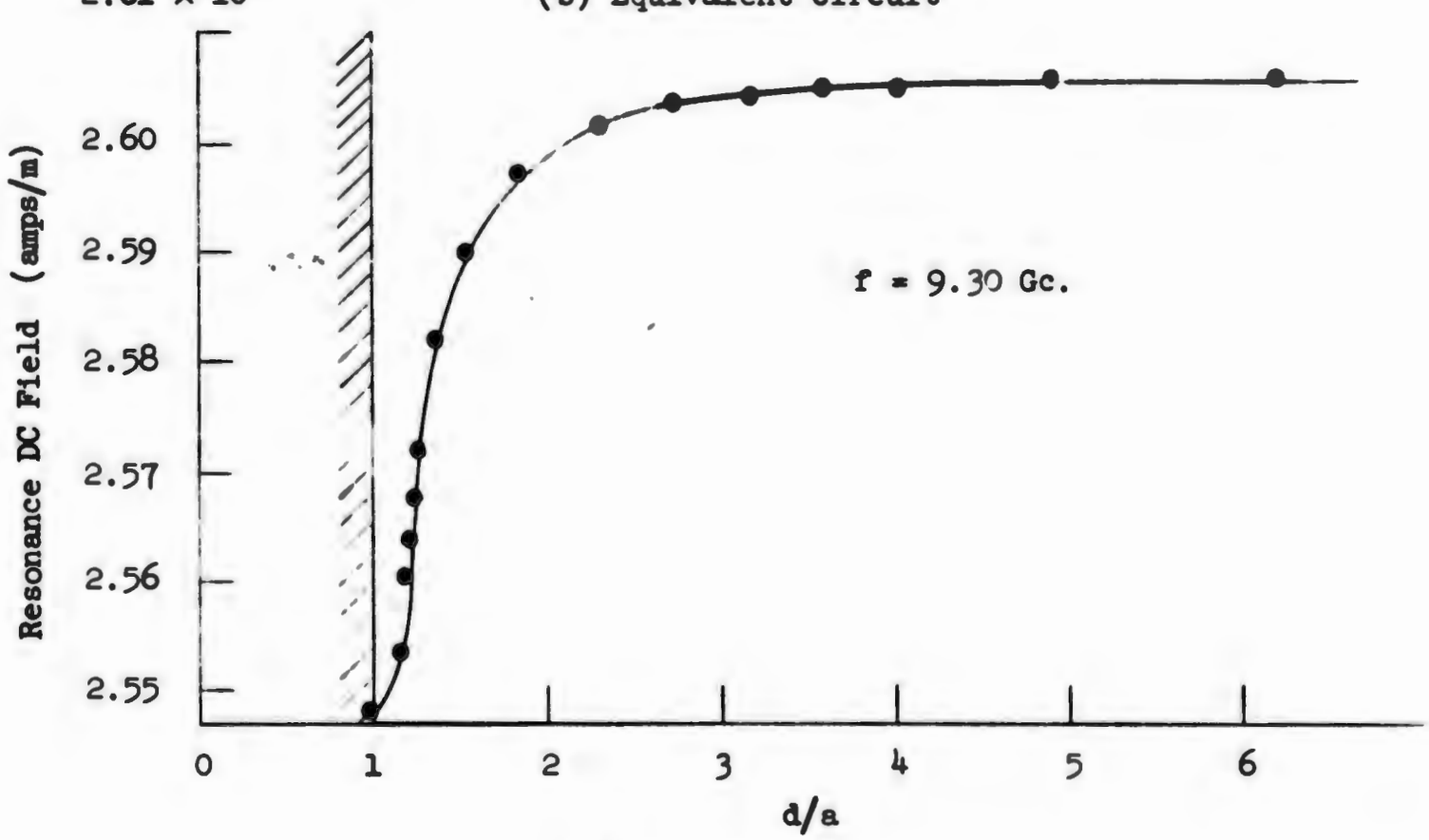

(c) Experimental Results

FIG. 2.18--Measurement of resonance shift as a function of the spacing of a ferrite sphere from a waveguide wall.

distance from the center of the sphere to the broad wall of the waveguide. In the absence of any wall effects, all of these quantities should be constants for the experimental configuration used, independent of the distance d. The observed variations are shown in Figs. 2.18c and 2.19a and b. The quantity $\beta\Delta H$ plotted in Fig. 2.19 is proportional to the reciprocal of the external Q of the sample, and hence is a measure of the geometrical coupling between the sample and the waveguide.

In addition to the preceding effects, it was also observed that for certain ranges of d, the resonance line became asymmetric, indicating within each such range a strong coupling between the uniform precession and some other magnetostatic mode degenerate in resonant frequency with the uniform mode. As the spacing d was varied, it was found that several modes could be "tuned through" the uniform precession, producing a distorted line whose shape changed as the sample was moved. Figure 2.20 is a series of photographs showing how the line shape varied as one such mode was tuned through the uniform precession. The coupling in this case is quite large, the two modes, as is evident from Fig. 2.20c, being in fact overcoupled.

Before proceeding to a theoretical discussion of these effects, it is well to consider their practical implications. In particular, it should be noted that, except in the immediate vicinity of the wall, the dominant effect is a shift in the resonant frequency of the sample. For example, with $d/a = 3$, corresponding to the surface of the sample being one diameter from the wall, the coupling has been reduced by less than 2%, the linewidth increased by less than 1%, but the resonant field shifted by over twice the linewidth. Since for many purposes a shift in the position of the resonance is unimportant, wall effects can usually be neglected for spherical samples spaced more than 1 diameter from the wall. This practice was adhered to in all of our relaxation experiments.

B. THEORETICAL INVESTIGATION

1. Frequency Shift.

A quantitative explanation of the observed frequency shift can be obtained on the basis of a simple argument using the method of images. We begin by supposing that a uniformly precessing dipole is placed in the

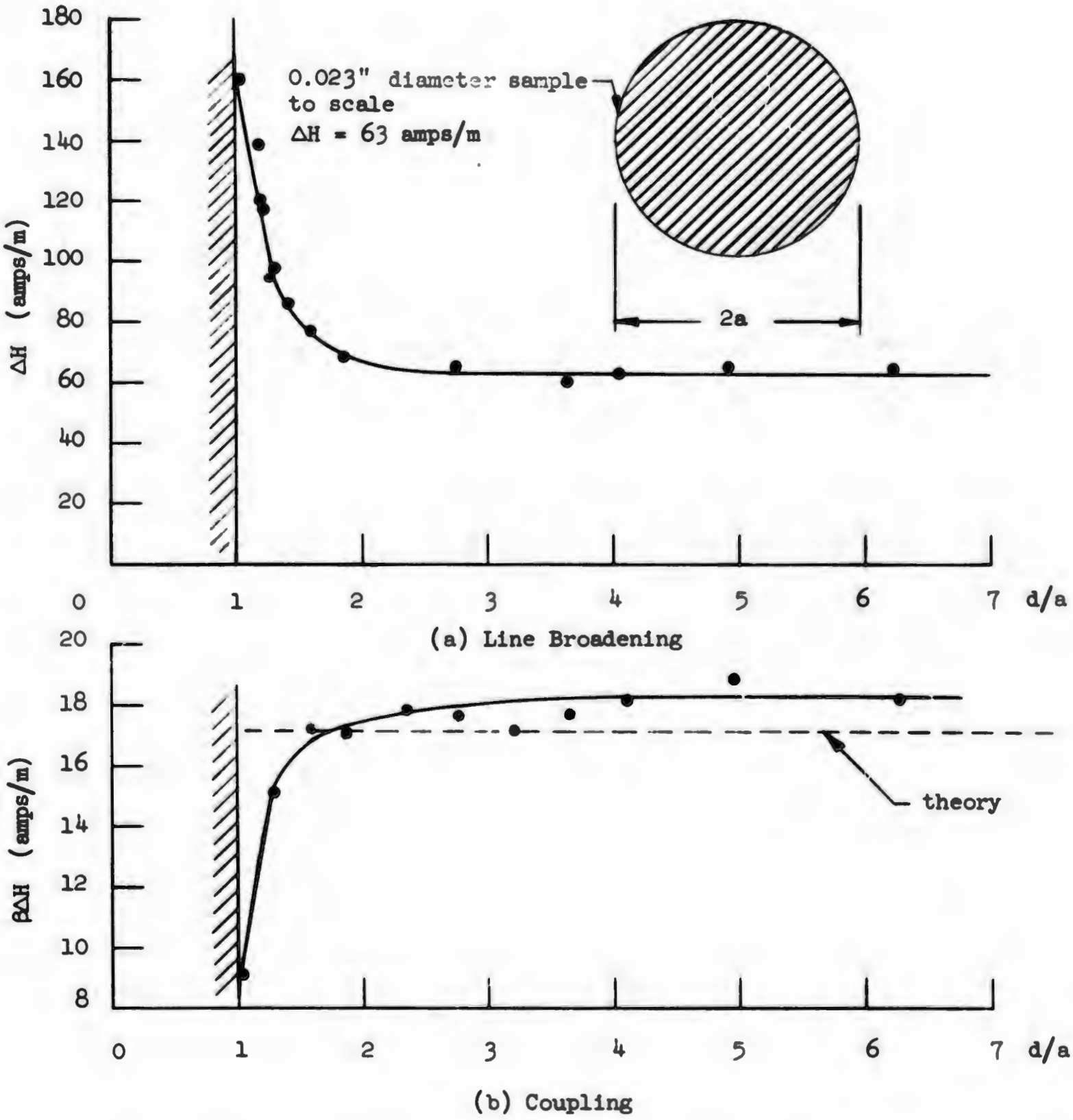

FIG. 2.19--Increase in linewidth and decrease in coupling produced by the proximity of a ferrite sphere to a waveguide wall.

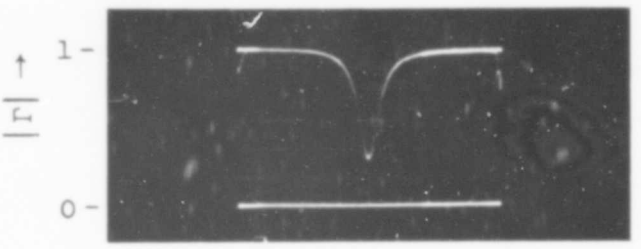

(a) $\frac{d}{a} \rightarrow \infty$

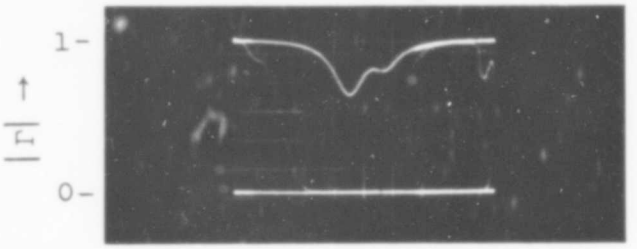

(b) $\frac{d}{a} \approx 1.235$

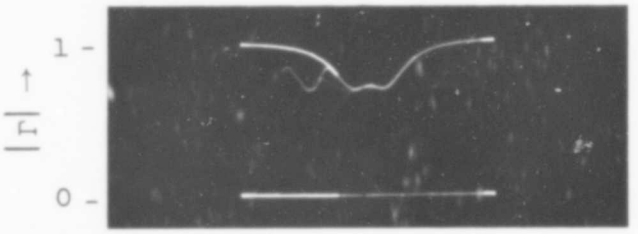

(c) $\frac{d}{a} \approx 1.23$

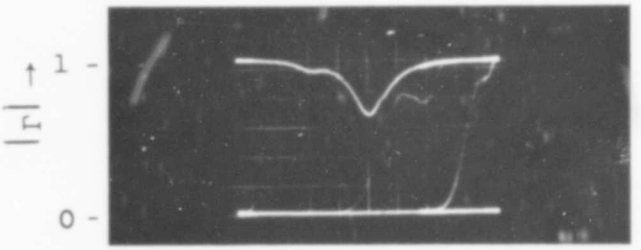

(d) $\frac{d}{a} \approx 1.24$

(approximately 80 amps/m per major division)

FIG. 2.20--Variation of line shape with distance of sample from waveguide wall

vicinity of a perfectly conducting plane of infinite extent. If the dipole is sufficiently close to the conductor, we may ignore retardation effects, and replace the plane by an image dipole in which the precession is oppositely directed, as shown in Fig. 2.21. The "reaction field," $\vec{h}_r$, produced by the image dipole, is[54]

$$\vec{h}_r = \frac{\overleftrightarrow{R}}{4\pi} \nabla \left[V_s \vec{m} \cdot \nabla \left(\frac{1}{\vec{r}'} \right) \right] , \qquad (2.40)$$

where $V_s\vec{m}$ is the rf component of the dipole moment of the sample, $\overleftrightarrow{R}$ is a reflection operator, and $\vec{r}'$ is the coordinate of the field point referred to the image dipole as the origin. The total field at the sample will be the sum of the reaction field and an applied field, $\vec{h}_{app}$, so that

$$\vec{m} = \overleftrightarrow{\chi}(\vec{h}_{app} + \vec{h}_r) \quad . \qquad (2.41)$$

Equation (2.41), with Eq. (2.40), represents a case where the concept of an effective susceptibility, discussed in Appendix A, may be used. There it is shown that whenever the total rf field may be written as the sum of two partial fields, $\vec{h}_1$ and $\vec{h}_2$, such that $\vec{h}_2 = \overleftrightarrow{k}\vec{m}$, an effective susceptibility tensor, $\overleftrightarrow{\chi}_{eff}$, may be so defined that $\vec{m} = \overleftrightarrow{\chi}_{eff}\vec{h}_1$. In the present problem there are two cases of interest, one in which the conducting plane is perpendicular to the dc field, for which

$$\overleftrightarrow{k} = \frac{-V_s}{32\pi d^3} \begin{pmatrix} 1 & 0 \\ 0 & 1 \end{pmatrix} , \qquad (2.42)$$

with d being the distance between the plane and the dipole, and the other in which the conducting plane is parallel to the dc field, in which case

$$\overleftrightarrow{k} = \frac{-V_s}{32\pi d^3} \begin{pmatrix} 2 & 0 \\ 0 & 1 \end{pmatrix} , \qquad (2.43)$$

when the conductor is parallel to the y-z plane. As shown in Appendix A, inclusion in the susceptibility tensor of a term of the form given by Eqs. (2.42) or (2.43) produces a shift in the dc field required for

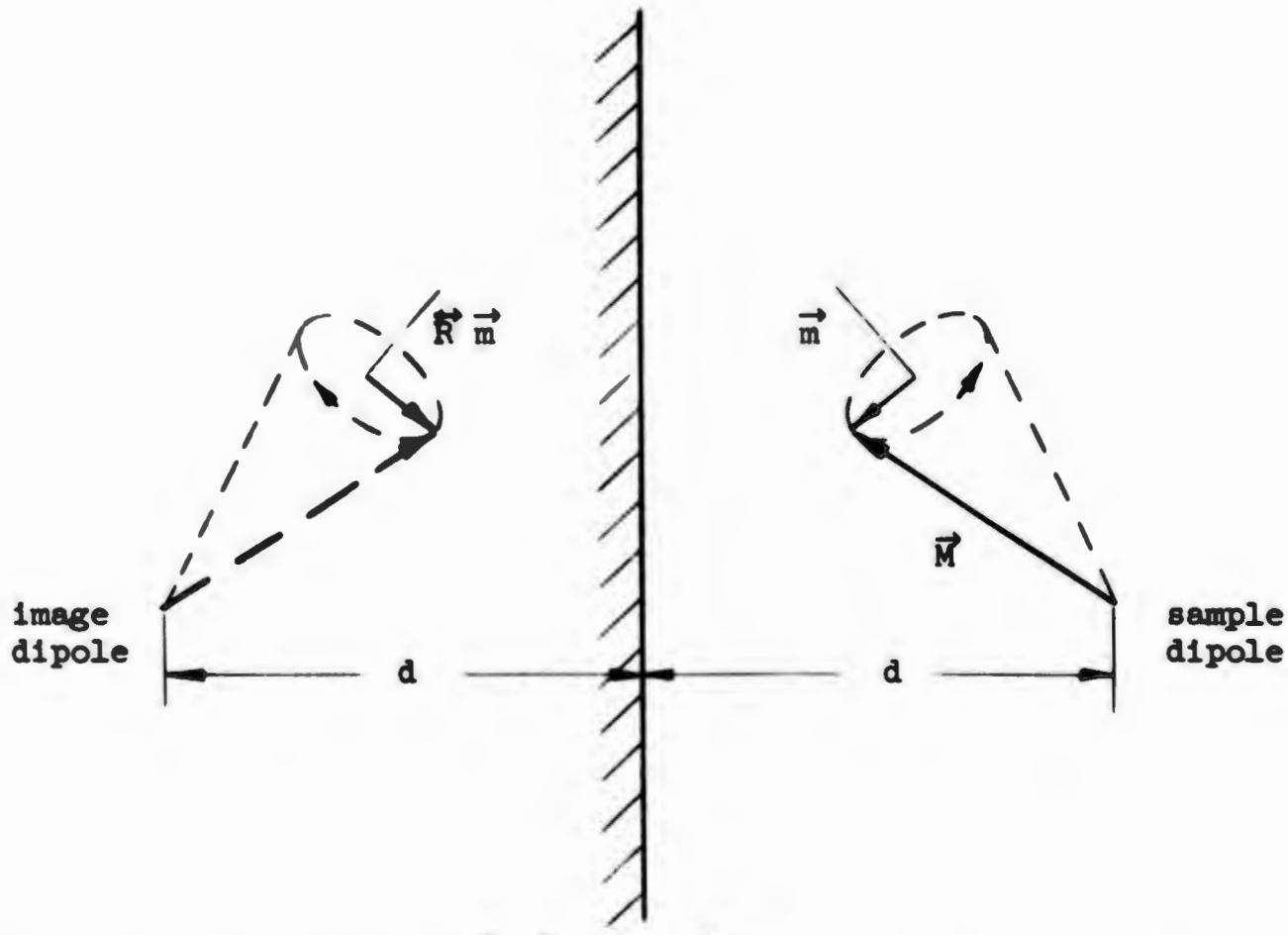

FIG. 2.21--A precessing dipole and its image in a conducting plane.

resonance at a given frequency by an amount

$$\delta H = M_s \frac{(k_{11}K^2 + k_{22})}{K^2 + 1} \quad , \qquad (2.44)$$

provided that $\delta H/M_s \ll 1$.[1]

To apply these results to the experiment discussed earlier, we may take $K = 1$, since our sample was a sphere. Then, since the waveguide wall was perpendicular to the dc field, Eq. (2.42) applies, and the

[1] The expression is exact whenever the uniform precession is circularly polarized, in the presence of the wall.

field shift is given by

$$\frac{\delta H}{M_s} = -\frac{1}{24}\left(\frac{a}{d}\right)^3 , \qquad (2.45)$$

"a" being the radius of the sample. Theory and experiment are compared in Fig. 2.22, where the experimental data of Fig. 2.18c are replotted on a logarithmic scale. Agreement is seen to be good except at the extremes of the range of d/a. The discrepancy at large distances (which actually may not be as great as indicated, since the very small field shifts involved are hard to measure accurately) is probably due to the neglect of retardation effects, and of the effects of the other walls of the waveguide.[1] The disagreement for values of d/a very near unity ($d/a = 1$ corresponds to the sample touching the waveguide wall) probably arises from the approximation of replacing the distributed magnetization of the sample by a single point source.

2. Line Broadening

The dipolar fields of the sample will induce currents in the adjacent wall of the waveguide. If the wall has a finite conductivity, there will be resistive losses associated with these currents which, inasmuch as they extract energy from the spin system, must act to broaden the resonance line. As in most calculations of this type, one may proceed approximately by assuming a current distribution appropriate to a perfectly conducting wall, and then calculate the dissipation produced by this current when the conductivity is finite. Considering only the case where the conducting plane is perpendicular to the dc field, and assuming the quasi-static approximation used in 2. above, one finds after a straightforward, somewhat tedious calculation, that the power lost in the waveguide wall as a result of currents induced by an adjacent precessing rf magnetization $\vec{m}$, together with its image, is just

$$P = \frac{3}{32\pi}\frac{R_s V_s^2 |m|^2}{d^4} , \qquad (2.46)$$

---

(1) It is evident from symmetry that the field shift must approach zero as the sample approaches the center of the waveguide.

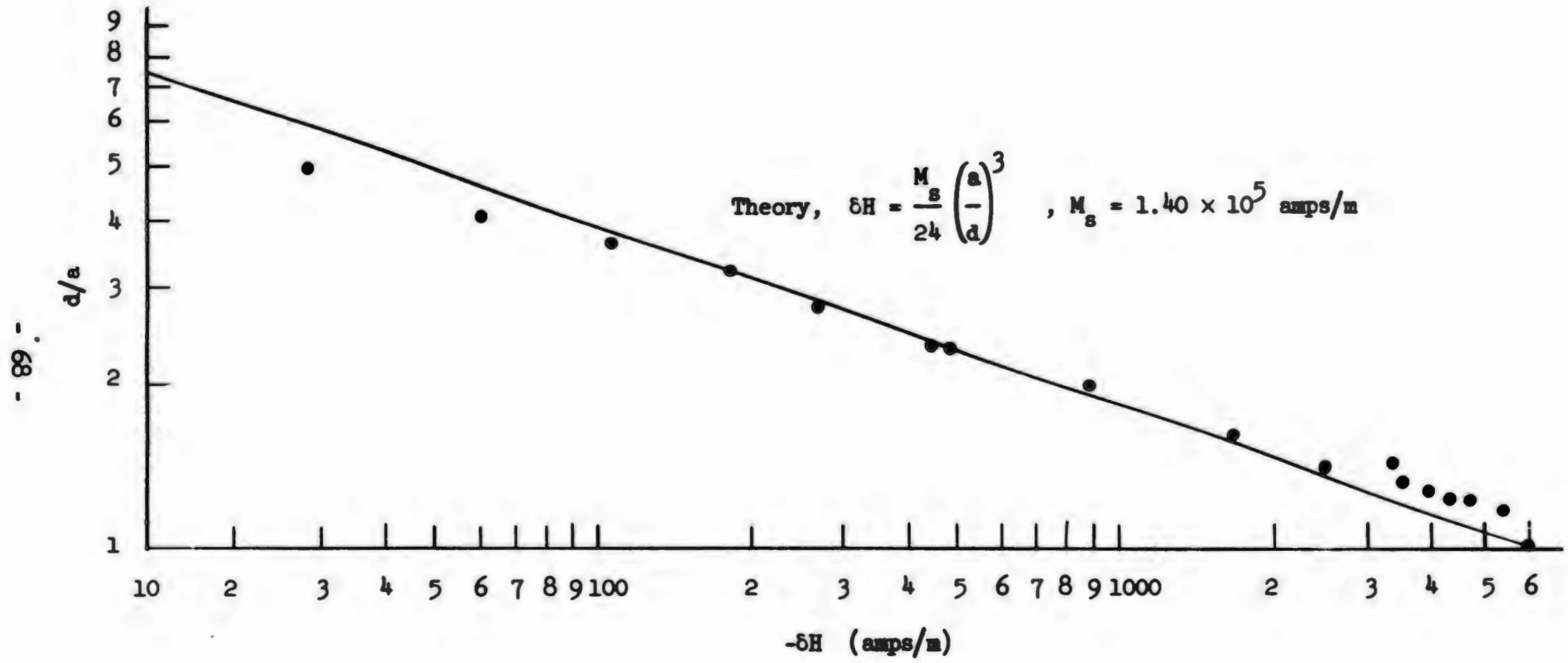

FIG. 2.22--Resonance shift as a function of the spacing of a ferrite sphere from a waveguide wall; comparison of theory and experiment.

where R_s is the surface resistivity of the wall, and as before, d is the distance from the wall to the center of the sample. To relate this dissipation to a contribution to the linewidth, we may equate the power lost to the product of the energy stored and a relaxation rate. According to the results of Part I, the energy stored is proportional to the square of the amplitude of the transverse magnetization, if the precession path is circular, while the relaxation rate may be written in terms of an equivalent linewidth, ΔH_w, with the result that

$$P = \frac{\mu_0 \Delta H_w \omega_0 |m|^2 V_s}{2M_s} \quad . \tag{2.47}$$

By combining Eqs. (2.46) and (2.47), and specializing to the case of a sphere of radius "a", we obtain

$$\frac{\Delta H_w}{M_s} = \frac{1}{4a} \frac{R_s}{\mu_0 \omega_0} \left(\frac{a}{d}\right)^4 \quad . \tag{2.48}$$

Because of the $1/d^4$ dependence, losses due to this mechanism evidently increase very rapidly as the sample is brought closer to the wall. An interesting feature of the result is that the line broadening, in contrast to the shift of the resonance, is <u>not</u> independent of the scale of the problem, but increases, for a fixed value of a/d, as the sample is made smaller. This result is not unexpected, of course, and comes about for the same reason that the Q of a microwave cavity ordinarily decreases as the cavity is made smaller.

To compare theory and experiment, we have plotted the <u>increase</u> in ΔH, as a function of d/a, in Fig. 2.23. Also shown is the theoretical result for a sphere of radius 0.29 mm, adjacent to a copper wall, for which $R_s = 2.5 \times 10^{-2}$ ohms at 9.3 Gc. Theory and experiment are seen to be in qualitative agreement. Indeed, the agreement would be quite good, for all but the closest spacings, if we were to assume an effective value for R_s some 50% higher than that given by simple skin-effect theory,[1]

[1] The wall losses in microwave resonant cavities are also found, invariably, to be higher than simple skin-effect theory predicts.

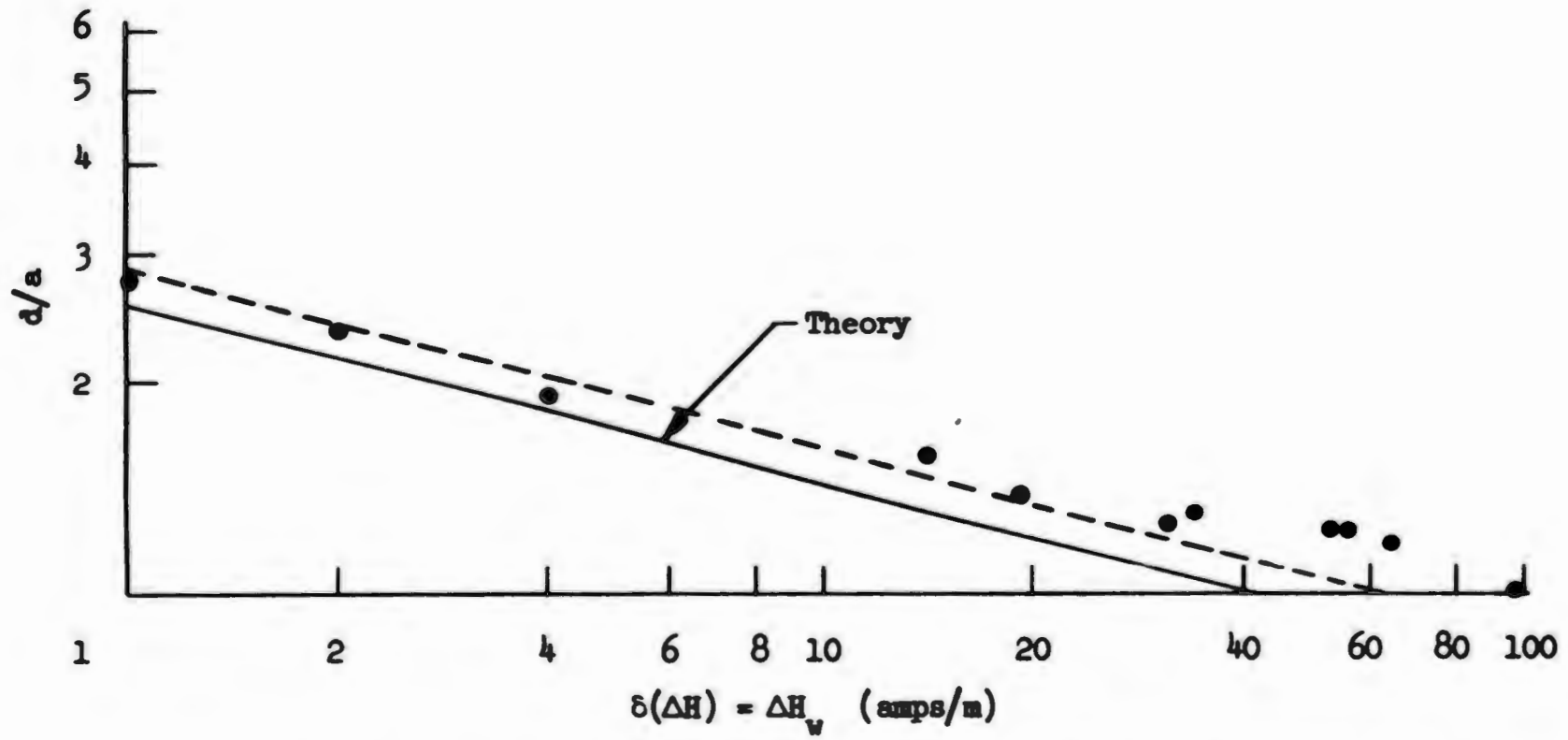

FIG. 2.23--Line broadening produced by the proximity of a ferrite sphere to a waveguide wall - comparison of theory and experiment.

thus giving the dotted line of Fig. 2.23. When d/a becomes very close to unity, it is impossible to separate the line broadening due to coupling to other magnetostatic modes from that due to the finitely conducting wall, so that in this region we would not expect agreement with our simple theory.

It thus seems certain that in the absence of coupling to other modes the line broadening of the uniform precession by an adjacent conductor can be largely, if not completely, accounted for by the finite conductivity of the conductor.

3. Coupling of the Uniform Precession to Other Modes

As can be seen from Fig. 2.20, coupling to other modes can profoundly alter the nature of the resonance line. In the experiment discussed previously, four separate modes, each coupled in turn to the uniform precession, could be observed as the sample was moved closer to the wall, the first appearing for $d/a \approx 2.35$. A simple argument can account qualitatively for this observed behavior. As we have seen, in the magnetostatic approximation, the waveguide wall may be replaced by an image dipole. Because the "reaction" field produced at the sample by the image is highly nonuniform, it is capable of exciting those magnetostatic modes having appropriate symmetry. In effect, then, there exist mutual coupling terms between the uniform precession and certain low order magnetostatic modes -- in the equivalent circuit of Fig. 1.1 of Part I, there will be additional mutual inductances M_{0k}" . The modes for which this coupling is appreciable will be in the discrete portion of the magnetostatic mode spectrum; since a strong interaction will occur only when the magnetostatic mode is degenerate, or almost degenerate, with the uniform mode, there will in general be only one mode coupled to the uniform precession at once, in contrast to the case of inhomogeneity scattering considered in Part I. The response of the system will thus be characteristic of any resonant system with two degrees of freedom -- for example, Fig. 2.17c will be recognized as quite typical of the response of a double-tuned electrical circuit in which the two resonant circuits have the same resonant frequency, and are slightly overcoupled.

Different modes appear for different values of the spacing d because the resonant frequency of the uniform mode depends strongly on the ratio d/a (cf. Fig. 2.18), whereas the resonant frequencies of the magnetostatic

modes presumably do not. Hence, as d is varied, the uniform mode is tuned through a succession of magnetostatic modes. The actual magnitude of the coupling will depend not only on the distance from the sample to the wall, but also on the symmetry of the magnetostatic mode relative to that of the inhomogeneous reaction field. For the four modes that could be positively identified in our experiment, the first to be discernible as the sample was brought closer to the wall was very much undercoupled, the second (shown in Fig. 2.20) was slightly overcoupled, the third approximately critically coupled, while the last, occurring for $d/a \approx 1$ was grossly overcoupled.

CHAPTER XII

SUMMARY

In this part we were concerned with the electrical representation of a section of waveguide containing a small, magnetically saturated ferrimagnetic ellipsoid. By assuming that the waveguide can propagate only one mode, and that only the uniform precessional mode of the ferrite is near resonance, we developed scattering matrix and lumped-element electrical equivalent circuit representations, both of which are valid for samples from which the scattering is large, and for which heretofore no adequate theory has existed. The scattering coefficients and equivalent circuit parameters are given absolutely in terms of the intrinsic properties of the ferrimagnetic material, and the geometry of the sample and waveguide.

The theory is particularly applicable to small ellipsoids of low-loss ferrimagnetic material, such as single crystal garnet. These materials are characterized by sufficiently low intrinsic losses that large electrical discontinuities can be produced by samples which are physically much smaller than a free-space wavelength. The theory is limited to such small samples because of the fundamental assumption that the motion of the magnetization in the sample can be characterized by a set of normal modes substantially independent of the external environment. The theory is further restricted to uniformly magnetized ellipsoids by the assumption that the dominant mode is a uniform precession.

The approach adopted here is equivalent to what is usually called, incorrectly, the "cavity perturbation technique," used to discuss the behavior of resonant cavities containing small ferrite samples. The essence of the procedure, in both cases, is to assume that the field configurations of the cavity or waveguide remain unchanged upon introduction of the ferrite, but that the amplitudes adjust themselves to satisfy conservation of energy.

The salient features of the theory have been verified experimentally through impedance measurements on sections of waveguide containing polished single crystal spheres of yttrium iron garnet. The equivalent circuits were shown to account quantitatively for the observed behavior even for samples large enough electrically to absorb all the power incident along the waveguide. Appreciable deviations from theory occurred only when the sample was placed within one or two diameters of the waveguide wall. Placing the sample close to the wall was found, experimentally, to shift the resonant frequency, as well as to broaden, and distort the resonance line. The shift in resonant frequency was explained quantitatively in terms of the "reaction" field of an image dipole produced by reflection of the sample in the waveguide mode. It was shown that the line broadening could be largely accounted for by the losses associated with the finite conductivity of the waveguide walls, while the distorted resonance line was explained qualitatively on the basis of a mutual coupling between the uniform precession and certain low-order magnetostatic modes. This coupling arises from the nonuniform reaction field produced, in the vicinity of the sample, by its image in the waveguide wall.

BLANK PAGE

PART III

MEASUREMENT OF FERRIMAGNETIC RELAXATION PARAMETERS

CHAPTER XIII

INTRODUCTION

A. CHARACTERIZATION OF THE RELAXATION PROCESSES

According to the spin mode theory outlined in Part I, small-signal ferrimagnetic relaxation processes are describable in terms of three relaxation parameters:

(i) η_0 , the intrinsic relaxation rate for the uniform mode,

(ii) η_k , an average relaxation rate characterizing the intrinsic relaxation of the S-modes (i.e., those spin modes degenerate in resonant frequency with the uniform mode), and

(iii) η_0' , a composite spin-spin relaxation rate which characterizes the net transfer of energy, by inhomogeneity scattering processes, from the uniform mode to other S-modes.

In Part I we outlined a derivation of the equations of motion which described the rate of change of the differential z-component of magnetization in terms of these relaxation parameters. Although the general equations could be immediately specialized to the conditions of our experiment, it is more instructive to re-derive them here using an approximate model which proves useful in visualizing the physical implications of the experimental technique. To do this, we first note that according to Eqs. (1.10) and (1.11) of Part I, the relaxation parameters describe very simply the rate at which energy is transferred among the modes of the spin system, and between these modes and the crystal lattice. In the experiments that we describe later, however, we do not measure the energy directly, but rather the deviation, ΔM_z , of the z-component of magnetization from its equilibrium value. Nevertheless, under certain circumstances the energy of each excited mode is uniquely determined by its differential z-component of magnetization, and when this is so, a simple characterization of the motion of the system is possible.

By combining Eqs. (1.9) and (1.14) of Part I, we find that

$$\Delta M_{zk} = \gamma \frac{A_k}{\omega_k^2} W_k \quad , \tag{3.1}$$

so that ΔM_{zk} will in fact be proportional to W_k, with a <u>proportionality constant independent of k</u> only for the special case where all the modes have (i) the same resonant frequency (ω_k independent of k), and (ii) the same ellipticity (A_k independent of k). Since the experiments to be discussed were all performed on spherical samples, in which the uniform mode is circularly polarized, so that $A_0 = \omega_0$, it would thus be convenient to assume that $A_k \approx \omega_k$ for the remaining modes as well. In our experiments, A_k and ω_k differ by less than 2%,[1] so that this assumption is in fact quite well justified, and is made in all that follows.

There remains, however, the question of whether we may assume that all the excited modes have the same resonant frequency. In a steady state small signal experiment, where only <u>linear</u> scattering processes occur, this assumption is justified, for then the only modes excited to an appreciable amplitude will have resonant frequencies lying in a small

---

[1] From Eqs. (1.3) and (1.15) of Part I we obtain, for the ratio of A_k to ω_k,

$$\frac{A_k}{\omega_k} = \sqrt{1 + \frac{\omega_M^2 \sin^4 \theta_k}{\omega_k^2}} \quad .$$

The maximum value of θ_k, for a given ω_k will occur for the lowest allowed value of k, which, for our experiments is $k \approx 0$, for which $\omega_M \sin^2 \theta_k = (\omega_k^2 - \omega_H^2)/\omega_H$. Hence in our experiments, where $\omega_k/2\pi \approx \omega_0/2\pi \approx 10 \times 10^9$ sec^{-1}, and $\omega_H = \omega_0 - \omega_M/3$, with $\omega_M/2\pi = 4.9 \times 10^9$ sec^{-1} for YIG, we obtain

$$\frac{A_k}{\omega_k} \approx \sqrt{1 + \frac{1}{30}} \quad .$$

It should be noted, however, that if these experiments were carried out at lower frequencies (smaller ω_k) on materials having a larger saturation magnetization (larger ω_M) the approximation $A_k \approx \omega_k$ could be seriously in error.

range, of order η_k, centered about the driving frequency. In addition, for the particular conditions of our experiment, this will also be true of those spin modes that are excited at moderate power levels through nonlinear coupling to the uniform precession. In such a case Suhl[13] has shown, for a spheroid, that whenever the angular driving frequency, ω, is greater than $2\omega_M N_t$, where N_t is the transverse demagnetizing factor, and the uniform mode is driven at resonance, the nonlinear coupling is such as to excite spin modes having very nearly the same resonant frequency as the uniform mode. This frequency condition is fulfilled in our experiments. Thus, as long as the excitation of the spin modes derives solely from the uniform precession, we are justified in assuming that all the magnetic energy is distributed among modes which have essentially the same resonant frequency.

Under these conditions, the distribution of energy will be the same as the distribution of ΔM_z, so that we can represent the steady state "motion" of the system by means of a stationary distribution of ΔM_z, and any <u>adiabatic</u>[(1)] changes in this motion by means of a redistribution or "flow" of ΔM_z. A simple representation of this sort is given in Fig. 3.1, which is a flow-chart similar to that first used by Fletcher,[8] et al., to describe the energy flow in a spin system. In this diagram, the ordinate is proportional to the differential z-component of magnetization, or equivalently, to the energy. The system is assumed to be driven by an external signal source which couples only to the uniform precession, thus exciting it to an appreciable amplitude, characterized by ΔM_{z0}. Some of the energy delivered to the uniform mode by the signal generator is then reradiated back into the microwave circuitry (at a time rate proportional to $\eta_R \Delta M_{z0}$), some is lost through various intrinsic processes ($\eta_0 \Delta M_{z0}$), while the remainder is scattered to the other spin modes, the rate of energy lost to the k^{th} mode being proportional to $\eta_{0k} \Delta M_{z0}$. This energy in turn is dissipated by the intrinsic relaxation processes of the individual spin modes, at a rate proportional to $\eta_k \Delta M_{zk}$ for the k^{th} mode. The total scattered energy will normally

---

(1) By "adiabatic" in this context we mean "slow" changes which occur over many cycles of the precession frequency.

be spread over a very large number of modes, so that each $k \neq 0$ spin mode will be excited to a level very much less than that of the uniform precession, i.e., $\eta_{0k} \ll \eta_k$.

Figure 3.1 is rather oversimplified in that we have ignored any coupling between individual spin modes. Also, it is not strictly correct to represent the inhomogeneity scattering in terms of a separate one-way energy transfer to each spin mode -- it is only the aggregate interaction of all the spin modes with the uniform precession that can be described in such a simple way, as was indicated in Part I. Nevertheless, the representation of Fig. 3.1 leads to a correct description of the observable behavior of the system. In particular, we can obtain a set of rate equations

$$\frac{d\Delta M_{z0}}{dt} = \text{DRIVE} - 2\left(\eta_0 + \eta_R + \sum_{k\neq 0} \eta_{0k}\right) \Delta M_{z0} \quad , \qquad (3.2a)$$

and

$$\frac{d\Delta M_z}{dt} = \text{DRIVE} - 2(\eta_0 + \eta_R - \eta_k)\Delta M_{z0} - 2\eta_k \Delta M_z \quad , \qquad (3.2b)$$

which reduce to the equations of motion described in Part I, for the special case of $A_0 = A_k$, if we make the identification

$$\sum_{k\neq 0} \eta_{0k} \equiv \eta_0' \quad ,$$

and assume, as discussed in Part I, that η_k is an effective intrinsic spin mode relaxation rate, obtained by averaging, in general with some weighting factor, over all the S-modes.

In the previous work, both here and in Part I, we have assumed that the processes which remove energy from the S-modes, and which we have characterized by a relaxation rate η_k , do so in such a manner that the total z-component of magnetization is destroyed as the energy is dissipated. This would of course be true for actual spin-lattice relaxation processes, in which, speaking quantum mechanically,

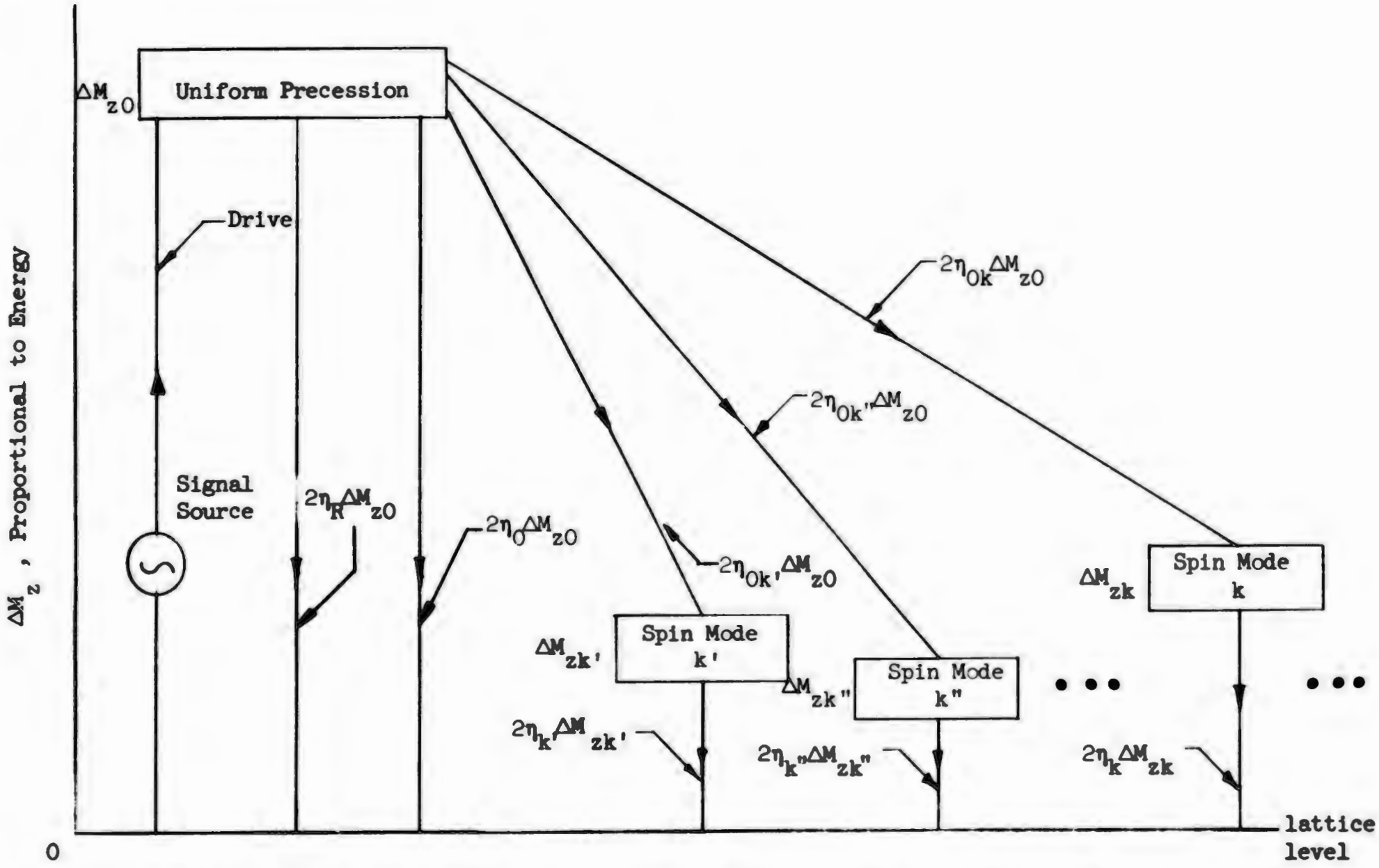

FIG. 3.1--Flow chart showing distribution of differential z-component of magnetization.

magnons[1] are destroyed and phonons are created. Recent calculations[5-7] have suggested, however, that the dominant relaxation mechanism for S-modes does not involve a direct transfer of energy to the lattice, but rather a gradual diffusion of energy to all the other spin modes by means of multiple quantum transitions and thence ultimately to the lattice. Although such processes will not in general result in the destruction of ΔM_z in an amount proportional to the energy removed from the S-modes, for the conditions of our experiment, it seems certain that they do, for the following reason. Of the possible multiple magnon transitions, the most important, as far as the first step in the removal of energy from the S-modes is concerned, are 3-magnon processes, of which we must distinguish two distinct kinds.[6]

In the first so-called "splitting" process, one magnon of frequency ω_k splits into two magnons with frequencies ω_k' and ω_k'' such that $\omega_k = \omega_k' + \omega_k''$. In the other "confluence" process two magnons of frequency ω_k and ω_k' coalesce to produce a single magnon of frequency ω_k'' such that $\omega_k + \omega_k' = \omega_k''$. Although the confluence process can always take place, the nature of the spin wave spectrum forbids the splitting process unless the frequency condition

$$\omega_k < 2/3\omega_M \qquad (3.3)$$

is satisfied.[6] The spin waves whose relaxation concerns us have the same resonant frequency as the uniform mode, so that in our (X-band) experiments, ω_k is of order 6×10^{10} sec^{-1}, whereas for yttrium iron garnet, ω_M is 3.7×10^{10} sec^{-1}; hence the inequality (3.3) cannot be satisfied, and the splitting process does not occur. In the confluence process, two magnons are destroyed -- one the magnon whose relaxation we are following, the other a thermal magnon -- and one is created. Since each magnon contributes an approximately equal share[2] to ΔM_z, the net result is

---

(1) A magnon is a quantum of magnetic energy, in analogy with the photon (electromagnetic energy) and the phonon (vibrational energy).

(2) This result is, of course, implicit in the quantum mechanical formulation. To demonstrate it within the present semi-classical framework, we note that if we ignore the ellipticity of the spin waves, and consider a single magnon with energy $\hbar\omega_k$, Eq. (3.1) reduces to $\Delta M_{zk} = \gamma\hbar$.

a decrease in ΔM_z equal to that which would have occurred if the relaxation had been directly to the lattice. It is believed that the further relaxation processes (by means of which the output magnons of the 3-magnon process which relax the S-modes are themselves destroyed) take place without any substantial change in ΔM_z ,[1] and in the interpretation of our experiments we shall assume that this is so.

B. METHODS OF MEASURING RELAXATION PARAMETERS

Most of the experimental techniques which have been described for the determination of relaxation parameters fall into two broad categories:

(a) small-signal measurements of both transverse and longitudinal (z) components of magnetization, using either

(i) steady-state (frequency domain),[8,46] or

(ii) transient (time domain) approaches,[10-12] and

(b) large-signal measurements of susceptibility, using either

(i) a transverse rf driving field,[13] or

(ii) a longitudinal rf driving field,[47] (the so-called "parallel-pump" experiment).

Small-signal, steady-state measurements using a sinusoidally modulated drive have been reported recently by Fletcher, LeCraw and Spencer,[8] who present a complete analysis of their results in terms of the spin-mode theory of ferrimagnetic relaxation. Earlier, transient measurements using a pulsed rf drive were made by Bloembergen and Wang,[10] Damon,[11] and Farrar.[12] Unfortunately, these transient measurements were made before the relaxation process, and the interaction between the sample and its microwave environment were as well understood as they are now. This places serious restrictions on the validity and interpretation of the experimental data.

In the present investigation, we have used conventional steady state linewidth measurements[2] to characterize the relaxation of the transverse component of magnetization, and transient methods to study

---

[1] See Ref. 9 and M. Sparks, private communication.

[2] Techniques for the measurement of linewidth, with special emphasis on methods suitable for low-loss materials, are considered in Appendix B.

the z-component. In essence, our technique is to apply step-functions of drive to the sample while monitoring the rate of change of the total z-component of magnetization by means of a loop or coil around the sample, specifically designed to minimize any interaction with the transverse component. Such a pulse technique, although perhaps not as accurate at small signal levels as the modulation method of Fletcher et al., has advantages in simplicity and directness, and perhaps more importantly, may be extended to the high power region where cw techniques cannot be used because of the difficulty of interpreting the results in the light of the resulting nonlinear equations of motion.[1]

CHAPTER XIV

USE OF THE TRANSIENT BEHAVIOR OF M_z TO PROVIDE RELAXATION INFORMATION

A. TRANSIENT BEHAVIOR OF THE Z-COMPONENT OF MAGNETIZATION

The rate equations (3.2) represent a particularly simple example of a coupled set of differential equations, and solutions may be easily obtained for the cases where the uniform mode is subjected to a suddenly applied sinusoidal drive at its resonant frequency, or when, after the steady-state has been reached, the drive is suddenly removed.

In the first case, ΔM_{z0} will grow exponentially towards its equilibrium value, which we shall denote by $\Delta\hat{M}_{z0}$, according to the equation

$$\Delta M_{z0} = \Delta\hat{M}_{z0}\left(1 - e^{-\eta_{2L}t}\right)^2 \quad , \qquad (3.4)$$

where

$$\eta_{2L} \equiv \eta_0 + \eta_R + \eta_0' \quad .$$

This is most easily seen by examining the equation of motion for the uniform mode, Eq. (1.8) of Part I. If we add a driving term of the form[2] $he^{j\omega t}u(t)$, where h is some constant, and $u(t)$ is the

---

[1] A more plebian difficulty would be excessive heating of the sample because of the high average power dissipation.

[2] To be perfectly general we would have to include another driving term of the form $h'e^{-j\omega t}u(t)$. The response of the system to this driving term is so small for low-loss samples near resonance, however, that it may be ignored.

unit step-function, Eq. (1.8) becomes

$$\dot{b}_0 = j[\omega_0 + j\eta_{2L}]b_0 + he^{j\omega t}u(t) \quad ,$$

for which a solution is

$$b_0 = \frac{he^{j\omega t}}{j(\omega - \omega_0) + \eta_{2L}}\left[1 - e^{-j(\omega-\omega_0)t-\eta_{2L}t}\right] \quad .$$

Since $\Delta M_{z0} \propto |b_0|^2$, at resonance $(\omega = \omega_0)$, this result leads at once to Eq. (3.4). To obtain a solution for the set of equations (3.2b), it is convenient to sum over all the spin modes, except for $k = 0$, and use the identity

$$\sum_{k\neq 0} \Delta M_{zk} = \Delta M_z - \Delta M_{z0} \quad .$$

If we do this, and remember that η_k was assumed to be independent of k , Eq. (3.2b) can be written in the form

$$\frac{d\Delta M_z}{dt} = \frac{d\Delta M_{z0}}{dt} + 2\Delta M_{z0}(\eta_0' + \eta_k) - 2\eta_k \Delta M_z \quad . \tag{3.5}$$

Substituting from Eq. (3.4) for the motion of the uniform mode then reduces Eq. (3.5) to a simple inhomogeneous linear differential equation in the single independent variable ΔM_z . By solving this in the standard way, subject to the initial condition that $\Delta M_z = 0$ at $t = 0$, we find that the rate of change of M_z when a step function of rf drive is applied is given by

$$\frac{d\Delta M_z}{dt} = \hat{\Delta M}_{z0} 2\eta_{2L}\left\{\frac{\eta_0 + \eta_R - \eta_0' - 2\eta_k}{\eta_{2L} - 2\eta_k} e^{-\eta_{2L}t}\right.$$

$$\left. + \frac{\eta_k - \eta_0 - \eta_R}{\eta_{2L} - \eta_k} e^{-2\eta_{2L}t} + \frac{\eta_0'\eta_{2L}}{(\eta_{2L} - 2\eta_k)(\eta_{2L} - \eta_k)} e^{-2\eta_k t}\right\} \quad . \tag{3.6}$$

In the case where the drive is suddenly removed after equilibrium has been established, it is evident from Eq. (1.8) that the uniform mode will decay exponentially, so that

$$\Delta M_{z0} = \hat{\Delta M}_{z0} e^{-2\eta_{2L}(t-t')}$$

if we suppose the drive to be cut off at $t = t'$. From the solution of Eq. (3.5) we then find that the rate of change of the total z-component of magnetization decays according to

$$\frac{d\Delta M_z}{dt} = - \frac{\hat{\Delta M}_{z0} 2\eta_{2L}}{\eta_{2L} - \eta_k} \left\{ (\eta_0 + \eta_R - \eta_k) e^{-2\eta_{2L}(t-t')} + \eta_0' e^{-2\eta_k(t-t')} \right\} . \quad (3.7)$$

The form of these solutions is sketched in Fig. 3.2. A significant feature of the waveform is that the leading edge takes a finite time, τ , to rise to its maximum value, d , in contrast to the behavior of the trailing edge. Furthermore, it is a mathematical consequence of the equations of motion that the amplitude of the trailing edge waveform at a time, $t = t' + \tau$ is also equal to d , regardless of the relative amplitudes of the relaxation parameters, a property readily subject to experimental verification.

At this point it is well to pause and list the assumptions that are necessary in order to obtain Eqs. (3.4) and (3.5). These are:

(i) All modes excited, including the uniform precession, have the same ellipticity and resonant frequency (i.e., A_k and ω_k are independent of k .)

(ii) The inhomogeneity scattering processes are such that either

(a) only spin modes having a narrow range of k , and hence of η_k are excited, or

(b) there is very tight coupling between S-modes, so that they remain equally populated, even though they may be selectively excited, and may relax intrinsically at different rates.

(iii) Scattering from the uniform precession occurs into a quasi-continuum of spin modes.

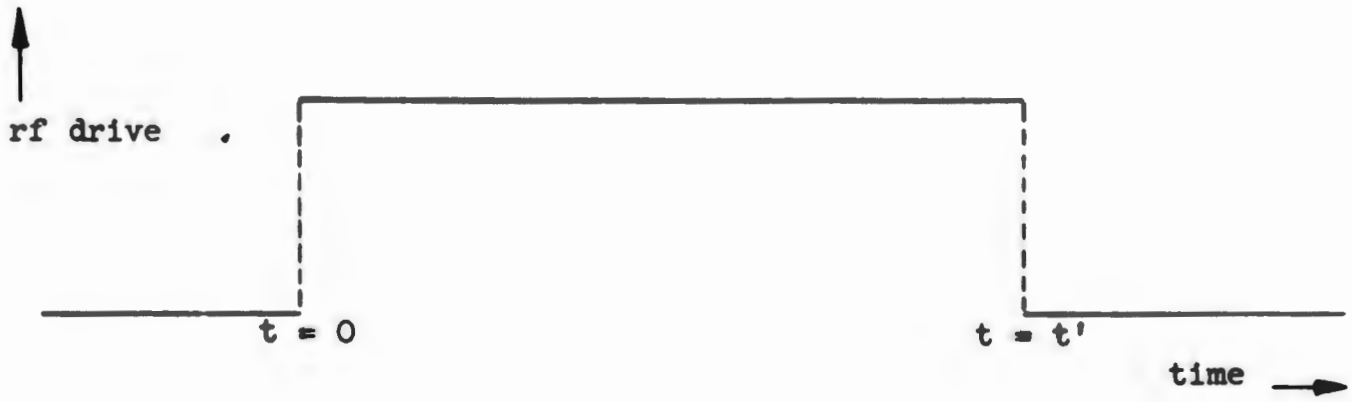

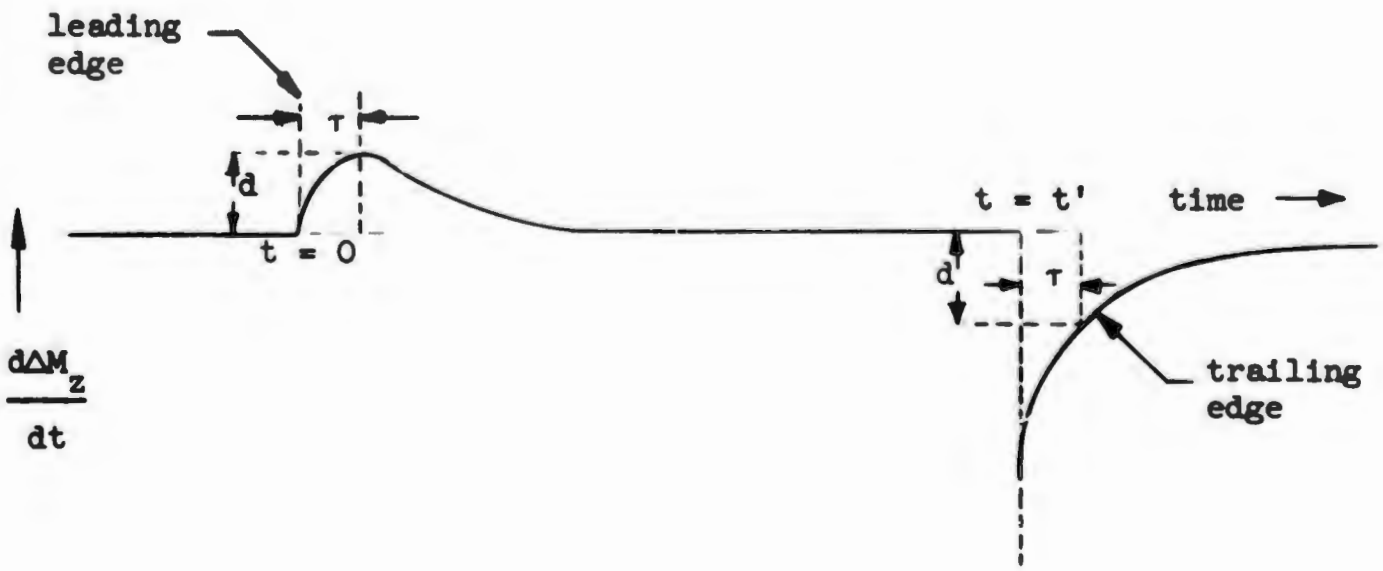

FIG. 3.2--Calculated response of the z-component of magnetization to a rectangular rf pulse.

These assumptions, in effect, are equivalent to lumping all the spin modes into a single mode which, however, has the rather peculiar property that it is unidirectionally coupled to the uniform mode, i.e., energy flows only from the uniform mode to the composite spin mode, and not vice versa. Under these circumstances, Fig. 3.1 actually reduces to the much simpler form shown in Fig. 3.3. This procedure of lumping all the spin modes together into a single mode is supported by experiment, as we shall discuss in detail later. Although we have justified such a step theoretically only for two particular assumptions concerning the inhomogeneity scattering, it is almost certainly more general than this, and is probably valid whenever the S-modes, among which the scattering occurs, form a quasi-continuum. In more general cases, however, the measured value of η_k will probably be a complicated average of the intrinsic relaxation rates for all the S-modes.

B. DETERMINATION OF THE RELAXATION PARAMETERS FROM THE dM_z/dt WAVEFORM

The voltage induced in a coil placed near the sample so as to couple to the z-component of magnetization will be proportional to $d\Delta M_z/dt$. From the waveform of this voltage the relaxation parameters may be deduced by fitting the experimental data to Eqs. (3.6) and (3.7). This curve fitting is rather tedious in general, because of the fact that $d\Delta M_z/dt$ contains contributions both from the uniform precession and from the spin modes. It becomes much simpler, however, for the special case that $\eta_{2L} \gg \eta_k$, for then we are left, after a sufficient time, with a trailing edge waveform that contains only the single exponential $\exp(-2\eta_k t)$, from which η_k may be deduced at once. By definition we have $\eta_{2L} = \eta_0 + \eta_R + \eta_0'$, so that for highly polished single crystals of garnet at room temperature the relative relaxation rates are such that $\eta_0 \sim \eta_k > \eta_0'$; it is evident that in the absence of radiation damping ($\eta_R = 0$) the inequality cannot generally be satisfied for such samples. However, by careful application of the circuit coupling theory developed in Part II, we have found that it is possible to make η_R sufficiently large so that the inequality is satisfied. In terms of Figs. 3.1 or 3.3, by this novel procedure we can ensure that the uniform mode has dropped down essentially to the lattice level before the spin modes have had a

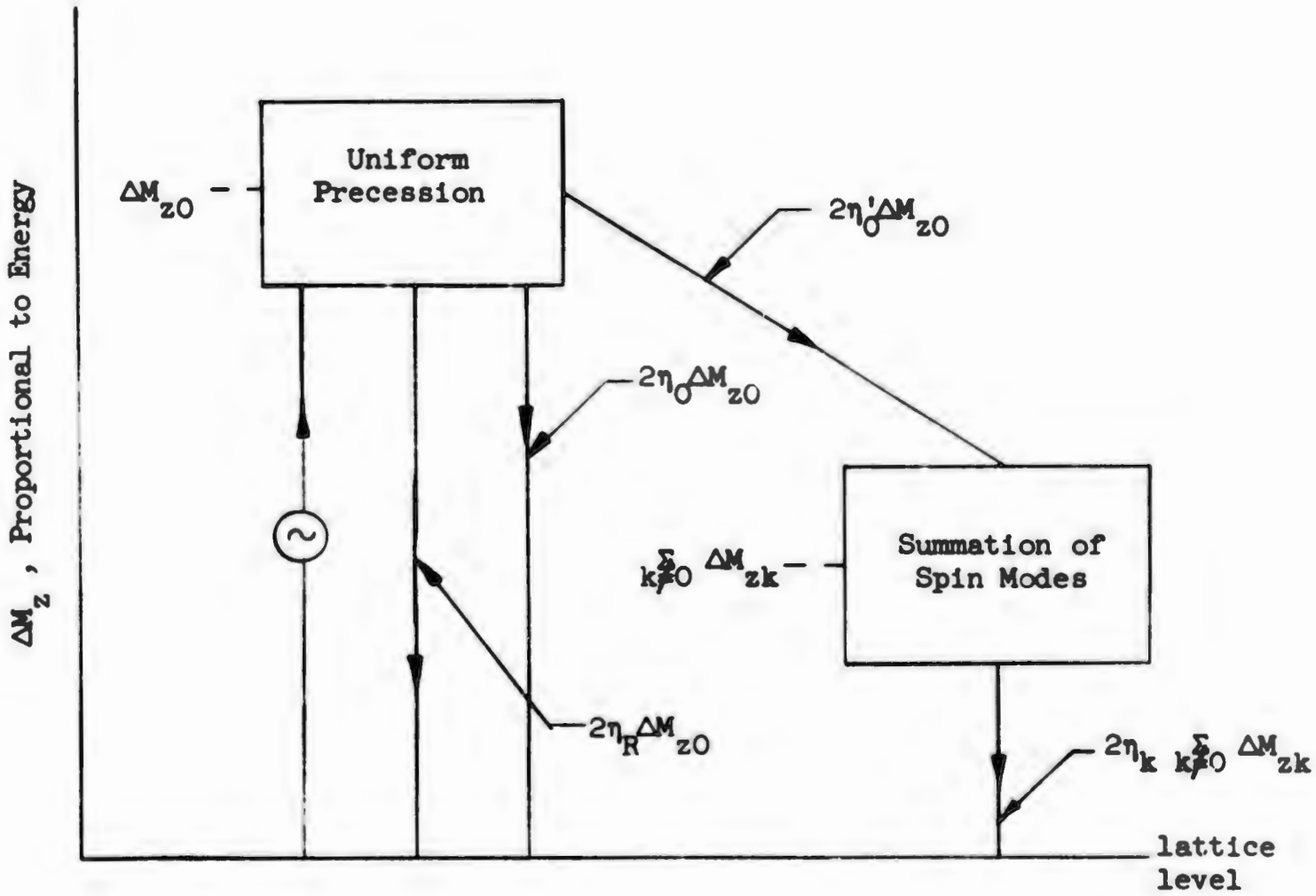

FIG. 3.3--Flow chart for case where all the spin modes may be lumped into a single mode.

chance to decay appreciably. In such a process, we make explicit use of the fact that it is only the uniform precession which interacts with the microwave fields. Since in most polycrystaline materials the relaxation parameters are such that $\eta_0' \gg \eta_k$, [16] radiation damping is not required to achieve the inequality $\eta_{2L} \gg \eta_k$ for these materials.

An important advantage of this technique is that it is applicable at power levels where there is appreciable nonlinear coupling between the uniform precession and the spin modes, because these nonlinear coupling terms, being proportional to various powers of the uniform precession amplitude, disappear rapidly, along with the uniform precession, in the presence of strong radiation damping, allowing the spin modes to decay freely. Of course, at sufficiently high levels of drive, the spin modes themselves may be excited to levels where nonlinear interactions make important contributions to their relaxation. In such a case, although one would not expect to get a simple exponential defining a unique relaxation rate, interesting information can nonetheless be obtained with the present techniques.

CHAPTER XV

PRACTICAL CONSIDERATIONS IN THE MEASUREMENT OF THE TRANSIENT BEHAVIOR OF THE MAGNETIZATION

Four main considerations are involved in the development of a practical system for studying the transient behavior of the z-component of magnetization:

(1) coupling to ΔM_z in such a way as to minimize the unwanted interaction with the microwave components of field and magnetization;

(2) amplification and presentation of the small signals produced by the coupling to ΔM_z ;

(3) production of truly rectangular rf pulses, and

(4) design of suitable microwave circuitry.

We shall consider each of these questions in turn.

A. COUPLING TO M_z

The most difficult problem has been to couple to the z-component of magnetization tightly enough to obtain a measurable signal without at the same time altering the relaxation processes in any essential way

through interaction with the transverse component. In our early experiments, the sample was placed in the center of a loosely-wound solenoidal coil whose axis was parallel to the dc field, a configuration similar to that used by Farrar. Such an arrangement was unsatisfactory for three reasons:

(i) The coil severely distorted the rf drive field, resulting in the direct excitation of magnetostatic modes. In the equivalent circuit of Fig. 1.1, this is describable in terms of an additional coupling, $M_{gk''}$, between the generator and the sample.

(ii) The presence of the coil also distorted the precessional path of the magnetization, resulting in unwanted coupling between the uniform mode and the magnetostatic modes, (the appearance of a coupling term $M_{gk''}$ in Fig. 1.1).

(iii) Finally -- although this effect was largely masked by the preceding two -- radiation damping produced by the coil resulted in an increase in the effective spin-lattice relaxation rate of the uniform precession.

From the results of these preliminary experiments and the later published work of Fletcher, et al.,[8] it became evident that to avoid these deleterious effects the pickup coil had to be very thin in a direction perpendicular to the applied rf drive field (to avoid field distortion), axially symmetric with respect to the dc field (to avoid distorting the precessional path), and accurately adjusted so as to be coplanar with the transverse magnetization. One design satisfying these requirements is shown in Fig. 3.4. It consists of a one-turn "loop" punched from copper foil 0.00018" thick, and sandwiched between two blocks of polystyrene. This assembly was then mounted on a brass plate, the leads projecting through a thin slot. To avoid the wall effects discussed in Part II, the center of the loop was spaced 1.5 mm (about two sample diameters) from the plate, which then formed part of the waveguide wall.

In many of our experiments the output from a single turn loop was inadequate, so another loop was constructed in which the foil was replaced by a 7-turn spiral coil formed from 0.001" diameter insulated copper wire, as shown in Fig. 3.5. In both of these cases the samples were mounted individually in polystyrene tubes, which could then be inserted into the block supporting the coil. In this way, it was possible not only to change samples readily, but also to center each one carefully within the coil.

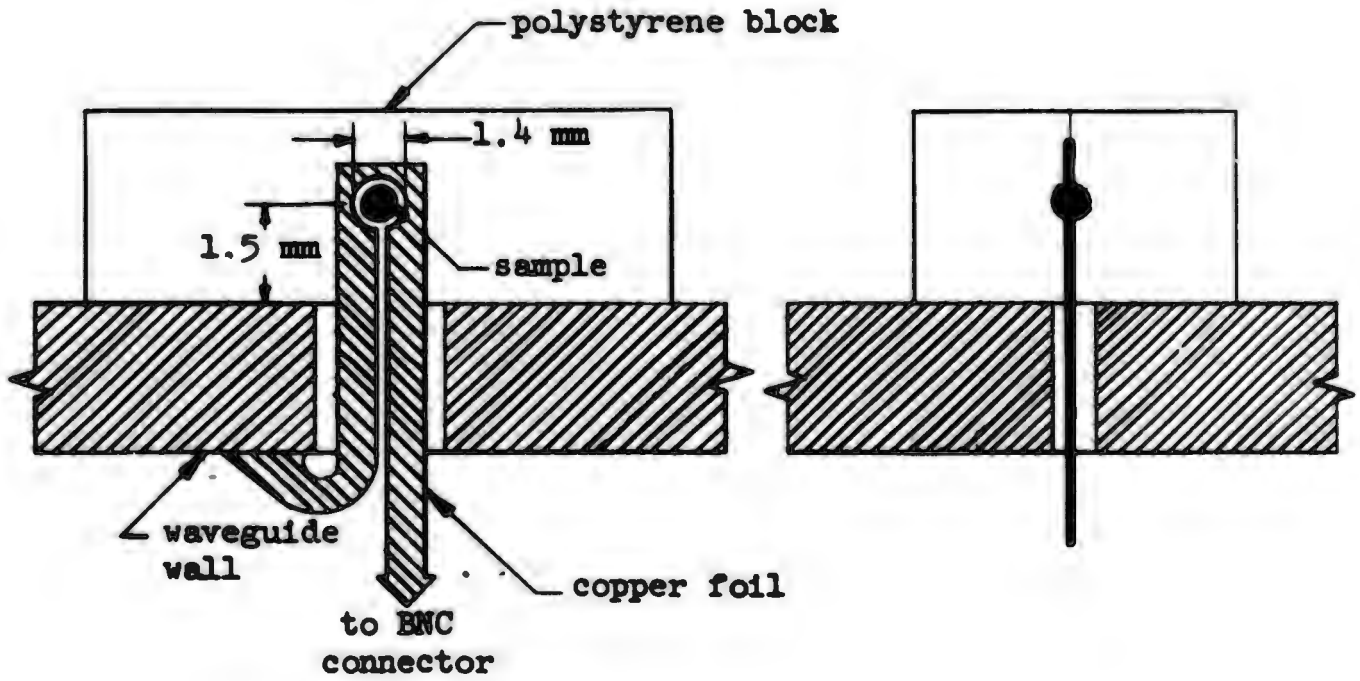

FIG. 3.4--Single-turn loop for coupling to M_z .

FIG. 3.5--Multi-turn loop for coupling to M_z .

As one would expect, the single turn foil loop was superior to the multi-turn spiral as far as the suppression of unwanted interactions was concerned. In the case of the single turn loop there was no evidence that magnetostatic modes were being excited, either directly, or via the uniform precession -- these conclusions being based on the fact that only a single, symmetrical, Lorentzian-shaped line was observed at all frequencies. With the multi-turn loop, some coupling between the uniform mode and another magnetostatic mode was observed, producing an asymmetrical resonance line, such as is shown in Fig. 3.6, at certain frequencies. However, since the magnetostatic mode tuned with dc field at a different rate than the uniform precession, it was always possible to choose the operating frequency so as to eliminate the unwanted coupling.

Despite careful construction and orientation, however, it was found that both loops broadened the uniform precession resonance line to some extent, an effect equivalent to an increase in the spin-lattice loss rate of the uniform mode.[1] This broadening was found to be 0.10 to 0.15 oersteds, and was about the same for both loops. The additional loss did <u>not</u> result simply from a direct coupling of the loop to the transverse component of magnetization, such as would be produced, for example, if the loop were canted slightly out of the transverse plane. Such loading would be strongly dependent on the impedance terminating the loop. By careful orientation of the loop it was possible to make the observed resonance line completely independent of the loop termination over the full range from open to short circuit. Any remaining broadening must then be due to purely local interactions between the sample and adjacent conductors. Such interactions could be decreased, of course, by increasing the diameter of the loop relative to that of the sample, at the expense of a decreased video signal. Since in our experiments we have been interested primarily in measuring η_k and η_0', rather than η_0, the additional damping, once understood, could be tolerated.

---

[1] An increase in the scattering parameter η_0' would also broaden the line, but it may be assumed that the field inhomogeneities produced by the loop are on too large a scale to excite spin waves. The modes so excited, as pointed out in the previous paragraph, fall in the discrete, magnetostatic-mode part of the spectrum.

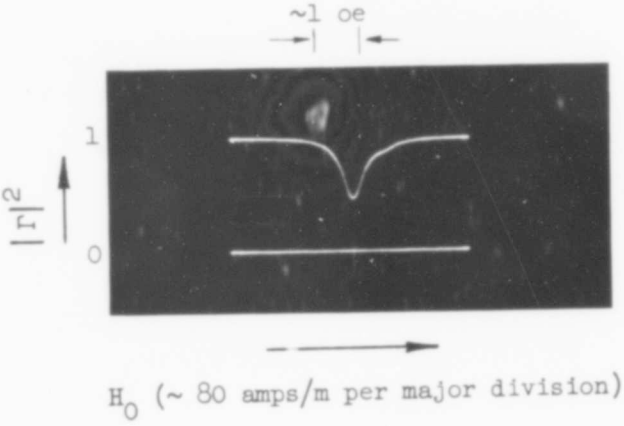

FIG. 3.6--Resonance line of sample in loop, showing asymmetric response produced by coupling to magnetostatic modes.

B. AMPLIFICATION AND PRESENTATION OF VIDEO SIGNALS

If a spherical sample of radius "a" is placed in the center of a circular loop of radius R, with its axis in the z-direction, the voltage induced in the loop by a changing magnetization is given, in the magnetostatic approximation, by

$$E = \mu_0 \frac{2\pi}{3} \frac{a^3}{R} \frac{dM_z}{dt} \quad . \tag{3.8}$$

We are interested primarily in that part of ΔM_z that decays at a rate $2\eta_k$, for which, according to Eq. (3.7),

$$\frac{d\Delta M_z}{dt} \approx - 2\eta_0' \hat{\Delta M}_{z0} e^{-2\eta_k t} \quad , \tag{3.9}$$

provided that $\eta_{2L} >> \eta_k$. Since $\hat{\Delta M}_{z0}$, being proportional to the square of the amplitude of the uniform mode, is limited by the unstable growth of spin waves to relatively small values,[1] the voltages induced in a practical loop will be small. As a numerical example, for a spherical sample 35 mils in diameter having $\eta_k = 6 \times 10^6$ sec^{-1}, and $\eta_0' = 3 \times 10^6$ sec^{-1}, the peak voltage induced in a circular loop of diameter 55 mils is about 45 μ volts. Since in practice $\Delta\hat{M}_{z0}$ must be restricted to values substantially less than the saturation value, in order to remain in the small signal region, the actual video voltage available from a single turn will be only a few microvolts for any measurements made in the small signal range. The signal voltage may be increased by using a multi-turn loop or an appropriate step-up transformer, although, because of bandwidth considerations, the process cannot be continued indefinitely. Some of the factors involved in obtaining the optimum signal to noise ratio for a given video bandwidth are discussed in Appendix C.

---

[1] The maximum amplitude of the uniform mode is (Ref. 21) $(b_0)_{max} = \sqrt{2\eta_k/\omega_M}$, so that from Eq. (1.14) (Part I) it follows that $(\Delta M_{z0})_{max} = \eta_k/\mu_0\gamma$.

Experimentally, the best results were achieved using a 7-turn pick-up coil (Fig. 3.5) and a specially constructed battery-operated transistor video amplifier with a noise figure of 8 db, an input impedance of 100 ohms and a maximum bandwidth of 30 Mc. The use of transistors in this application was of fundamental importance, for it allowed the amplifier to be placed, in a fully shielded enclosure, in the dc field immediately adjacent to the pick-up loop. It was only by such drastic measures that stray pick-up could be eliminated, and the low-noise capabilities of the system realized.

Even under optimum conditions, the signal to noise ratio in small-signal experiments on highly-polished single crystals (where η_C' is small) is inherently low. Fortunately, however, it is possible to extract a considerable amount of information from relatively noisy signals by using the integrating properties of cathode ray tube screens and photographic film. The procedure generally adopted was to photograph the oscilloscope display and, by examining the photograph carefully under a traveling microscope, construct a semi-logarithmic plot of the decay. In this way time constants, reproducible within 5%, could be obtained under circumstances where the signal to noise ratio was ten or even less. In effect, the noise bandwidth of the system was reduced by taking advantage of the repetitive nature of the signal.

C. PRODUCTION OF FAST RF PULSES

In order to obtain useful information from a transient study of the spin system, it is necessary to use rf drive signals with rise and fall times substantially shorter than the shortest relaxation time encountered -- in our case about 10 nsec. Furthermore, since such fast pulses imply broad-band microwave circuitry, the rf source must be capable of moderate power output in order to obtain adequate drive fields at the sample. Because conventional klystrons and magnetrons are not capable of producing sufficiently fast pulses, a medium power broad-band traveling-wave tube, with a saturation power output of 3 watts c-w, was used. The traveling-wave tube was driven, through a semiconductor rf switch, by a low-power reflex klystron. A block diagram of the setup is shown in Fig. 3.7a. The heart of the apparatus is a two-section semiconductor switch[49-51] used

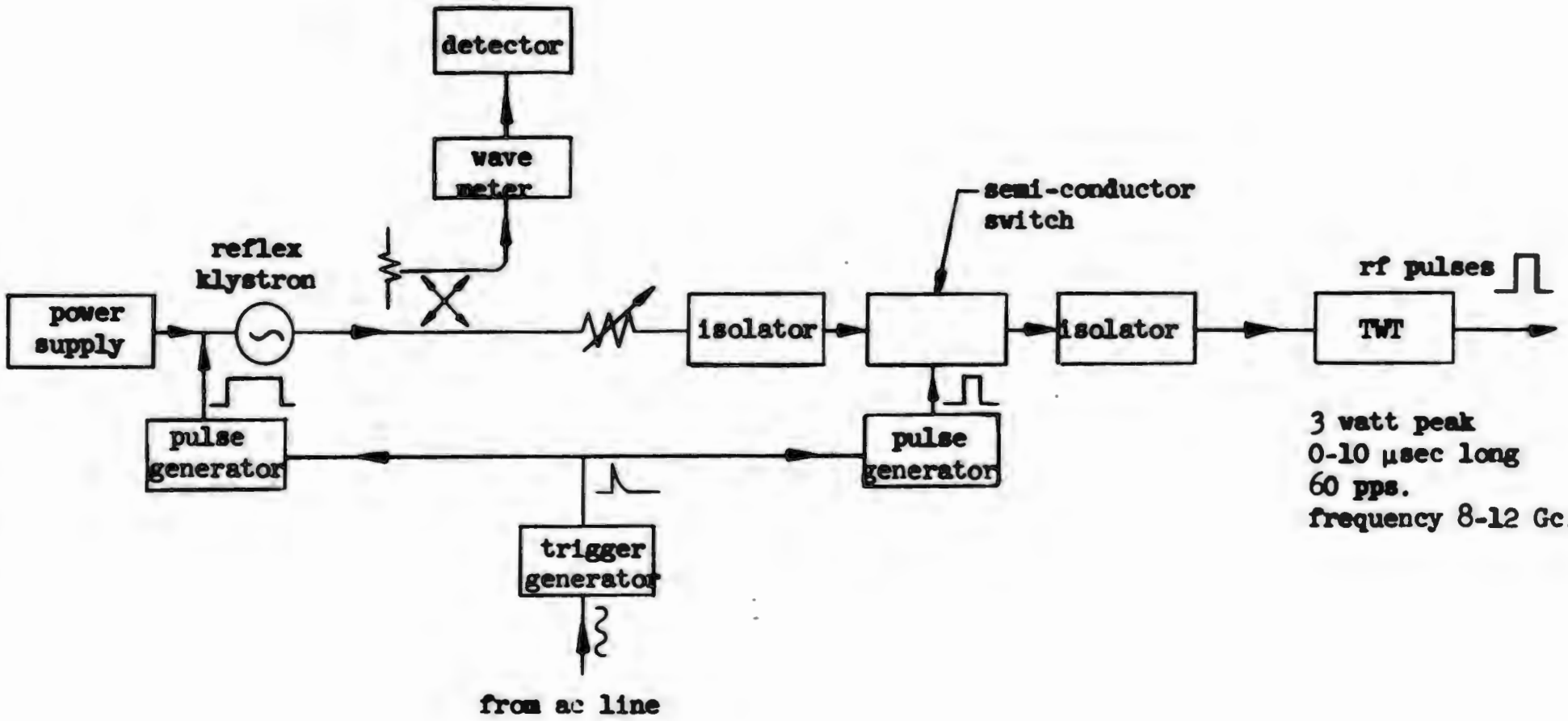

FIG. 3.7a--Block diagram of system for generation of fast microwave pulses.

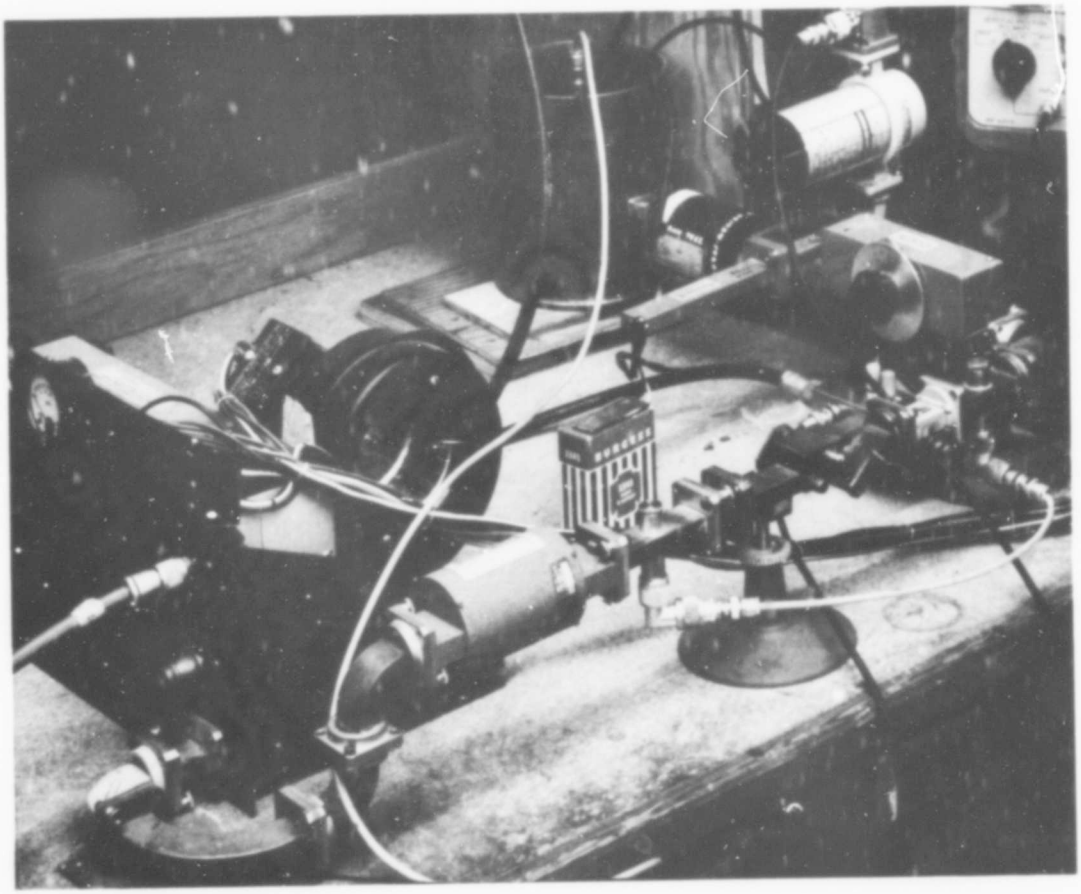

FIG. 3.7b--Apparatus for generation of fast microwave pulses.

to provide the fast rf pulses which are then amplified by the traveling-wave tube. Each switch section consists of a 1N3093 germanium diode mounted in a conventional waveguide transmission crystal mount. Switching action results from the strong dependence of the rf impedance of the crystal on its dc bias. Such a switch is inherently very fast (rise time < 2 nsec) , and requires little switching power (a conventional laboratory pulse generator may be used). A schematic diagram of the switch and its associated circuitry is shown in Fig. 3.8. When phased for optimum operation, the switch had an insertion loss of about 3 db and a switching ratio of 38 db. The switching speed was about 5 nsec, determined solely by the 20 nsec rise time of the pulse generator used to drive the switch.(1)

The driver klystron could have been operated continuously, but it was found more convenient to pulse modulate it with a pulse much longer than that applied to the switch, and then select a relatively short section from the center of this pulse to be amplified by the traveling-wave tube. In this way the stability associated with c-w operation could be effectively realized, and at the same time, the presence of modulation allowed the driver to be monitored, and the phasing of the semiconductor switch adjusted for optimum performance. Pulsing the driver also reduced the average power dissipated in the semiconductor switch, thus prolonging the life of the diodes. To avoid the effect of 60 cycle ripple on any of the supply voltages, the system was triggered directly from the ac line.

When adjusted for correct operation, the system was capable of producing rf pulses of variable length having a peak power of 3 watts, rise and fall times of 5 and 9 nanoseconds, respectively, and a minimum of frequency and amplitude modulation. Such pulses are very close to the ideal rectangular pulses which were assumed in the solution of the equations of motion for the magnetization, although we have not exploited these properties to the full in our experiments, which made use primarily

---

(1) A useful feature of the switch is that the diode nonlinearity results in the production of rf pulses considerably faster than the dc switching pulse.

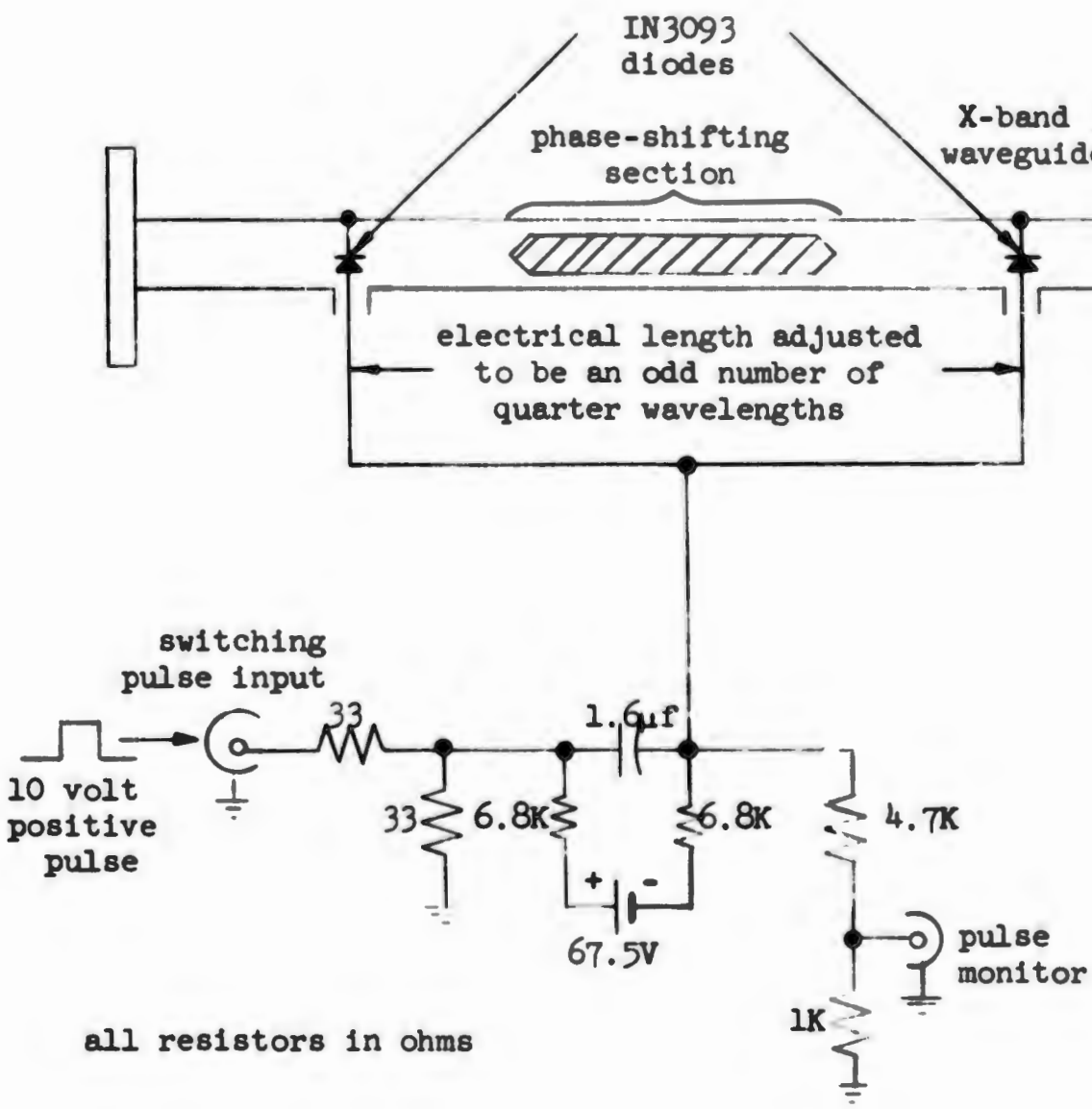

FIG. 3.8--Schematic diagram of semiconductor switch.

of the rapid fall. A more demanding application would be to the study of the transient behavior of the transverse component of magnetization in the nonlinear region, where the freedom of the pulse from frequency and amplitude modulation, particularly near the leading edge, would facilitate the study of such phenomena as spin wave build-up times. In such studies it is essential that the driving pulse be truly rectangular if any analytical progress is to be made.

D. MICROWAVE CIRCUITRY

The experiments were carried out in a shorted section of X-band rectangular waveguide, with the sample being mounted on the shorting plate, in the middle of the waveguide cross-section, as shown in Fig. 3.9. Extra radiation damping, when needed, was obtained by placing an iris in front of the sample so as to form a $TE_{1,0,2}$ reflection cavity of low external Q, resonant at the operating frequency. A small-signal equivalent circuit for this configuration is simply:

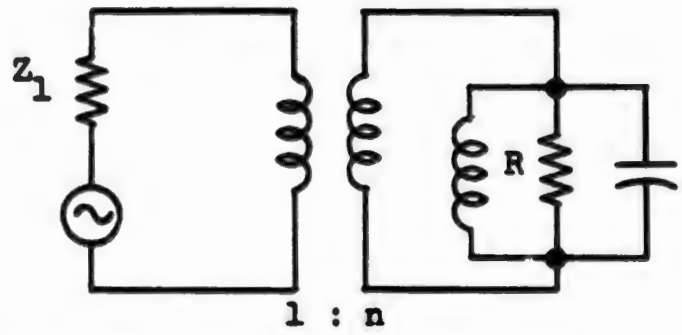

where, according to the results of Part II, the normalized shunt impednace of the ferrite is given by

$$\frac{R}{Z_1} = \frac{2\pi V_s}{ab\lambda_t} \frac{\omega_M}{\eta_0 + \eta_0'} \quad . \tag{3.10}$$

For a $TE_{1,0,2}$ cavity the turns ratio is given by

$$n^2 = \pi \left(\frac{\lambda_t}{\lambda_0}\right)^2 \frac{1}{Q_{ext}} \quad , \tag{3.11}$$

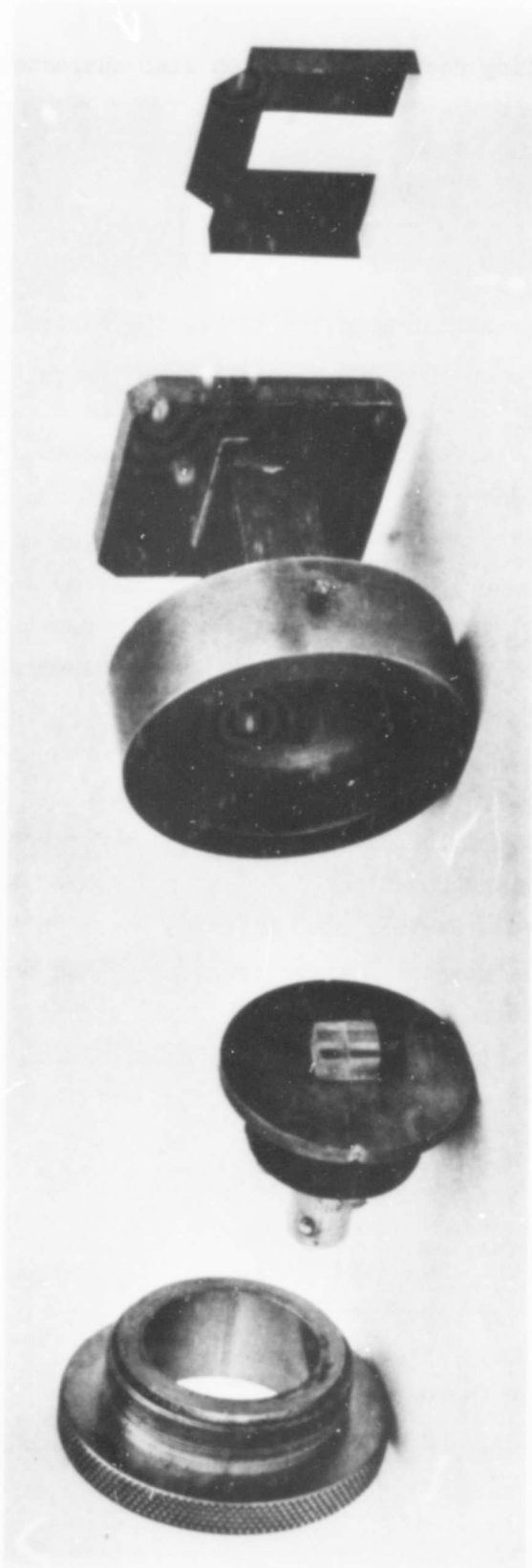

FIG. 3.9--Mounting of sample in microwave circuit.

so that for the coupling coefficient, which also characterizes the radiation damping, we obtain

$$\beta = \frac{R}{n^2 Z_1} = \frac{2V_s}{ab\lambda_t} \frac{\omega_M}{\eta_0 + \eta_0'} \left(\frac{\lambda_0}{\lambda_t}\right)^2 Q_{ext} \quad . \qquad (3.12)$$

The samples used were sufficiently large that the desired coupling ($\beta \sim 5$-10) could be obtained with cavities whose Q's were low enough not to interfere with the rapid rise and fall of the rf driving pulse.

In practice, it was found that the coupling obtained was somewhat greater than that predicted by Eq. (3.12), an effect due to the relatively massive polystyrene block in which the sample was mounted,[1] which tended to concentrate the rf fields in the vicinity of the ferrite. For samples mounted in polyfoam, the agreement between the theoretical and measured coupling coefficients is quite good, the discrepancy never being more than 10%.

A block diagram of the experimental setup is shown in Fig. 3.10a. In selecting the components, an effort was made to obtain a broadband match looking back from the sample cavity towards the generator. Aside from this, the arrangement is quite conventional. That portion of the circuit enclosed by the dotted lines was used only for power calibration purposes, the procedure being to compare a known fraction of the peak pulse power with a carefully measured c-w signal. For small-signal measurements of the transverse component of magnetization, the precision directional coupler was replaced by a slotted line, so that detailed impedance measurements could be made.

CHAPTER XVI

EXPERIMENTAL RESULTS FOR SINGLE CRYSTAL YTTRIUM IRON GARNET

That portion of our experimental program dealing with relaxation measurements had two main objectives:

(i) to establish the validity of the transient procedures discussed in the previous chapter, and gain familiarity with the experimental technique, and then

---

[1] It was originally intended to machine off the excess polystyrene once the loop was mounted. One such attempt, however, ended in disaster, and since good loops were difficult to make, it was decided not to tempt fate further.

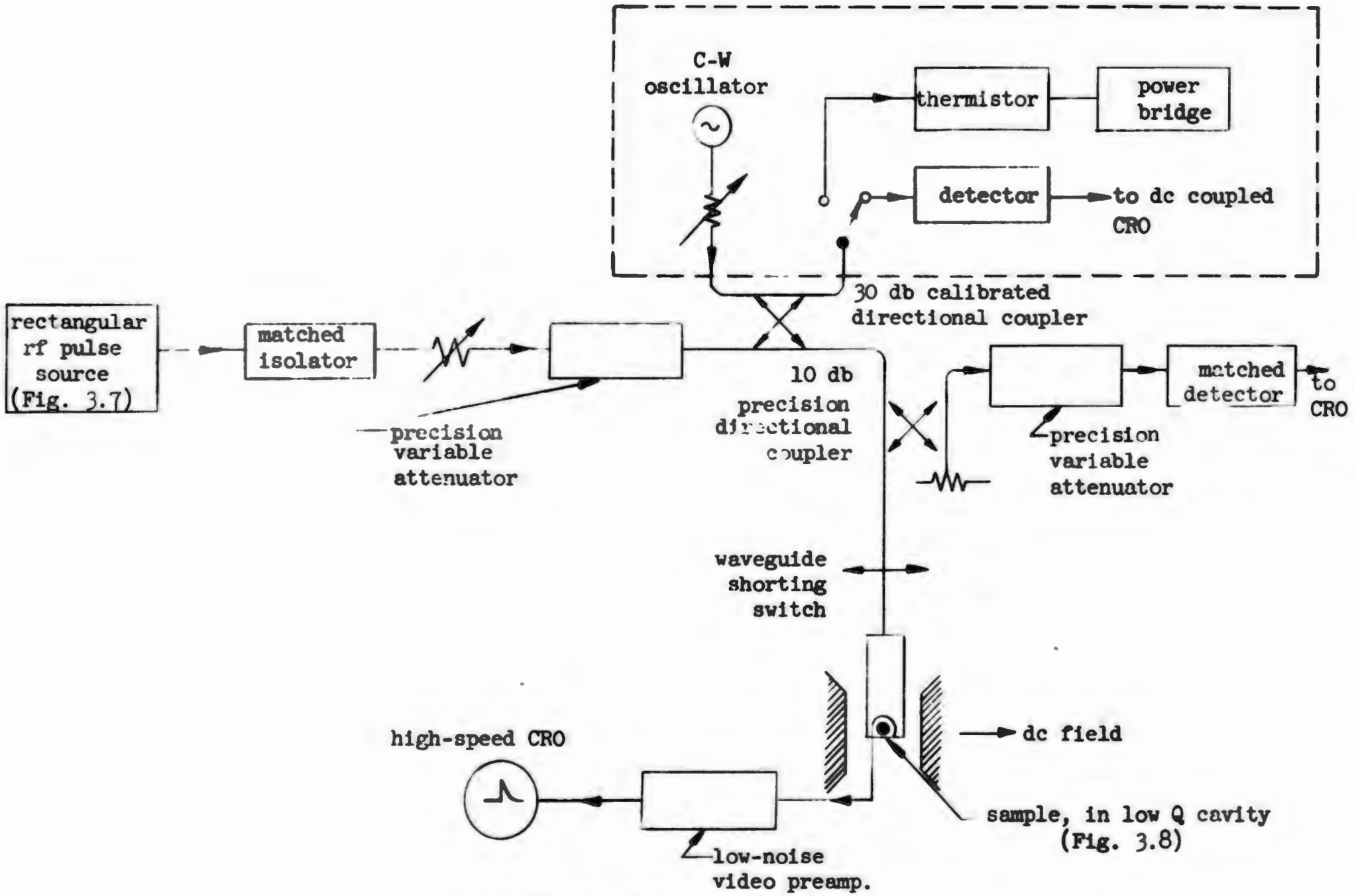

FIG. 3.10a--Block diagram of test set-up.

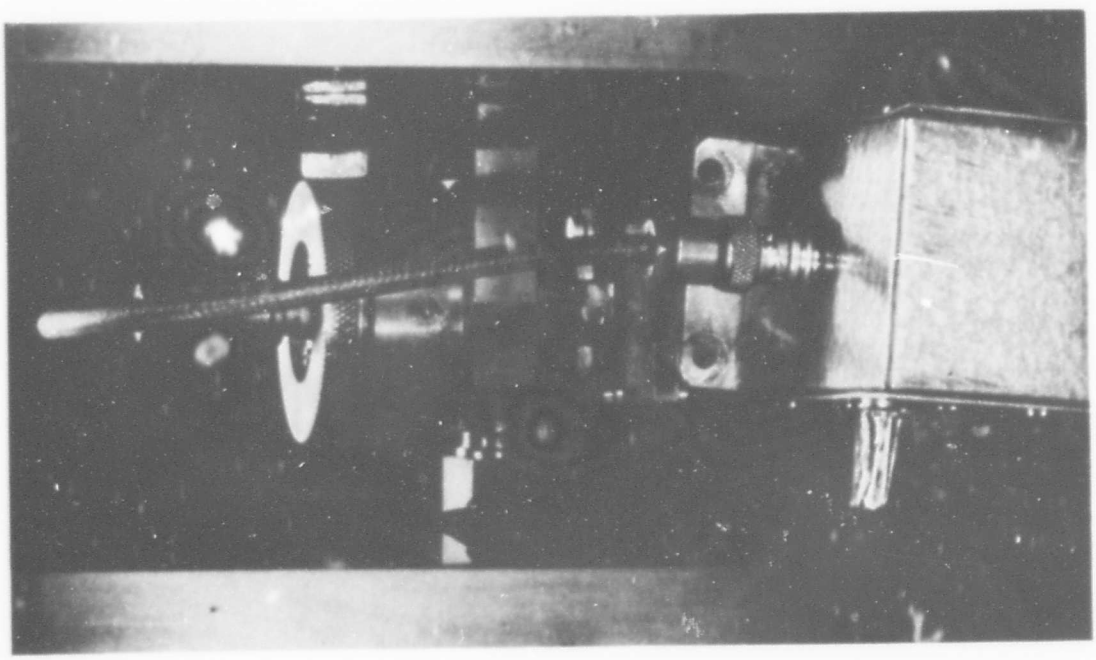

FIG. 3.10b--Arrangement of apparatus in magnet.

(ii) to extend the direct relaxation measurements into the large signal region which hitherto has been inaccessible.

Our transient procedure is based on an equation of motion first derived, in the form we have used it, by Fletcher et al.,[8] who also carried out a comprehensive set of small signal experiments, the results of which seem to support the theory. Nonetheless, some objections have recently been raised[52] concerning the validity of these equations of motion, so that it was felt that an independent and more direct experimental verification was of value. Our experiments, as were those of Fletcher et al., were carried out on single crystals of yttrium iron garnet, thus enabling us not only to compare the observed transient response of the magnetization with the theory developed in Chapter XV, but also to compare our values for the relaxation parameters with those obtained by Fletcher et al.

Because the techniques that we have developed are of quite general applicability, we have tried in what follows to present the essential features in sufficient detail to enable similar measurements to be carried out with different materials or under different conditions.

A. SMALL-SIGNAL MEASUREMENTS

Small-signal measurements were made on polished single-crystal spheres of yttrium iron garnet, ranging in diameter from 0.5 to 1.25 mm. The samples were prepared by the air-tumbling technique,[53] final polishing being done using Linde A abrasive powder. The most complete set of measurements was made at 9.0 Gc on a sample 0.898 mm in diameter, and having a linewidth of 82 amps/m, (≈1 oe.) and which we designate hereafter as sample MC-20. At the time these measurements were carried out, the x-ray facilities necessary to establish the directions of the crystal axes were not available to us, so that the measurements were made with an arbitrary orientation of the sample with respect to the dc field, although care was exercised to maintain the same alignment for all measurements. The dependence of the relaxation parameters on crystal orientation for YIG is not particularly pronounced, so that this omission, while complicating some hat the numerical comparison of our results with those of other experimenters, does not affect the validity of the conclusions we draw.

1. Measurement of η_k

The relaxation rate of the spin modes was measured using the configuration of Fig. 3.9, with the iris selected to provide a coupling coefficient of 5.45. In Fig. 3.11 is shown the voltage induced in the pick-up loop by the free decay of the magnetization. The incident power was about 40 milliwatts, low enough to avoid nonlinear effects.[1] Just visible at the left of the photograph is a portion of the large spike produced by the decay of the uniform precession, with a time constant, determined almost completely by the radiation damping, of about 8 nanoseconds. The much longer tail results from the decay of the spin modes. Figure 3.12 is a semilogarithnic plot made from the photograph. The tail of the curve is seen to be characterized quite accurately by a single time constant $\tau = 116 \pm 5$ nanoseconds. By averaging many such determinations,[2] a value of $4.31 \pm 0.15 \times 10^6$ sec^{-1} was obtained for $\eta_k = 1/2\tau$. Similar values were obtained for other samples made from the same batch.

2. Measurement of η_0'

According to Eq. (3.7), the relative amplitude of the two decaying exponentials appearing in Fig. 3.11 is a measure of the scattering parameter η_0'. In the presence of strong radiation damping, however, the rapid decay of the uniform mode is masked by the finite response time of the video system. Much more accurate information can be gleaned by studying the transient behavior of the magnetization at the leading edge of the rf pulse, using a minimum of radiation damping. Under these circumstances dM_z/dt grows relatively slowly from its initial value of zero, as shown in Fig. 3.2, producing a video signal whose frequency components lie well within the capabilities of the detection equipment.

---

[1] At this drive level the susceptibility had actually declined about 0.5% from its small signal value. Subsequent measurements showed, however, that the values obtained for η_k were independent of input drive until the saturation of the resonance became quite pronounced (see Fig. 3.18).

[2] Figure 3.11 was taken with an unnecessarily large bandwidth which does exhibit conclusively, however, the separate contributions of the uniform precession and the spin modes to the total z-component of magnetization. Subsequent determinations were made using a reduced bandwidth and hence better signal to noise ratio (cf Fig. 3.17).

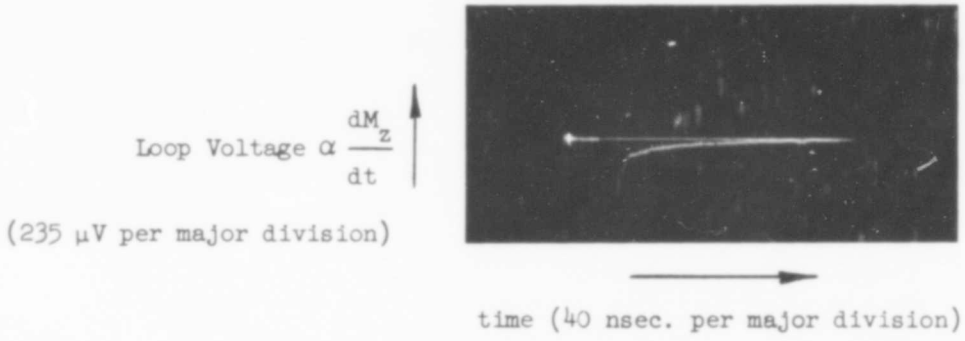

FIG. 3.11--Radiation damped decay of magnetization.

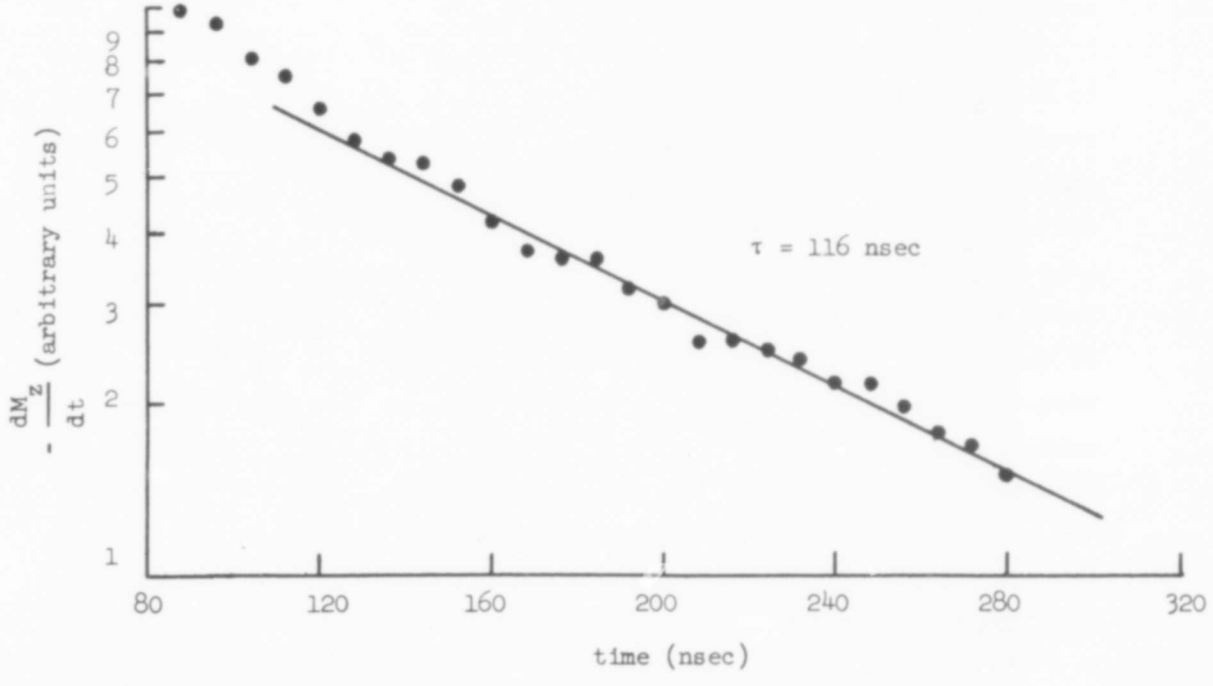

FIG. 3.12--Semilog plot of tail of Fig. 3.11.

In our geometry, the minimum radiation damping was obtained by removing the iris, thus reducing the coupling roughly to unity. Still less coupling would have been desirable, but with this sample this could have been achieved only by going to a completely different circuit configuration, a procedure not considered worthwhile. The small-signal response of the z-component of magnetization is shown in Fig. 3.13. The power level was about 3 db less than that required to produce an observable (0.1%) decline in χ'' . A value for η_0' was obtained by curve-fitting Eq. (3.6) to the $d\Delta M_z/dt$ waveform produced at the leading edge of the rf pulse, assuming for η_k the value obtained previously from Fig. 3.12. The result was $\eta_0' = 1.65 \pm 0.15 \times 10^6$ sec^{-1} . From the observed linewidth of 82 amps/m we find that $\eta_0 + \eta_0' = 9.0 \times 10^6$ sec^{-1} , so that $\eta_0 = 7.35 \times 10^6$ sec^{-1} . The computed curves, together with the experimental points, for the leading and trailing edge waveforms are shown in Figs. 3.14 and 3.15, respectively. The fit is seen to be excellent, except in the immediate vicinity of $t = 0$, where the finite rise and fall times of the rf pulse and the video system produce an appreciable deviation.

In order to fit Eq. (3.6) to the experimental data, it was necessary to assume a value of η_{2L} about 10% lower than that obtained from a steady-state measurement of the loaded linewidth. Such a discrepancy can result from a mismatched generator, or from nonnegligible loss in the microwave circuit in which the ferrite is placed, and is important only in that not knowing the exact value of η_{2L} to begin with greatly increases the labor of curve-fitting. If both η_{2L} and η_k are known at the outset all the exponential factors in Eqs. (3.6) and (3.7) are known so that only the coefficients need be fitted, a relatively simple matter. When one exponent has also to be determined, the computation becomes much more tedious, and if both exponents are unknown initially, the labor involved is generally prohibitive. It is for this reason that the radiation damping technique for obtaining η_k independently of the other relaxation parameters is so valuable.

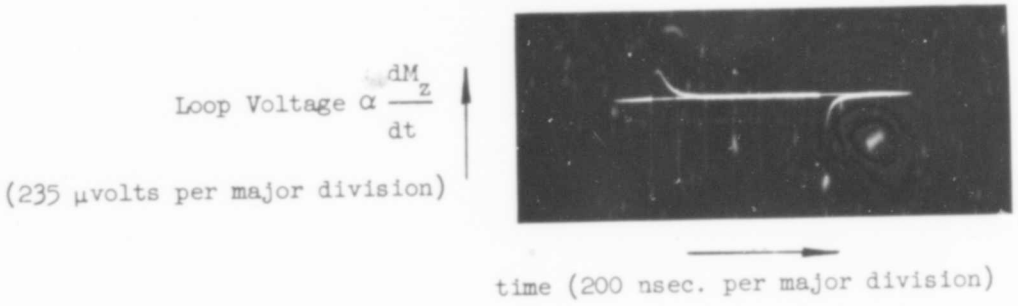

FIG. 3.13--Response of magnetization to a rectangular rf pulse.

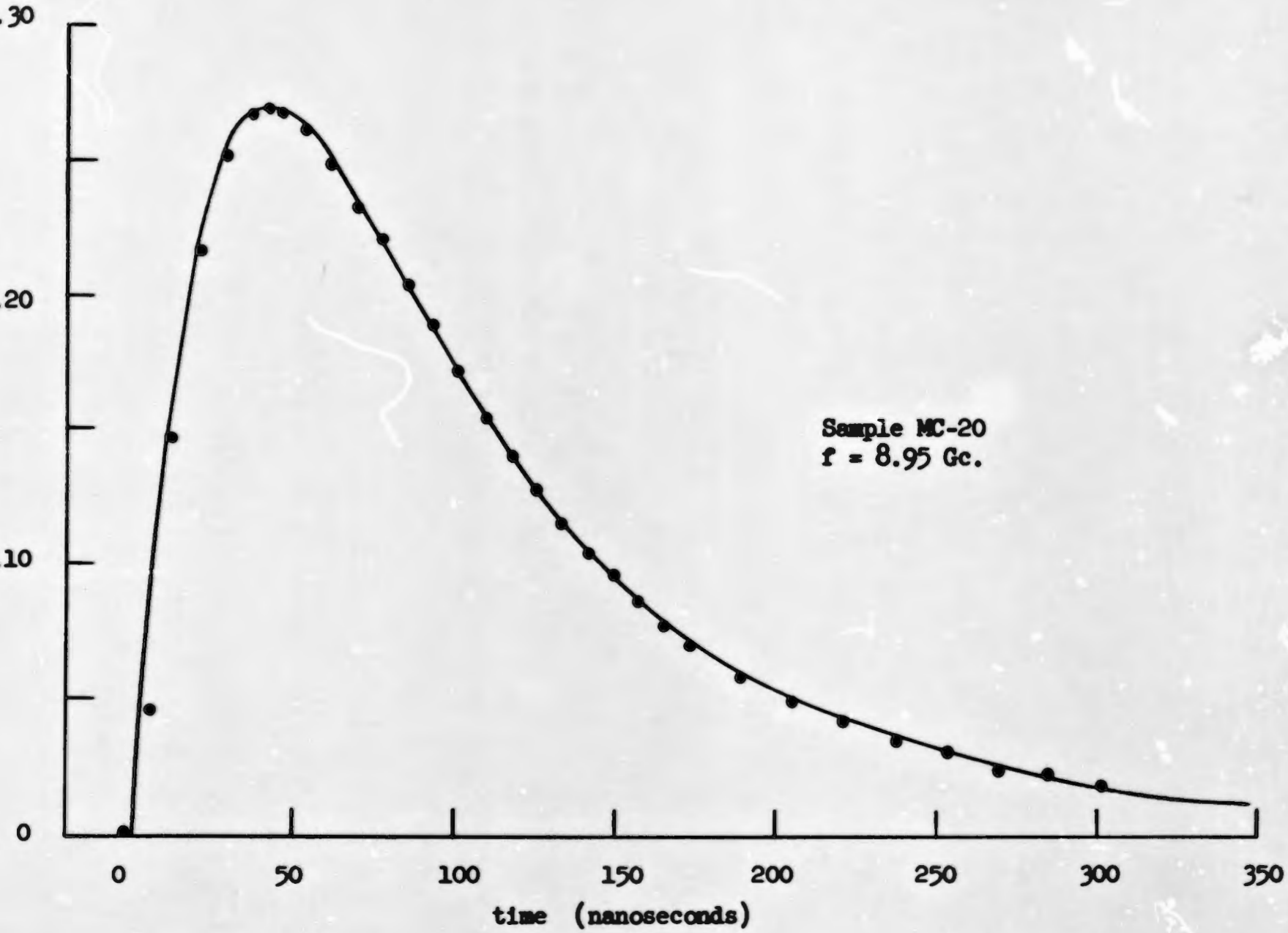

Fig. 3.14--Response of the z-component of magnetization to the leading edge of the rf pulse.

BLANK PAGE

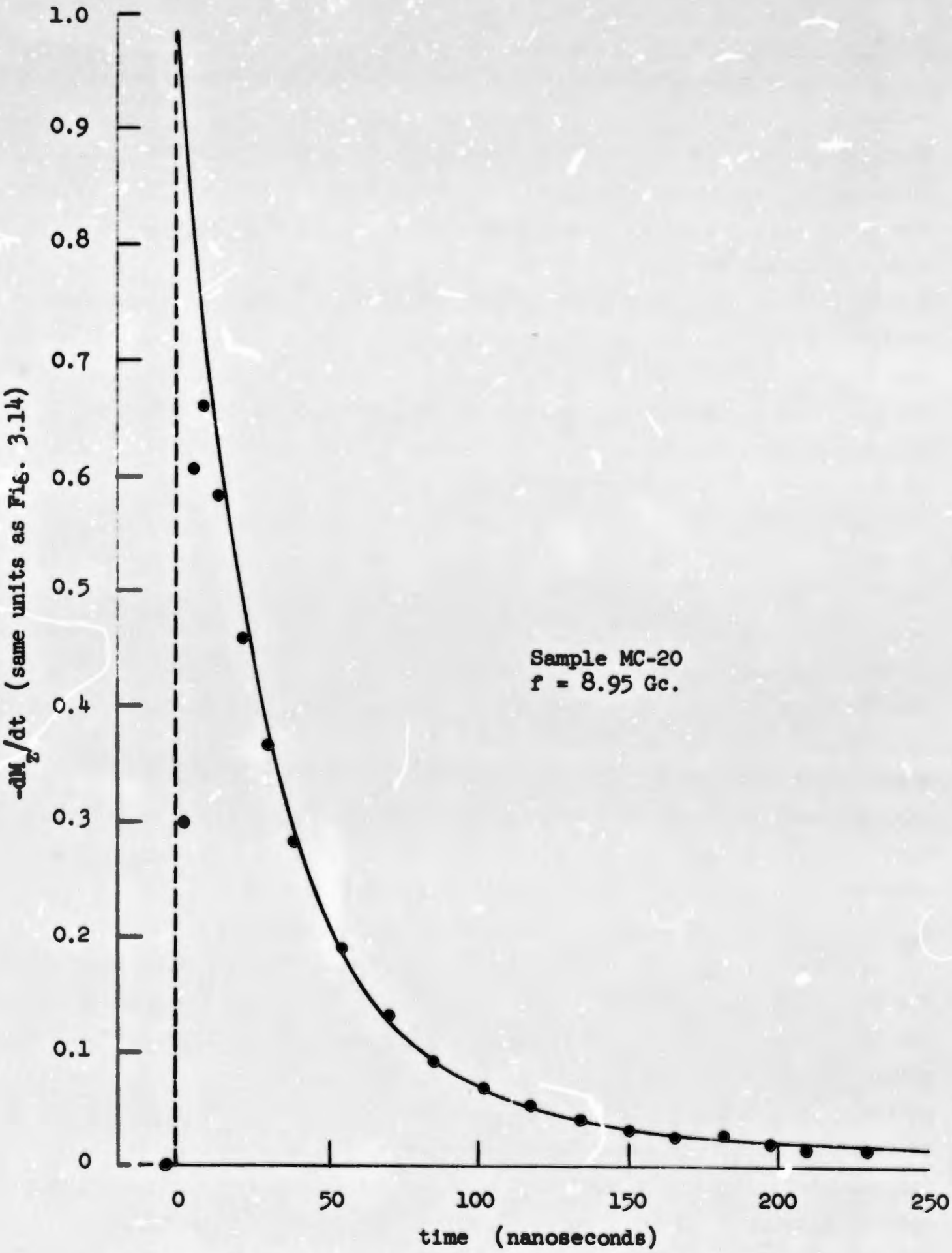

FIG. 3.15--Response of the z-component of magnetization to the trailing edge of the rf pulse.

3. Comparison with Existing Data

The only other complete set of measurements of the small signal relaxation parameters for single-crystal YIG available are those of Fletcher et al.,[8] made at 6.2 Gc on spherical samples oriented with their [111] axes along the direction of the applied field. Their results for their most highly polished sample are compared with ours in Table IV. A meaningful comparison is made difficult by the fact that the two determinations were made at different frequencies, with different orientations of the crystal axes. In addition, the extent to which spin modes are excited by inhomogeneity scattering, as well as the wave vector of the spin modes so excited, is expected to depend strongly on surface polish and disorder in the crystal lattice,[23] and hence on the details of the individual sample preparation.

To compare these two sets of data, we must take up the question of frequency scaling. Some theoretical[5] and experimental[7] results suggest that η_0 should be scaled in direct proportion to frequency. This has been done in Table IV, by scaling the FLS value to our frequency range. In addition, our value has been reduced 10 per cent to account for an observed contribution of the coupling loop to η_0. The parameter η_0' is expected to be independent of frequency, and no scaling of this quantity has been done in the table. For η_k the situation on frequency scaling is unclear at the present time. Existing theories[5,6,7] suggest that there should be two contributions, one proportional to ω, and the other proportional to k and inversely proportional to ω. As a result, η_k has also been left unscaled in the table.

With these adjustments, the only significant difference between the two sets of data is in η_0'. Our sample is seen to have the larger value, and thus evidently, larger inhomogeneity scattering. This is entirely possible, since surface scattering is a sensitive function of sample polish. This could easily be different for the two samples, in spite of the fact that both had a final polish with the same grit size (Linde A, approximately .3 μ). In our sample, surface inspection was limited to optical microscope checks, and as a result the final polish could easily have been less than ultimate for the grit size used.

TABLE IV

COMPARISON OF SMALL-SIGNAL RELAXATION PARAMETERS FOR SINGLE-CRYSTAL YIG
(f = 9.0 Gc.)

	Fletcher et al.	Anderson
η_0	5.25×10^6 sec^{-1}	6.2
η_0'	0.48	1.65
η_k	3.6	4.31

A notable feature of the results in Table IV, on which both sets of data agree, is that η_0 is greater than η_k. This is in contradiction to certain theories which predict a relaxation rate arising from three-magnon processes that is a linearly increasing function of k, which is also borne out in parallel pumping experiments,[7] which would call for η_k greater than η_0. This suggests the existence of further processes which can strongly relax the uniform mode. The presence of rare earth impurities may possibly provide such a mechanism.[54]

B. LARGE SIGNAL MEASUREMENTS

The small-signal measurements discussed in the previous section are important in that they represent independent and direct verification of the spin-mode theory of ferrimagnetic relaxation, and establish techniques which are of universal applicability. Although in the small-signal application the techniques do not provide information that cannot be obtained by other means, this is not true in the large signal region. Here, as indicated previously, the modulation technique is inapplicable, both because of fundamental difficulties in interpreting the results in the light of the nonlinear equations of motion, and the more prosaic problem of excessive average power dissipation in the sample. Thus, in the past, information about the behavior of the spin system at high power levels has been largely restricted to what may be gleaned[8,21,56,58,61] from measurements on the decline of the susceptibility with increasing drive. By using the techniques described in previous sections, we have been able, in addition, to measure directly the spin mode relaxation rates and spin mode amplitudes as a function of rf drive. This information, when combined with that obtained from the susceptibility decline, has provided a much more complete description of the spin system. We shall now consider these measurements in turn.

1. Measurement Procedure

a. Susceptibility Decline. This most basic of all high-power measurements was made in the standard way[8,45,56] by monitoring the power reflection from the sample, at resonance, as a function of the incident power. All measurements were made with the sample in a shorted waveguide or low-Q resonant cavity, using the basic set-up of Fig. 3.10. By increasing the attenuation in the reflected power arm as the incident

power was increased, so as to maintain a constant level at the detector, the absolute value of the reflection coefficient was obtained as a function of the incident power. From this, the coupling coefficient β was deduced, and since β is proportional to χ'', the susceptibility decline curve was obtained at once. By adjusting the coupling so that the sample is close to being critically coupled to the input waveguide, the method becomes quite sensitive, since then the initial small-signal reflection from the sample is small, allowing small changes in the reflection coefficient, and hence susceptibility, to be measured with precision. The susceptibility decline curve obtained in this way for sample MC-20 at 8.95 Gc is shown in Fig. 3.16, in which the normalized susceptibility is plotted as a function of the reciprocal of the rf driving field.[1]

At this juncture, it may be appropriate to digress briefly and mention a practical difficulty which arises when susceptibility decline measurements are made under certain circumstances. This is the presence of instabilities, often in the form of relaxation oscillations, in the power reflected from the sample in some regions of the susceptibility decline curve. Such instabilities have been commented on by several investigators.[55,56] Although they may arise from a number of detailed mechanisms within the sample, a particularly simple process is possible whenever the sample is tightly coupled to the microwave circuit. Under these circumstances the rf drive field is a function of the sample susceptibility which in turn, in the nonlinear region, depends on the rf drive. The conditions under which this coupling can lead to instability are examined briefly in Appendix E, the principal result being that this form of instability can never occur in practice when the sample is less than critically coupled to the circuit. This condition was fulfilled in all of the cases reported here. It is perhaps worth emphasizing that the presence of an instability of this kind is <u>not</u> predicated on the existence of any energy storage element other than the ferrite itself. Although in practice it may not be possible to obtain the necessary tight coupling without placing the sample in a resonant structure of some sort, the presence of a cavity is not a fundamental requirement.

---

[1] The procedure for determining h in terms of the incidnet power is given in Appendix D.

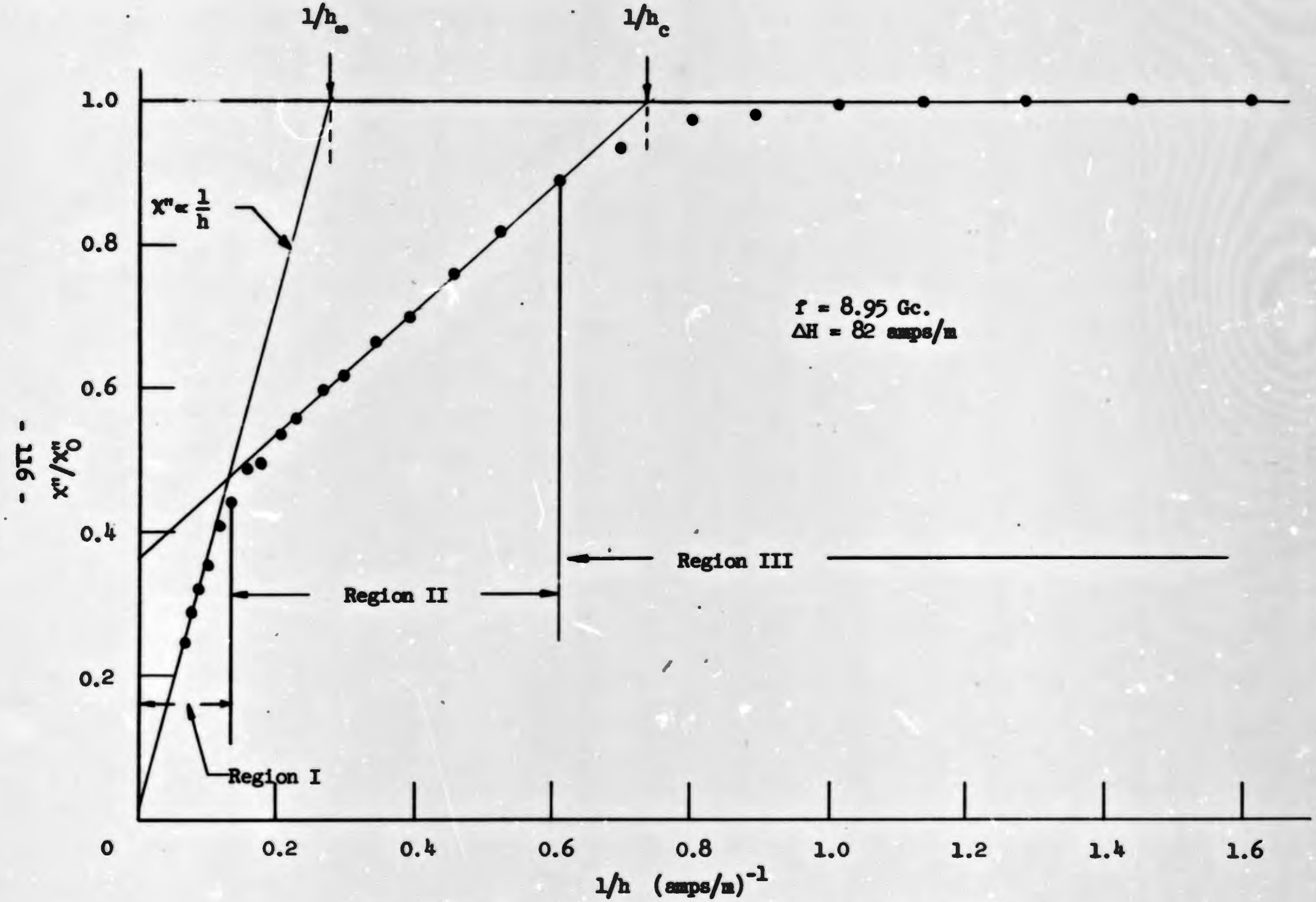

FIG. 3.16--Susceptibility decline curve for sample MC-20.

b. Variation of η_k with rf Power Level This measurement was made as described in a previous section by observing the free decay of the magnetization in the presence of sufficient radiation damping to clearly separate the contributions of the spin modes from that of the uniform precession. The type of video information obtained is shown in Fig. 3.17. In these photographs, as in Fig. 3.11, the initial spike is produced by the rapid decay of the radiation damped uniform precession, while the longer tail characterizes the free decay of the spin modes. Photograph (a) shows the small signal response of the magnetization, and (b) the large signal response. The value of η_k obtained from the time constant of this decay is shown as a function of the rf driving field in Fig. 3.18. To demonstrate the levels involved, the susceptibility decline data of Fig. 3.16 has also been plotted here.

c. Measurement of the Amplitude of the Modes[1] The steady state amplitude of the uniform precession may be obtained at once from the susceptibility decline, since we know from the definition of the resonance susceptibility that

$$\frac{\Delta M_{z0}}{M_s} = \frac{1}{2}\left(\frac{\chi''}{\chi''_0}\frac{h}{\Delta H}\right)^2 \quad , \qquad (3.13)$$

where ΔH is the small signal linewidth. The equilibrium spin mode population, on the other hand, can be obtained directly by observing the decay of ΔM_z, and determining the initial amplitude of that component having an $\exp(-2\eta_k t)$ time dependence. Experimentally, this involves extrapolating the tails of the decay curves in Fig. 3.17 back to $t = 0$. This intercept is proportional[2] to $\sum_{k\neq 0} \eta_k \Delta M_{zk}$, and since η_k is

---

[1] The actual amplitudes of the normal modes defined in Part I are given in terms of their differential z-component of magnetization as $|b_k| = \sqrt{2\Delta M_{zk}/M_s}$, when ellipticity is ignored. In what follows we shall often, for brevity, speak of the fraction $\Delta M_{zk}/M_s$ or even the quantity ΔM_{zk} itself as "amplitude" of the mode, when no confusion can arise.

[2] Here, and in what follows, ΔM_{zk} is the steady-state differential z-component of magnetization, i.e., the equilibrium value obtaining before the drive was shut off.

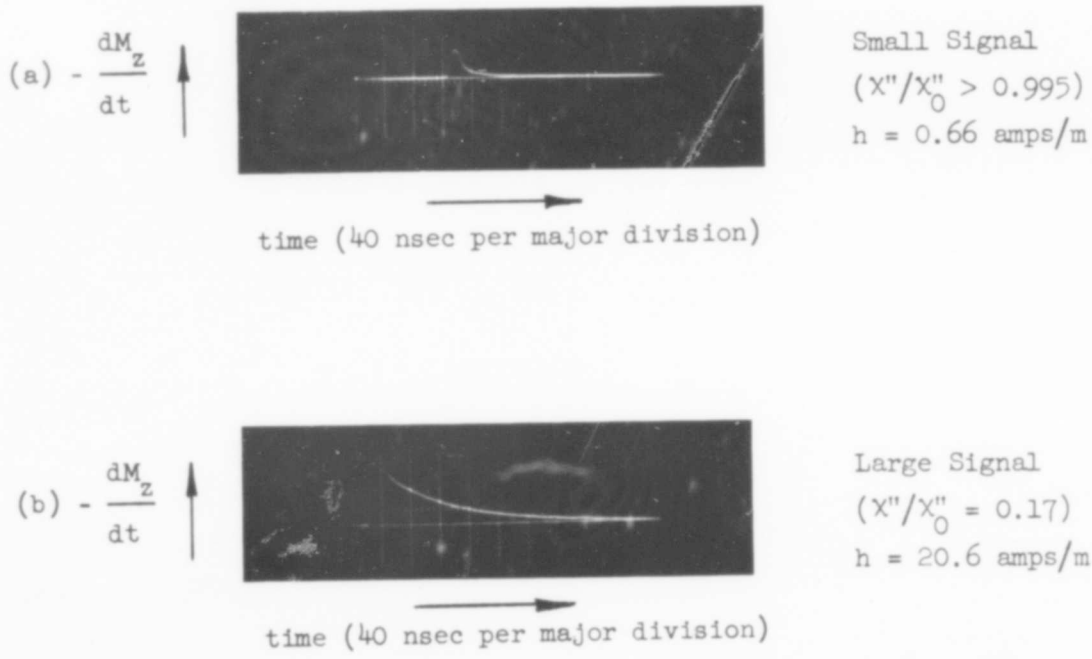

FIG. 3.17--Decay of z-component of magnetization, showing effect of increasing drive on relative amplitudes of the uniform precession and spin modes.

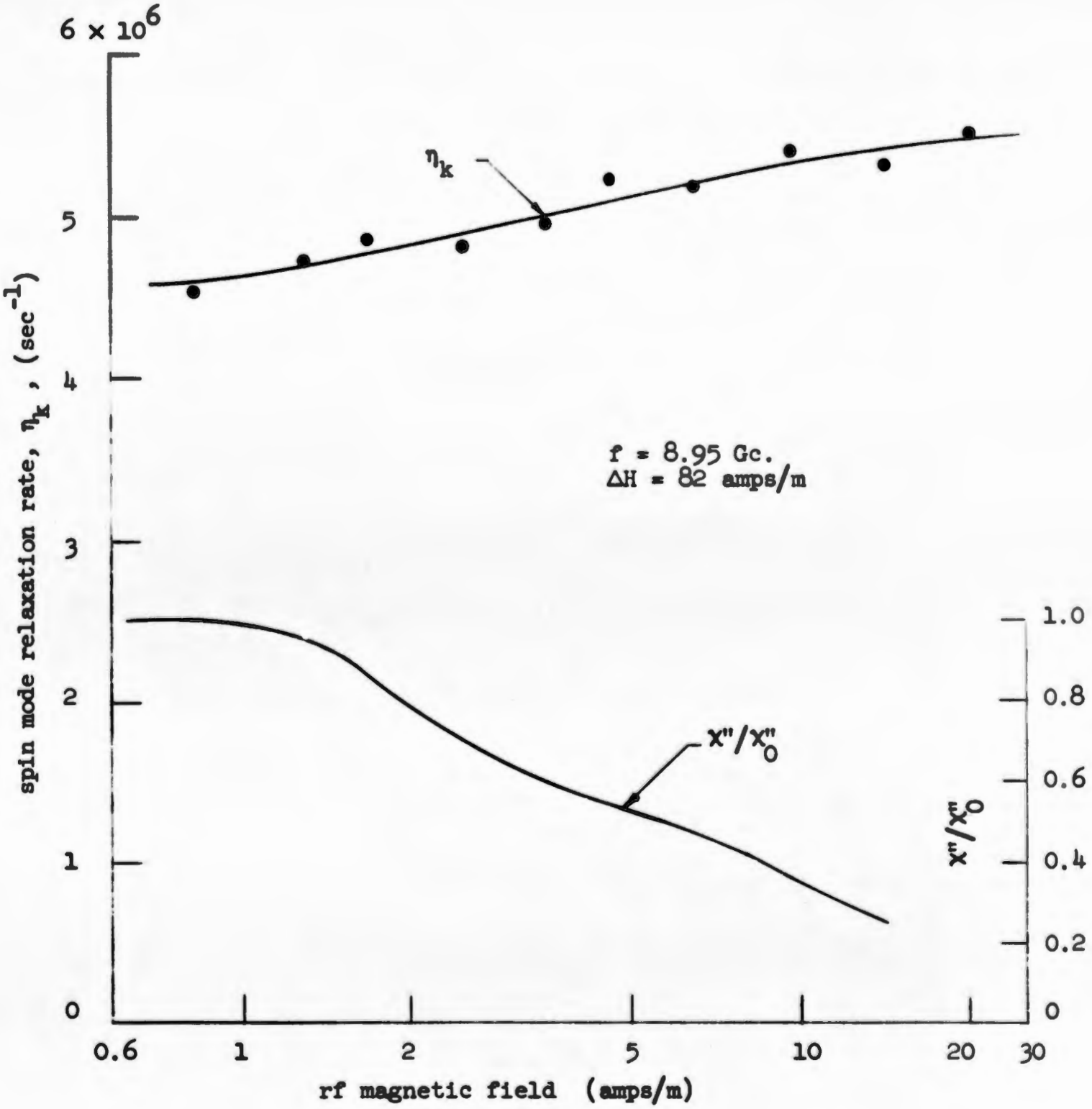

FIG. 3.18--Spin mode relaxation rate as a function of the rf drive level for sample MC-20.

known, relative values of $\sum_{k\neq 0} \Delta M_{zk}$ as a function of rf drive may be deduced at once.(1)

An absolute value of $\sum_{k\neq 0} \Delta M_{zk}$ would be quite hard to obtain with this procedure, however, both because of the uncertainty in determining the effective origin of time in the face of the finite fall time of the rf pulse and rise time of the video system,(2) and the difficulty of obtaining an absolute calibration of the multiturn loop. Instead, we may use the fact that in the small signal region

$$\sum_{k\neq 0} \frac{\Delta M_{zk}}{\Delta M_{z0}} = \frac{\eta_0'}{\eta_k} \quad , \tag{3.14}$$

as may be seen at once from Fig. 3.1. Since η_0' and η_k are known, this pins down one end of the curve, and in effect provides an absolute calibration. We show in Fig. 3.19 a plot of mode amplitude vs rf drive obtained in this way, in which we have expressed the amplitude of each mode in terms of its contribution to the fractional deviation of M_z from M_s .

---

(1) This statement holds regardless of which of the two assumptions, mentioned in the first section of Chapter XIV, that we choose to make about the inhomogeneity scattering. In the presence of sufficiently strong coupling between the S-modes, ΔM_{zk} is independent of k , and the quantity $\sum_{k\neq 0} \eta_k \Delta M_{zk}$ can be written as

$$\left(\sum_{k\neq 0} \Delta M_{zk}\right)\left(\frac{\sum_{k\neq 0} \eta_k}{\sum_{k\neq 0} (1)}\right) \quad ,$$

in which the last factor is just the average value of η_k that we deduce from our ΔM_z decay curve, and the first is the desired total spin mode population. In the other case, where η_k is taken to be independent of k , the statement is obvious.

(2) This uncertainty does not appreciably affect the validity of the relative values, since η_k is almost the same at all power levels (see Fig. 3.18).

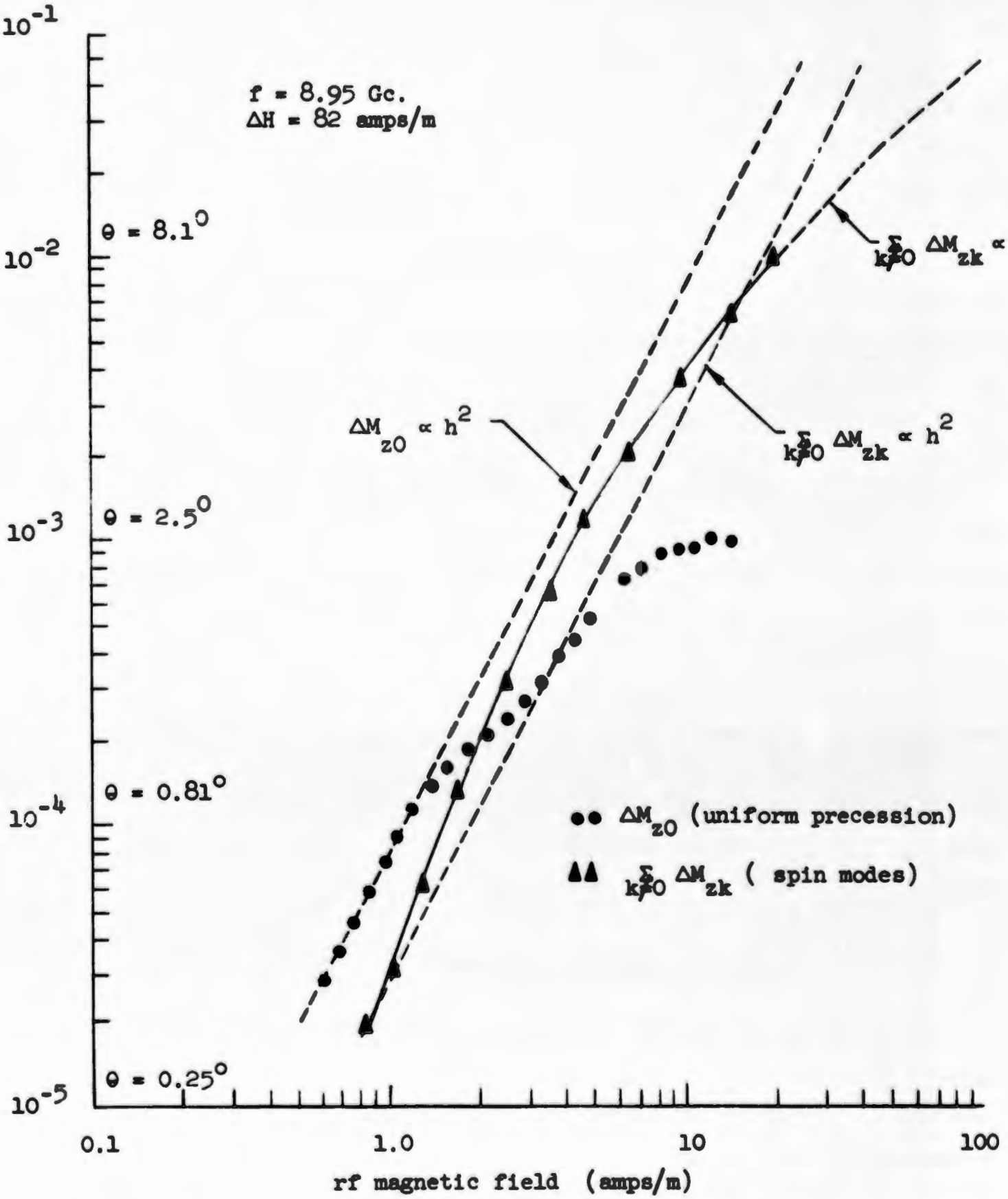

FIG. 3.19--Variation of mode amplitudes with rf drive for sample MC-20.

2. Discussion of Results

a. Susceptibility Decline The susceptibility decline curve shown in Fig. 3.16 is substantially different from those previously published for polycrystalline[56,21,58] and relatively poorly polished single crystal[21,58] samples of YIG, in that the decline is more gradual, with saturation occurring only at very high drive levels, although the behavior is very similar to that observed at 1980 Mc, by Smith and Watanabe in a polished single crystal disk.[55] Because of the unexpected nature of this result, susceptibility decline measurements were made on two other samples from the same batch. In order to compare the results for the three samples, which had different linewidths, the normalized susceptibility was plotted against $\Delta H/h$, ΔH being the small-signal linewidth. With this normalization, in the small-signal region, a given abscissa then corresponds to the same precession angle in all samples. The curves are shown in Fig. 3.20. Despite some differences in detail, all are seen to have substantially the same form. In particular, the curves consist, asymptotically, of two distinct portions linear in $1/h$, and an initial region of gradual decline, labelled Regions I, II, III, respectively, in Fig. 3.16. We shall consider each of these regions in turn.

(1). Region I. In Region I the susceptibility is directly proportional to the reciprocal of the driving field, a result which implies, from Eq. (3.13), that the uniform mode "sticks" at the amplitude for which

$$\left(\frac{\Delta M_{z0}}{M_s}\right)_{max} = \frac{1}{2}\left(\frac{h_\infty}{\Delta H}\right)^2 \quad , \qquad (3.15)$$

where $1/h_\infty$ is the intercept defined in Fig. 3.16. This saturation, which is clearly evident in Fig. 3.19, occurs for $\Delta M_{z0}/M_s = 9.9 \times 10^{-4}$, corresponding to a maximum precession angle of about 2.5°. Suhl[13] and Schloemann[21] have shown that such limiting of the uniform precession can be produced by nonlinear coupling between it and z-directed spin waves having the same resonant frequency. In one way of viewing this process the effect of the nonlinear coupling is to decrease the effective

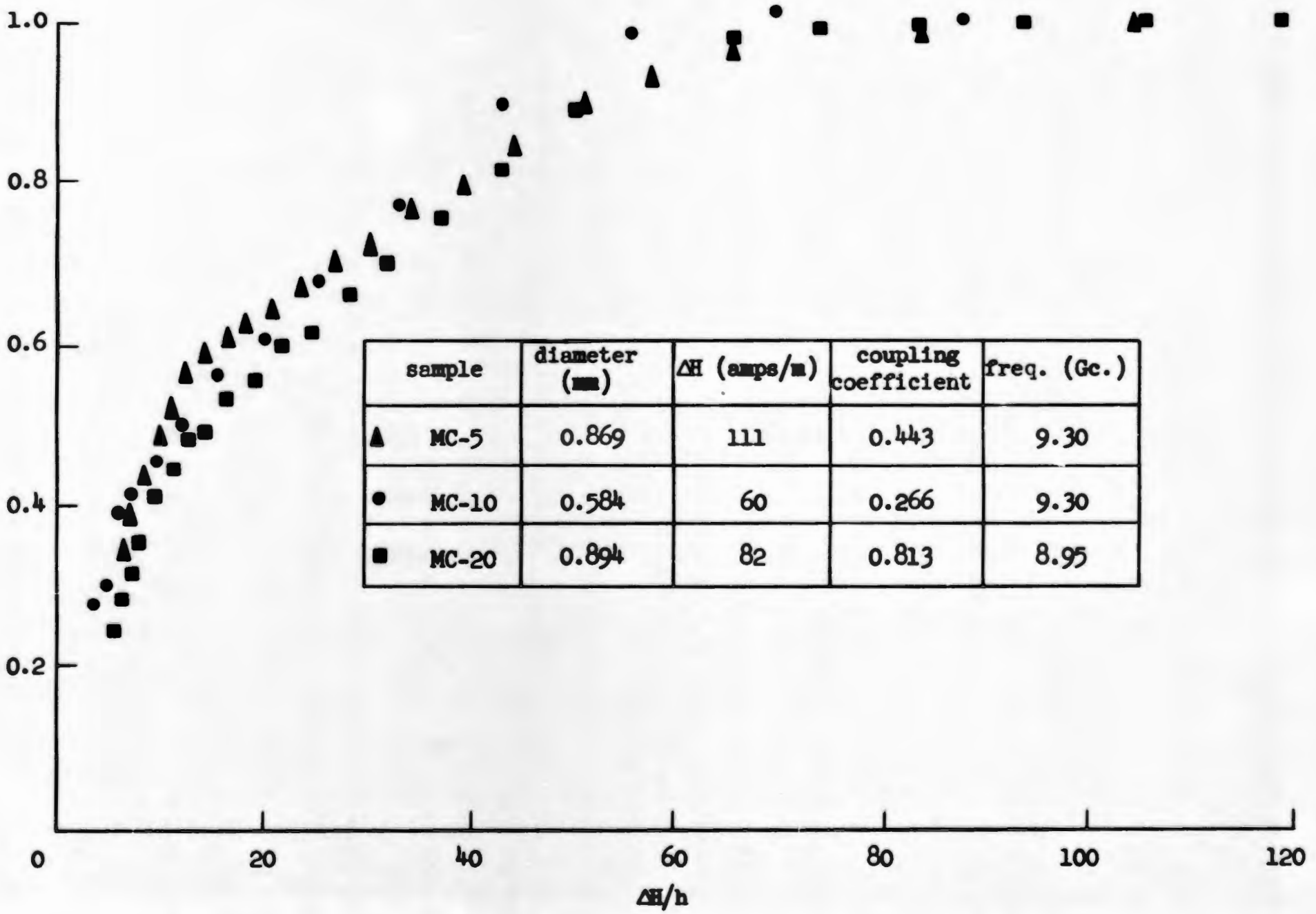

sample	diameter (mm)	ΔH (amps/m)	coupling coefficient	freq. (Gc.)
▲ MC-5	0.869	111	0.443	9.30
● MC-10	0.584	60	0.266	9.30
■ MC-20	0.894	82	0.813	8.95

FIG. 3.20--Normalized susceptibility decline curves for polished single crystal YIG samples.

relaxation rate for these spin waves, so that they become unstable as soon as the uniform mode reaches the critical amplitude for which[1]

$$\left(\frac{\Delta M_{z0}}{M_s}\right)_{crit} = \frac{\eta_{kz}}{\omega_M} \quad , \tag{3.16a}$$

where η_{kz} is the small-signal relaxation rate of the z-directed spin wave. The existence of this instability thereafter "clamps" the uniform mode at this level. If we suppose that this theory is applicable in Region I of Fig. 3.16, we obtain a value of 30.5×10^6 sec^{-1} for η_{kz}. Such spin waves should contribute to the decay of ΔM_z a component with a time constant of 16 nanoseconds, which, although short, is still within the capabilities of our video system. Figure 3.21 is a semi-logarithmic plot of the observed decay of ΔM_z, taken from Fig. 3.17b. Virtually the entire curve is characteristic of a decay with a time-constant of 90 nanoseconds, and although there is a small contribution from a faster decaying component in the region $t < 35$ nanosec., this is attributable entirely to the fast, radiation damped decay of the uniform mode. On the strength of this evidence then, we can conclude that if there <u>are</u> present spin waves with $\eta_k = 30.6 \times 10^6$ sec^{-1}, they represent a small fraction of the total spin-mode population.

In an effort to establish beyond doubt the existence or not of modes other than the uniform precession and spin-modes for which $\eta_k \sim 5 \times 10^6$ sec^{-1}, we used the fact that ΔM_z is proportional to the area under the decay curve to obtain relative values of ΔM_z at the two highest drive levels that were used, the ratio of the two values of ΔM_z being 0.652. At these same two drive levels, the ratio of the

---

[1] This is a special case of a more general result which states that the threshold for the unstable growth of arbitrarily directed spin modes, in a spherical sample, is

$$\left(\frac{\Delta M_{z0}}{M_s}\right)_{crit} = \frac{\eta_k}{\omega_M\left(1 - \frac{\beta}{2}\sin^2\theta_k\right)} \quad , \tag{3.16b}$$

where η_k is the relaxation rate of spin waves with polar angle θ_k.

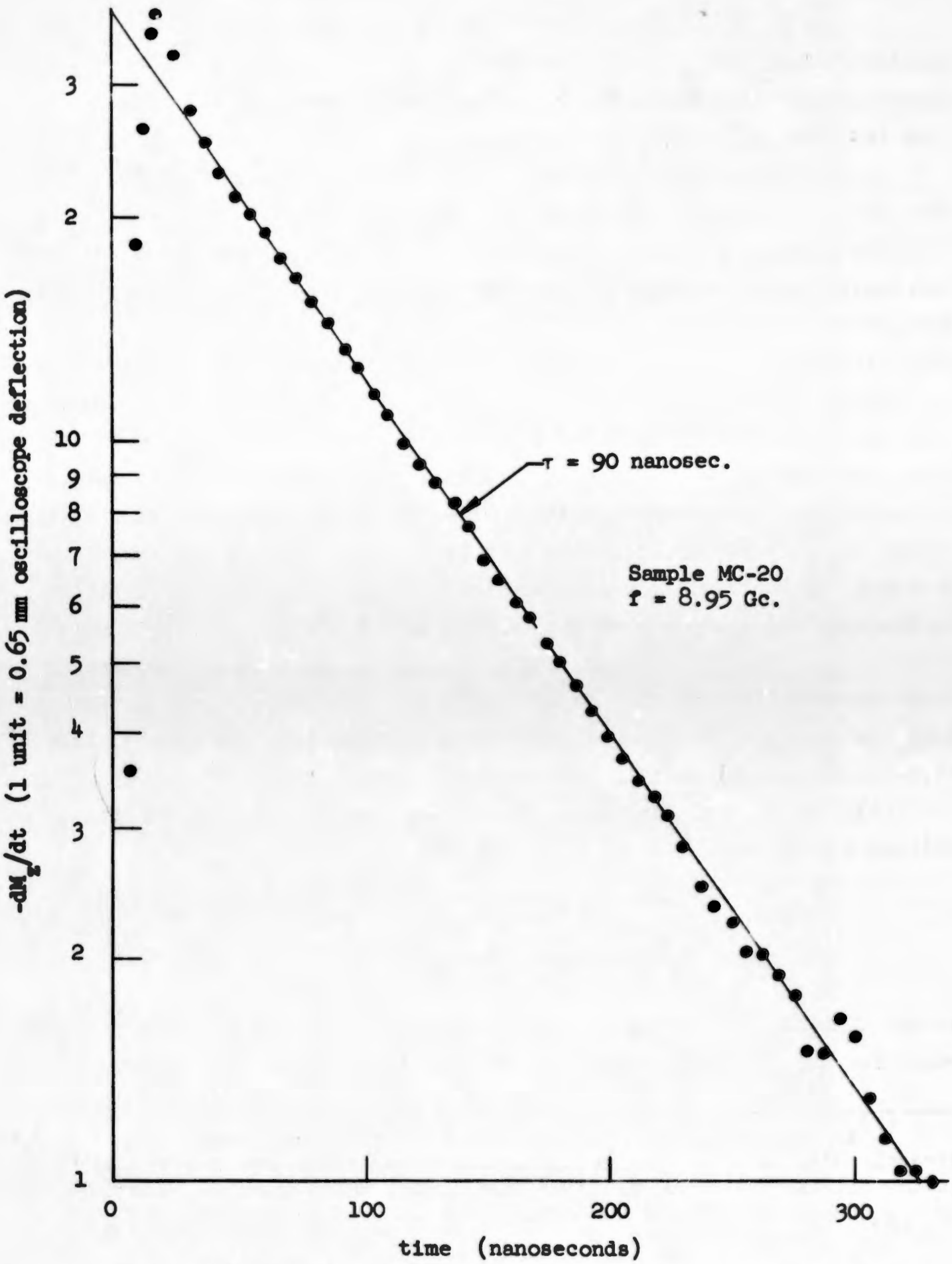

FIG. 3.21--Free decay of the z-component of magnetization from a large-signal steady state value.

quantities $\Delta M_{z0} + \sum_{k\neq 0} \Delta M_{zk}$, obtained from Fig. 3.19, was 0.648, i.e., almost exactly the observed ratio of the total ΔM_z for the two cases. From this result[1] we are forced to conclude that either

(i) there are no modes other than those plotted in Fig. 3.19 (i.e., the uniform mode and spin modes with $\eta_k \approx 5 \times 10^6$ sec^{-1}), or

(ii) there are other modes, but that their amplitude increases, with increasing drive, in exactly the same ratio as ΔM_z.

The latter alternative is quite improbable -- we would expect a much more rapid increase, at least as fast as that first observed in $\sum_{k\neq 0} \Delta M_{zk}$ at the initial onset of saturation. It is on this basis that we discount the existence of any spin modes other than those observed directly. In particular, the spin waves predicted by a simple application of Suhl's theory to Region I of the susceptibility decline curve do not exist, so that the theory is, in fact, inapplicable in this region. This is not surprising, perhaps, for Suhl's theory is essentially a small-signal theory, as far as the spin modes are concerned, and throughout Region I the spin mode amplitude, as Fig. 3.19 makes clear, is in fact quite large. It thus seems certain that in our case, the ultimate saturation of the uniform mode, in Region I, is brought about by mechanisms more complicated than those postulated by Suhl in his original theory.[2]

(2). Region II. In Region II of Fig. 3.16, the susceptibility follows the curve

$$\frac{\chi''}{\chi''_0} = C_1 + \frac{h_c}{h} \quad , \tag{3.17}$$

where C_1 and h_c are positive constants. This existence of a positive value for C_1 is rather difficult to explain. Seiden[57] has obtained

---

[1] We are barred from the obvious approach of comparing $\Delta M_{z0} + \sum_{k\neq 0} \Delta M_{zk}$ directly with ΔM_z by the ract, mentioned earlier, that uncertainty in the origin of time prevents us from assigning an accurate, absolute value to $\sum_{k\neq 0} \Delta M_{zk}$ in terms of the actual oscilloscope deflection.

[2] One possible explanation is advanced in a later section.

saturation curves for polycrystalline garnets which contain a region describable by Eq. (3.17) but with a negative value of C_1, which he explains in terms of a linear decrease in the magnetization with increasing h. As Fig. 3.19 shows, ΔM_z does, for our sample, approach a linear dependence on the rf drive at sufficiently high powers. This mechanism, however, leads to an extremely small value of C_1, about -10^{-5} for sample MC-20, so that this effect clearly is of no importance in our work. In fact, it is extremely doubtful whether for <u>any</u> material the decrease in the magnetization would significantly affect the susceptibility.(1)

The observed form of the susceptibility decline curve in Region II might lead one, in the absence of any other knowledge about the spin system, to suppose that there existed two essentially independent degenerate modes within the sample, both coupled to the microwave fields, but with the amplitude of one of the modes "clamped" by the Suhl instability while the other remained unaffected. If two such degenerate modes existed, however, it would be essential that they be completely decoupled; otherwise, the resonance line would not have had the simple Lorentzian shape at small signal levels that was always observed. Since the existence of two such degenerate modes is highly unlikely, especially in a number of samples, at different frequencies, we are forced to conclude that Region II of the susceptibility decline curve, like Region I, cannot be explained by a simple application of Suhl's theory.

(3). Region III. In this region, the susceptibility shows a gradual decline with increasing drive. Suhl[20] and Schloemann[21] have recently extended their theory to cover this effect by including in it the inhomogeneity scattering from the uniform precession into the spin modes. Because of the linear scattering there will exist, as we have demonstrated experimentally, a finite spin-mode amplitude, even in the small signal region, the effect of which is to cause the amplitude of the uniform mode to attain its maximum value only asymptotically at high powers, rather than abruptly at some critical threshold. Under these circumstances the

---

(1) Richards has pointed out that the <u>definition</u> of χ'' precludes this possibility.

susceptibility is given by

$$\frac{\chi''}{\chi''_0} = \frac{1 + \frac{\eta_0}{\eta'_0}}{\frac{\eta_0}{\eta'_0} + \left[1 - \left(\frac{h}{h_m}\frac{\chi''}{\chi''_0}\right)^4\right]^{-1/2}} \quad , \qquad (3.18)$$

where h_m is a constant, related to the maximum amplitude of the uniform mode by

$$\left(\frac{\Delta M_{z0}}{M_s}\right)_{max} = \frac{1}{2}\frac{h_m^2}{\Delta H^2} \quad , \qquad (3.19)$$

with ΔH being the small-signal linewidth. We have fitted this curve to our susceptibility decline data, using the previously determined values[1] for η_0 and η'_0. The value of h_m was selected so as to provide the best fit for values of χ''/χ''_0 greater than 0.8, since the theory is expected to apply best to the initial part of the susceptibility decline. The result is shown in Fig. 3.22. For sufficiently small values of χ''/χ''_0, the fit is adequate, but becomes increasingly poor for values of χ''/χ''_0 less than 0.75. The value of h_m selected corresponds to a value of 2×10^{-4} for $(\Delta M_{z0}/M_s)_{max}$; the fact that the amplitude of the uniform mode continues to increase beyond this value underscores the inadequacy of the theory.

We may, however, adopt the attitude that the uniform precession would have saturated at this level if other, as yet not understood, effects had not intervened. The relaxation rate of the spin modes responsible for this "saturation" can then be determined from Eq. (3.16a)[2] as 6.3×10^6 sec^{-1}, compared to an observed value of about 4.8×10^6 sec^{-1} in this region (Fig. 3.18). The discrepancy arises from two sources:

---

[1] The fit could not be improved by assuming a different value for the ratio η_0/η'_0.

[2] Or more generally, it can be determined by Eq. (3.16b). This expression, however, has a minimum value (corresponding to the lowest threshold) for $\Theta_k = 0$, even when the experimentally observed increase of η_k with increasing k (and hence decreasing Θ_k) is allowed for.

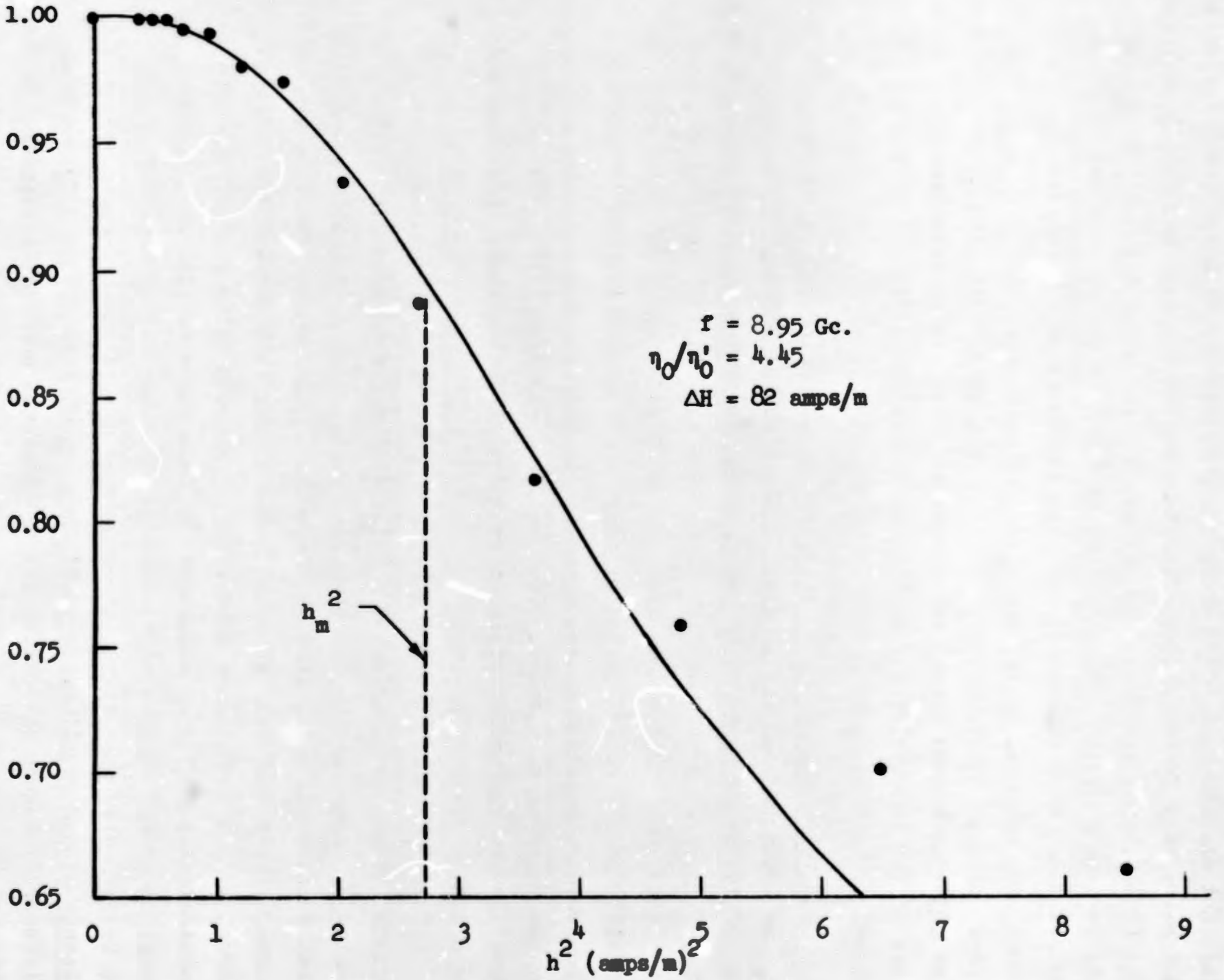

FIG. 3.22--Initial susceptibility decline for sample MC-20.

(a) not all the spin waves whose decay we observe directly are z-directed, and hence they do not all have the same relaxation rate and (b) in deriving Eq. (3.18), Suhl was forced to neglect the variation with k of η_k and the various coupling constants linking the uniform mode and the spin modes, an omission which apparently[8] results in too large a value for h_m, and hence, through Eqs. (3.19) and (3.16), too large a value for η_k. The error involved is perhaps 25%, so that when this correction is made, theory and experiment come into good agreement. Thus, it appears that the initial part of the susceptibility decline is adequately described by the current theories.

b. Variation of η_k with Drive Our experimental measurements of η_k as a function of the rf drive exhibit two significant features:

(i) η_k depends little on h, the variation, as may be seen from Fig. 3.18 being less than 20% over a more than 20 : 1 range of h, and

(ii) the ΔM_z decay curves (e.g., Figs. 3.11, 3.12, 3.17 and 3.20) consist, at all power levels, of only two exponentials, one produced by the heavily radiation damped decay of the uniform precession, the other by the decaying spin modes. Thus we find, experimentally, that at all power levels the decay of the spin modes can be uniquely characterized by a single relaxation rate.

Taken together, these two features provide strong evidence that there exists strong coupling between individual S-modes (so-called "S-S scattering"). Although not indisputable, ours is the first substantial evidence that such coupling is, in fact, important. The reasons for this may be summarized as follows: We would normally expect the spin modes excited directly from the uniform precession by inhomogeneity scattering to have substantially different values of k from those excited by nonlinear coupling to the uniform mode. We would further expect this difference to be reflected in a different value for η_k in the two cases. In the absence of S-S coupling, we would then expect there to be a fundamental difference between the values of η_k measured under small-signal conditions, when all the spin modes would be produced by inhomogeneity scattering and very large signal conditions, when the bulk of the spin mode excitation would result from nonlinear coupling to the uniform mode. At intermediate

signal levels we would expect the decay of the spin modes to be characterized by two exponentials corresponding to the existence of spin modes excited by both processes. Our experimental results are in direct contradiction to such a hypothesis. On the other hand, the fact that η_k is almost independent of the drive is consistent with the assumption of strong S-S coupling, since such coupling would tend to equalize the spin mode population regardless of which mode, or group of modes was being directly excited. The fact that the measured value of η_k tends to increase somewhat at the highest drive levels may be evidence of a partial saturation of the coupling between the directly excited z-directed spin modes and the remaining spin modes. Such a saturation would produce an overpopulation of the z-directed modes and a corresponding weighting of the averaging of η_k over all S-modes in favor of the higher values of η_k.

The results are not absolutely conclusive, however, for it is not impossible, even in the absence of S-S coupling for the spin modes excited by linear scattering to have the same value of η_k, more or less by chance, as those excited by nonlinear coupling to the uniform mode. It is, nonetheless, unlikely.

c. Variation of Spin-Mode Amplitude with Drive The amplitudes of the uniform precession and the spin modes are shown, as a function of the rf drive, in Fig. 3.19. In the absence of any nonlinear coupling, both ΔM_{z0} (proportional to the square of the amplitude of the uniform precession), and $\sum_{k\neq 0} \Delta M_{zk}$ (proportional to the sum of the squares of the spin mode amplitudes) would be proportional to h^2, following the dotted lines in the figure. In actual fact the uniform mode increases less rapidly, finally saturating when $\Delta M_{z0}/M_s \approx 10^{-3}$, corresponding to an angle of about 2.5°. This information, of course, is also contained in the susceptibility decline curve from which ΔM_{z0} was deduced, although perhaps less graphically. The spin mode amplitude, on the other hand, at first increases rapidly as the nonlinear coupling to the uniform mode becomes important, and then approaches a linear dependence on h as the uniform mode saturates. To demonstrate this latter behavior, we may

according to the results of Part I, write the power absorbed in the sample, per unit volume, as

$$\frac{P_{abs}}{V_s} = \frac{2}{\gamma}\left[\eta_0\omega_0\Delta M_{z0} + \sum_{k\neq 0}\eta_k\omega_k\Delta M_{zk}\right] \quad , \qquad (3.20)$$

provided that we ignore the ellipticity of the spin modes. On the other hand, from the definition of the susceptibility, the power absorbed is always given by

$$\frac{P_{abs}}{V_s} = \frac{1}{2}\omega\mu_0\chi''h^2 \quad . \qquad (3.21)$$

In the saturation region, where ΔM_{z0} is a constant, χ'' is simply $h_\omega/h\chi_0''$, so that if $\omega = \omega_0 = \omega_k$, Eq. (3.20) can be rewritten as

$$\sum_{k\neq 0}\eta_k\,\Delta M_{zk} = \frac{\mu_0\gamma h_\omega\chi_0''}{4}\,h - \eta_0(\Delta M_{z0})_{max} \quad . \qquad (3.22)$$

Thus, if η_k is independent of k and h, $\Sigma\Delta M_{zk}$ will increase linearly with h, becoming proportional to h in the limit when $\Sigma\eta_k\Delta M_{zk} \gg \eta_0(\Delta M_{z0})_{max}$ This asymptotic behavior is evident in Fig. 3.19, at sufficiently high drive levels.

The results shown in Fig. 3.19 may be displayed in an alternative way which permits a ready comparison with the results of our small-signal measurements. By combining Eqs. (3.13), (3.20), and (3.21), and assuming that $\omega = \omega_0 = \omega_k$, we may eliminate ΔM_{z0} and h, obtaining a linear relationship between the quantity $\sum_{k\neq 0}(\eta_k\Delta M_{zk}/P_{abs})$ and the normalized susceptibility, χ''/χ_0''. This lationship can be written in the form

$$\sum_{k\neq 0}\frac{\eta_k\Delta M_{zk}}{P_{abs}} = \frac{\gamma}{2\omega_0 V_s}\left[1 - \frac{\eta_0}{(\eta_0 + \eta_0')_0}\frac{\chi''}{\chi_0''}\right] \quad , \qquad (3.23)$$

where we have written the small-signal resonance susceptibility as $\mu_0\gamma M_s/2(\eta_0 + \eta_0')_0$, adding the subscript to underscore the fact that this is a small-signal quantity. Since $\sum_{k\neq 0}\eta_k\Delta M_{zk}$, P_{abs} and χ''/χ_0'' are

all quantities which we have measured directly, the predicted linear relationship may be checked at once. The experimental data are shown in Fig. 3.23. Although there is some scatter as a result of the accumulated errors in the individual measurements of $\Sigma \eta_k \Delta M_{zk}$, χ'' and P_{abs}, particularly the first of these, the experimental points do in fact define a straight line in the region $\chi''/\chi''_0 > 0.5$, although the curve tends to flatten out for smaller values. Equation (3.23) predicts that the (χ''/χ''_0)-intercept should be just $1 + \eta'_0/\eta_0$. Extrapolating the linear portion of the curve in Fig. 3.23 down to the (χ''/χ''_0) axis yields an intercept of 1.20 ± 0.03, giving a value of 0.20 ± 0.03 for η'_0/η_0, in excellent agreement with the value of 0.22 ± 0.03 obtained from the small signal measurements described in Section A. This agreement justifies our experimental procedures, especially the technique used to obtain the spin mode amplitude which, as we shall see, is not beyond criticism on theoretical grounds.

The departure of the experimental data from the expected linear behavior, which sets in at roughly the same drive level as that for which the uniform precession saturates, must arise from the basic nonlinearity of the system. To see in detail how this is so, we shall have to examine more closely the assumptions that are inherent in Eq. (3.23), and in our measurement procedure.

Equation (3.20), describing the power absorbed in the sample <u>in the steady state</u>, is very general, and aside from the relatively trivial assumption that all the modes are circularly polarized, requires only that there exist a set of modes in each of which the actual <u>dissipation</u> is proportional to the amplitude of the mode. The presence of coupling, either linear or nonlinear, among these modes then serves only to establish in a complicated way, the steady state energy distribution. In going from Eq. (3.20) to Eq. (3.23), however, we have added the important restriction that all the modes have essentially the same resonant frequency, so that the energy of each mode can be taken to be proportional to its differential z-component of magnetization. Also, in our experimental procedure, we have assumed that the steady state value of the quantity $\sum_{k\neq 0} \eta_k \Delta M_{zk}$ can be inferred from a transient measurement of the free decay of ΔM_z. This will not be true, in general, if there exists arbitrary coupling between the individual spin modes, <u>unless all the spin modes have the same</u>

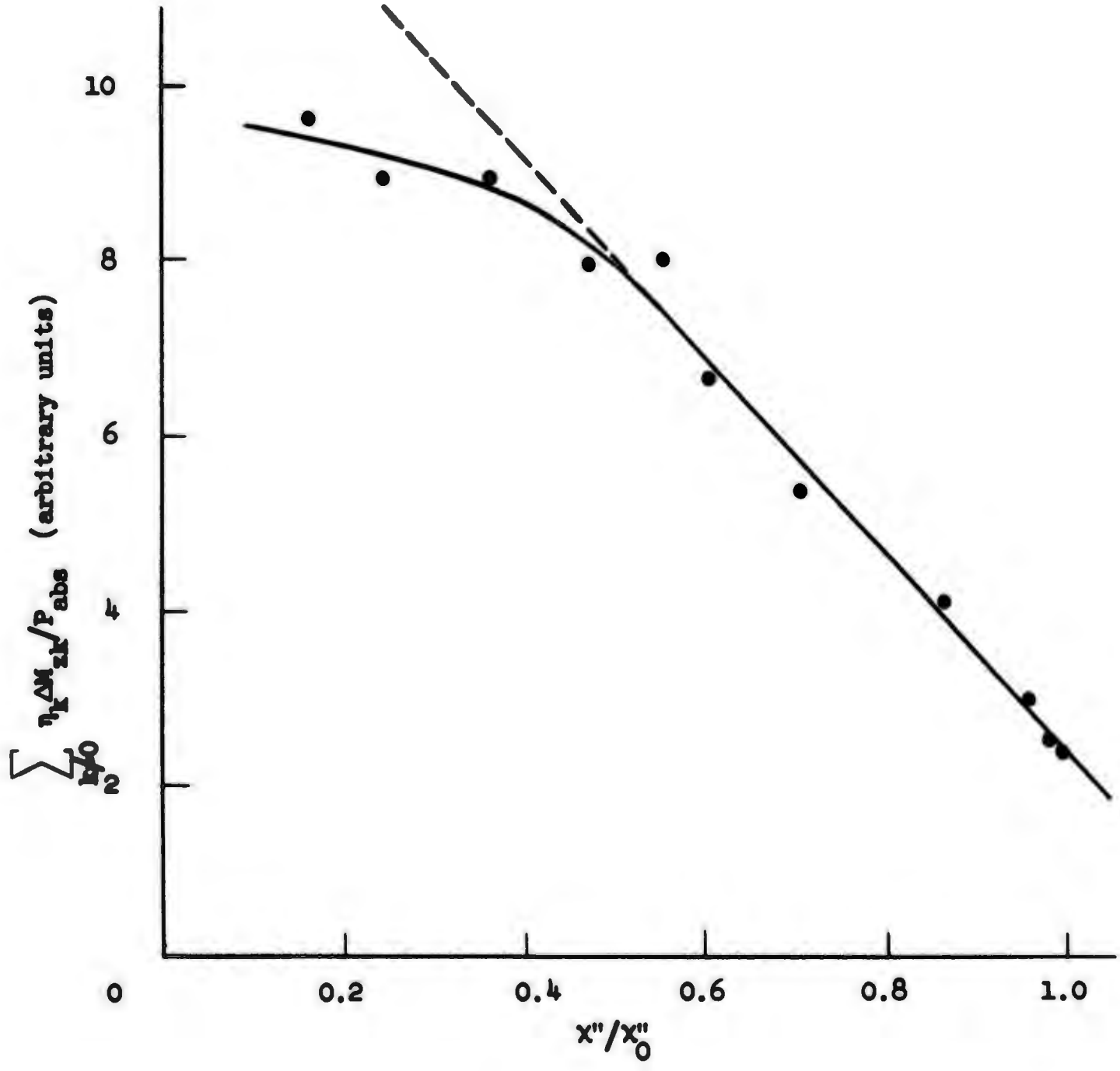

FIG. 3.23--Relation of spin mode amplitude to susceptibility decline.

relaxation rate. If they do not, there will be a continuous redistribution of energy within the spin system as the decay proceeds, with those spin modes having the highest relaxation rate contributing proportionately more to the total dissipation. Such a mechanism, however, would lead to the measured value of $\sum_{k\neq 0} \eta_k \Delta M_{zk}$ being too large, contrary to observation. In addition, as we have pointed out before, once the uniform mode has died out, the remaining decay of ΔM_z is characterized by a single exponential, showing that we are justified, at all power levels, in lumping all the spin modes together in one large "super mode" having a well defined relaxation rate.

For a number of reasons, then the crucial question appears to be whether or not a substantial fraction of the nonthermal energy in the spin system resides in modes whose resonant frequencies differ appreciably from that of the uniform mode. The experimental evidence suggests that the answer is "no," since we expect spin modes with different frequencies to have different relaxation rates, and, excited as they are by nonlinear processes, to have amplitudes which are a strong function of the drive level, features which seem incompatible with the experimental observation that the spin mode decay is characterized by a single relaxation rate which is only a slowly changing function of the rf drive.

If we accept the validity of our procedure for determining the spin mode amplitude, and the related assumption that all modes have approximately the same resonant frequency, the observed departure of the experimental data shown in Fig. 3.23 from the linear behavior predicted by Eq. (3.23) can then only be due to an increase in η_0 at high power levels. Since the magnetostrictive spin-lattice coupling will in general consist of both linear and nonlinear parts, just as the spin-spin coupling does, it is possible that for a sufficiently large amplitude of the uniform mode there could exist a line broadening similar to that produced by nonlinear spin-spin coupling, but leading, in this case, to an increase in η_0 instead of η_0'. Such nonlinear coupling is known to exist between the uniform mode and certain low frequency acoustic modes,[60] and it seems reasonable that it should be present for higher frequency vibrational modes as well.

We are thus led to hypothesize that the ultimate saturation of the uniform mode occurs as a result of the nonlinear coupling not to spin modes, but to vibrational modes, the evidence for such an hypothesis being summarized as follows:

(i) The power absorbed by the sample is greater than can be accounted for by linear dissipation processes within the spin system, yet the spin modes themselves exhibit a perfectly linear decay.

(ii) The ultimate saturation of the uniform mode occurs quite abruptly, in a manner strongly suggestive of the limiting action produced by the parametric excitation of an initially unexcited mode (or pair of modes), as in the original Suhl theory.[13] After the onset of the final saturation, however, there appears to be no rapid change in the spin mode distribution or amplitude, and in particular, no evidence of the existence of spin modes having a relaxation rate, as calculated from Suhl's theory, which is appropriate to the observed threshold.

It should be pointed out, however, that such evidence is suggestive rather than conclusive, in the face of the lack of a detailed understanding of the behavior of the spin system at the rather large signal levels at which the effect occurs, and further investigation is called for.

C. SUMMARY

We have measured the small signal relaxation parameters of polished single crystal spheres of yttrium iron garnet by observing directly the transient response of the z-component of magnetization to step-functions of rf drive, obtaining values which are consistent with those obtained by other experimenters. By judicious control of the radiation damping of the uniform precession, we have been able to separate its contribution to the decay of the z-component of magnetization from that of the spin modes, thus permitting a direct measurement of their decay, independently of the other relaxation parameters. We find that the decay of the spin modes can be accurately described by a single exponential, thus justifying the assumption, made in the theory, that we may define a single intrinsic spin mode relaxation rate, η_k . This provides the first substantial evidence to support a recent theory[9] that predicts strong mutual coupling between those important spin modes which have the same resonant frequency as, and are initially excited by, the uniform precession.

The fact that we are able to measure η_k in the presence of arbitrary coupling between the uniform precession and the spin modes, coupled with the fact that we are able to use short rf pulses, has allowed us, for the first time, to measure the amplitude and relaxation rate of the spin modes as a function of the rf drive level. This information, when combined with that obtained from conventional susceptibility decline measurements, leads to a picture of the high-power behavior of the spin system which is at variance, in some essential details, with that provided by currently available theories.

We find that as the rf drive level is increased the rf susceptibility shows a gradual decline, the initial part of which is correctly accounted for by existing theories in terms of nonlinear coupling to spin modes having the experimentally observed relaxation rate. The uniform mode, however, does not saturate at the amplitude predicted by the theory, corresponding to a precession angle of about 1°, but instead increases beyond this level as the drive increases, finally saturating rather abruptly at an amplitude corresponding to a precession angle of about 2.5°. Careful observation of the spin modes excited in this region indicates that this ultimate saturation of the uniform mode does not result from nonlinear coupling to the spin modes. A tentative explanation is offered in terms of a nonlinear magnetostrictive coupling to the lattice. At the present time, the reason why the nonlinear coupling to the spin modes does not produce a saturation of the uniform precession at a much lower level is not understood.

CHAPTER XVII

EXPERIMENTAL RESULTS FOR POLYCRYSTALLINE YTTRIUM IRON GARNET

A. INTRODUCTION

As a result of our successful application of transient methods to the study of relaxation processes in narrow linewidth single crystal materials, we were led to investigate the possibility of applying these techniques to polycrystalline samples as well. On first thought, the large linewidths of these materials, ranging typically from 3000 to over 40,000 amps/m, corresponding as they do to relaxation rates of from 3×10^8 to 4.5×10^9 sec^{-1}, would seem to preclude any such transient

investigation because of the very short times involved. However, available values for the spin-mode relaxation rates in polycrystals,[57,59] all inferred from an application of Suhl's theory to the susceptibility decline at high power, indicated that they were of the same order of magnitude as those observed in single crystals, ranging from 0.5×10^6 to 30×10^6 sec^{-1}, and hence well within the range of our experimental technique. Furthermore, there are theoretical[17] grounds for believing that in these materials virtually the entire loss in the uniform precession arises from inhomogeneity scattering into spin modes (i.e., $\eta_0' \gg \eta_0$) , so that there should exist, even at low power, a very substantial spin-mode population. The success of the experiment thus seemed ensured.

Accordingly, measurements were made on several spherical samples of polycrystalline yttrium iron garnet, made from material prepared by the Lockheed Missile and Space Division, and differing somewhat in the ratio of iron to yttrium, and in the details of the firing. The steady-state behavior of these same samples, both at low and high power, had been previously investigated in this laboratory by Seiden.[57]

B. DESCRIPTION OF MEASUREMENTS

The experimental setup was identical to that used for the single crystal measurements, the sample being placed in a rectangular cavity having an external Q of about 20, and resonant at 8.95 Gc. One example of the experimentally observed relaxation is shown in Fig. 3.24, which is a photograph of the video signal produced by a free decay of the magnetization for a sample having a linewidth of 3,650 amps/m. The trailing edge of this response can be resolved approximately into two exponentials, having time constants of 15.5 and 4.5 nanoseconds, respectively, the latter being characteristic of the impulse response of the video system. Measurements on other samples of different composition, and hence of different linewidth, showed the same unexpected behavior -- a large initial pulse, indicating that a substantial fraction of ΔM_z was relaxing more rapidly than our video system could respond, followed by an approximately exponential tail having a time constant of about 15 nanoseconds.

Although quantitative information has been hard to obtain in the face of these rapid relaxation rates, we have been able to establish the fact that the uniform precession alone cannot account for the size of the

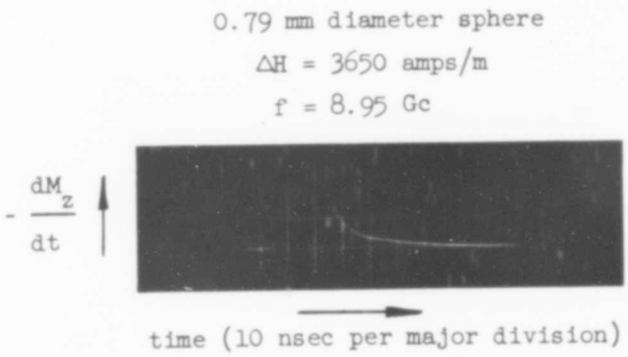

FIG. 3.24--Free decay of ΔM_z in polycrystalline yttrium iron garnet.

initial spike, but that it must also contain contributions from spin modes having relaxation rates faster than those to which our detection system could respond. To do this we estimated ΔM_z by measuring the total area under the response curve of Fig. 3.24, using the previous single crystal measurements to provide an absolute calibration, as discussed in Section B of Chapter XVI. The amplitude of the uniform precession was obtained from the known rf driving field and linewidth, using Eq. (3.13). The amplitude of those spin modes responsible for the tail of Fig. 3.24, which we denote by $\Sigma_1 \Delta M_{zk}$, was obtained, approximately, by extrapolating this exponential decay back to $t = 0$, and correcting for the finite fall time of the rf pulse and rise time of the detection system. The results are summarized in Table V for three different samples. The quantity in the last column of this table, which we have denoted by $\Sigma_2 \Delta M_{zk}/M_s$, is defined by

$$\sum_2 \Delta M_{zk} = \Delta M_z - \left(\Delta M_{z0} + \sum_1 \Delta M_{zk} \right) \quad , \qquad (3.24)$$

and represents that portion of ΔM_z which is not accounted for by the sum of the uniform precession and the spin modes that produce the tail of the decay curve. Although the absolute accuracy of the data presented in Table V is poor, it is believed to be good enough to justify the conclusion that there do exist spin modes with very fast relaxation rates, whose contribution to the decay of ΔM_z cannot be separately resolved by our detection system.

Additional evidence for the existence of such spin modes can be obtained by considering the steady-state energy distribution in the sample, which as we have seen before, is such that

$$\eta_0' \Delta M_{z0} = \sum_{k \neq 0} \eta_k \Delta M_{zk} \quad . \qquad (3.25)$$

Under the conditions that $\eta_0' \gg \eta_0$, so that scattering to spin modes accounts for most of the loss in the uniform precession, we find that Eq. (3.25) cannot be satisfied unless some of the spin modes relax substantially faster than those in the tail of the decay.

TABLE V

MODE AMPLITUDES IN POLYCRYSTALLINE GARNET

SAMPLE	ΔH - amps/m	$\frac{\Delta M_{z0}}{M_s}$	$\frac{\Delta M_z}{M_s}$	$\sum_1 \frac{\Delta M_{zk}}{M_s}$	$\sum_2 \frac{\Delta M_{zk}}{M_s}$
A	3650	1.39×10^{-5}	9.85×10^{-5}	7.6×10^{-5}	0.8×10^{-5}
B	4620	0.83	5.76	3.7	1.2
C	7030	0.49	6.36	5.2	0.7

Spin mode relaxation rates for these samples were obtained by Seiden[57] from susceptibility decline measurements. From his measurements he obtained two values, one for those spin modes that give rise to the initial decline, and one for those responsible for the final saturation. These values are compared with those we obtained directly from the tail of the ΔM_z decay curve in Table VI, for the same three samples as in Table V. There is seen to be no agreement, Seiden's values in all cases being smaller than ours. Since it is impossible to conceive that our direct measurement technique would give a value of η_k that is too large, we must conclude that Seiden's procedure for deducing η_k from the initial susceptibility decline data is in fact incorrect.

An interesting feature of the transient measurements is that the values of η_k obtained in this way are essentially independent of ΔH. The three samples that we have been discussing differ only in that they contain different, nonstochiometric, ratios of iron to yttrium. Since Seiden[57] has shown that the garnet lattice can exist only in stochiometric proportions, with the excess iron or yttrium going into a second phase, we expect, as he has pointed out, that η_k should be independent of composition, just as we observe.

C. SUMMARY AND CONCLUSIONS

In our attempt to apply the previously developed transient techniques to the measurement of the small-signal relaxation parameters of polycrystalline yttrium iron garnet, we have found that the spin-lattice relaxation rate is much faster than previous measurements, based on the decline of the susceptibility at high powers, would indicate, indeed being too rapid for accurate measurement with the existing apparatus. We have been able to determine that for most of the excited spin modes η_k is about 30×10^6 sec^{-1}, but there is also indirect evidence that some spin modes having η_k greater than 10^8 sec^{-1} are also excited.

In order to obtain more accurate information by the transient technique, and thus, perhaps, resolve some of these anomalies, it will be necessary to considerably shorten the overall response time of the system, a process which does appear to be feasible. Thus, with the samples that have been used in the present experiment, it should be

TABLE VI

SPIN MODE RELAXATION RATES IN POLYSCRYSTALLINE YIG				
SAMPLE	STEADY STATE MEASUREMENTS			TRANSIENT MEASUREMENTS
	$\eta_0 + \eta_0' = \frac{\mu_0 \gamma \Delta H}{2}$	η_{kz} saturation	η_k' initial susceptibility decline	η_k tail of ΔM_z decay
A	403×10^6 sec^{-1}	28.1×10^6 sec^{-1}	0.64	32
B	510	9.2	0.27	34
C	777	18.8	0.62	30

possible to increase the drive field by a factor of 5, corresponding to an increase of 25 in the incident power, up to about 25 watts, and still remain in the linear region. This would produce a 25-fold increase in ΔM_z, and permit the use of a single turn loop instead of the 7-turn loop with which the measurements described here were made. By constructing the loop of a relatively wide strip of thin foil, as described in Section E.1, and following it with a low-noise amplifier having a 200 Mc bandwidth, it should be possible to reduce the rise time of the video system to 2 nanoseconds or less, while retaining, by virtue of the higher power, the same signal to noise ratic as in the present experiment. The main limitation on the transient behavior of the system would then be the finite fall time of the rf pulse, at present about 6 nanoseconds, determined completely by the fall time of the switching pulse applied to the microwave diodes. These diodes have an inherent switching time of less than two nanoseconds,[1] which could be realized by using a faster switching pulse.[2] At present the fall time of the rf cavity represents no limitation, a Q of 20 corresponding, at 10 Gc., to a time constant of less than a nanosecond. It should thus be possible to develop a system whose overall pulse response, as measured by the rise time of the voltage induced in the pickup loop at the trailing edge of the drive pulse, would be only 2 nanoseconds, in contrast with the present rise time of 9 nanoseconds.

---

[1] This figure is according to the manufacturer's specification.

[2] Because of the nonlinearities in the diodes, the switching pulse can, however, still be considerably slower than the desired rf pulse.

APPENDIX A

THE EFFECTIVE SUSCEPTIBILITY TENSOR

1. General Form of the Effective Susceptibility Tensor

In a saturated ferrimagnetic material, the transverse rf magnetization is related to the transverse rf magnetic field inside the sample through the intrinsic susceptibility tensor, so that

$$\vec{m} = \overleftrightarrow{\chi}\,\vec{h} \quad . \tag{A.1}$$

If we now suppose that the internal rf field is made up of two parts, so that

$$\vec{h} = \vec{h}_1 + \vec{h}_2 \quad , \tag{A.2}$$

and that $\vec{h}_2$ is linearly related to $\vec{m}$, so that

$$\vec{h}_2 = \overleftrightarrow{k}\,\vec{m} \quad , \tag{A.3}$$

then Eq. (A.1) can be written in the form

$$\vec{m} = (1 - \overleftrightarrow{\chi}\,\overleftrightarrow{k})^{-1}\,\overleftrightarrow{\chi}\,\vec{h}_1 \quad , \tag{A.4}$$

whenever the inverse matrix exists. Equation (A.4) then defines an effective susceptibility,

$$\overleftrightarrow{\chi}_{eff} \equiv (1 - \overleftrightarrow{\chi}\,\overleftrightarrow{k})^{-1}\,\overleftrightarrow{\chi} \quad , \tag{A.5}$$

relating the magnetization to the partial field $\vec{h}_1$. If $\overleftrightarrow{k}$ has the form

$$\overleftrightarrow{k} = \begin{pmatrix} k_{11} & k_{12} \\ k_{21} & k_{22} \end{pmatrix} \quad , \tag{A.6}$$

and the intrinsic susceptibility is written in the usual notation as

$$\overleftrightarrow{\chi} = \begin{pmatrix} \chi & -j\kappa & 0 \\ j\kappa & \chi & 0 \\ 0 & 0 & 0 \end{pmatrix} \quad ,$$

then

$$\overleftrightarrow{\chi}_{eff} = \frac{1}{A}\begin{pmatrix} \chi - (\chi^2 - \kappa^2)k_{22} & -j\kappa + (\chi^2 - \kappa^2)k_{12} \\ j\kappa + (\chi^2 - \kappa^2)k_{21} & \chi - (\chi^2 - \kappa^2)k_{11} \end{pmatrix} \qquad (A.8)$$

where $A = 1 - \chi(k_{11} + k_{22}) - j\kappa(k_{12} - k_{21}) + (\chi^2 - \kappa^2)(k_{11}k_{22} - k_{12}k_{21})$.

The case where $\vec{h}_2$ arises from the surface demagnetizing fields of an ellipsoid has been considered by Steinert.[32] For this case $\overleftrightarrow{k}$ is the transverse part of the demagnetizing tensor, $\overleftrightarrow{N}$, having the diagonal form

$$\overleftrightarrow{k} = -\overleftrightarrow{N} = \begin{pmatrix} -N_x & 0 \\ 0 & -N_y \end{pmatrix} \quad , \qquad (A.9)$$

provided that the coordinate axes coincide with the principal axes of the ellipsoid.

In another application of interest to us, $\vec{h}_2$ is the reaction field that arises when a sample is placed close to a waveguide wall, as discussed in Chapter XI. In this case $\overleftrightarrow{k}$ is real, and also has the same diagonal form,

$$\overleftrightarrow{k} = \begin{pmatrix} k_{11} & 0 \\ 0 & k_{22} \end{pmatrix} \quad , \qquad (A.10)$$

as the demagnetizing tensor. As is well-known, one of the major effects of the inclusion of a term of this form in the effective susceptibility tensor is a shift in the resonant frequency of the sample. Thus, in analogy to the usual Kittel resonance relation (Eq. (1.5), Chapter II), we obtain

$$\omega_0^2 = [\omega_H + (N_x - k_{11})\omega_M][\omega_H + (N_y - k_{22})\omega_M] \quad . \qquad (A.11)$$

If the signal frequency is held fixed, this corresponds approximately to a shift

$$\delta H \equiv (H_0)_w - H_0 = \frac{M_s(k_{11}K^2 + k_{22})}{K^2 + 1} \quad , \qquad (A.12)$$

in the dc field required for resonance. Here $(H_0)_w$ is the dc field required for resonance in the presence of the wall, H_0 the resonant field in the absence of wall effects, and K is the form factor defined in Chapter VIII.

2. Form of the Effective Susceptibility Matrix Elements

The steady-state, small-signal solution of the transverse part of the equation of motion for the rf magnetization in terms of the internal rf fields leads to an intrinsic susceptibility tensor whose matrix elements are

$$\chi = \frac{\omega_M \omega_H}{(\eta_D + j\omega)^2 + \omega_H^2}$$

and (A.13)

$$\kappa = \frac{j\omega_M(\eta_0 + j\omega)}{(\eta_D + j\omega)^2 + \omega_H^2} \quad ,$$

$\eta_D \equiv \eta_0 + \eta_0'$ being the damping rate discussed in Part I, where all the remaining symbols are defined.

The matrix elements of the external susceptibility for a finite ellipsoid are then obtained by combining Eqs. (A.8), (A.9), and (A.13), with the result that

$$\chi_{11} = \frac{\omega_M(\omega_H + N_y\omega_M)}{(\eta_D + j\omega)^2 + \omega_0^2} \quad , \qquad (A.14)$$

$$\chi_{22} = \frac{\omega_M(\omega_H + N_x\omega_M)}{(\eta_D + j\omega)^2 + \omega_0^2} \quad , \qquad (A.15)$$

and

$$\chi_{12} = -\chi_{21} = \frac{\omega_M(\eta_D + j\omega)}{(\eta_D + j\omega)^2 + \omega_0^2} \quad , \qquad (A.16)$$

where

$$\omega_0^2 = (\omega_H + N_x\omega_M)(\omega_H + N_y\omega_M) \quad . \tag{A.16}$$

A quantity of interest for evaluation of the scattering matrix in Chapter V is the combination $\chi_{11}\chi_{22} - \chi_{12}\chi_{21}$, which is seen to be just $\omega_M^2/[(\eta_D + j\omega)^2 + \omega_0^2]$, of the same order of magnitude, and with the same resonant denominator as the individual matrix elements thenselves, so that terms containing this combination are <u>not</u> second order in the susceptibility, a fact which allows considerable simplification of the scattering admittance and impedance matrices discussed in Part II. For example, consider Eq. (2.13f), defining one of the parameters that appears in the scattering matrix. By substituting explicit values for the susceptibility matrix elements from Eqs. (2.14-2.16), we can write Eq. (2.13f) in the form

$$E = \frac{2}{j\beta_1 V_s} + \frac{\omega_M(\omega_H + N_y\omega_M)}{(\eta_D + j\omega)^2 + \omega_0^2}\, h_x^2 - \frac{\omega_M(\omega_H + N_x\omega_M)}{(\eta_D + j\omega)^2 + \omega_0^2}\, h_y^2$$

$$- \frac{j\beta_1 V_s}{2}\, h_x^2 h_y^2 \frac{\omega_M^2}{(\eta_D + j\omega)^2 + \omega_0^2} \quad . \tag{A.17}$$

It is then evident that the last term can be neglected, since the ratio of it to the second term is $[\omega_M/j(\omega_H + N_y\omega_M)][(\beta_1 V_s h_y^2)/2]$, in which the first factor is of order unity, but the second is of order[1] V_s/λ^3 , and hence, because of the basic assumption that the sample is very much smaller than a wavelength, very small.

[1] Since $\beta_1 \sim 1/\lambda$, and $h_y^2 \sim 1/\text{waveguide cross-section} \sim 1/\lambda^2$.

APPENDIX B

MEASUREMENT OF LINEWIDTH

Experimentally, the most readily accessible damping parameter is the total relaxation rate of the uniform mode, $\eta_0 + \eta_0'$, which, as we have seen in Chapter II, is uniquely determined for a sample of a given shape, by a steady-state measurement of the linewidth, ΔH. In this appendix, we shall review a number of techniques that have been found useful for such a measurement. Although some of these procedures have been discussed in the literature,[3,38,45] in some cases exhaustively, the equivalent circuit approach that we have developed allows all of the techniques to be treated simply and concisely within a single framework, with their limitation and ranges of applicability clearly delineated.

We begin by assuming that a small ferrite ellipsoid is placed in a two-port resonant cavity, at a point where the rf magnetic field is linearly polarized, and that both ferrite and cavity are resonant in but a single mode at the operating frequency, so that the equivalent circuit of Fig. 2.8 applies. This circuit may be specialized to the cases of a reflection cavity or uniform waveguide by an appropriate choice of the network parameters.

In the ensuing discussion, it will become evident that the choice of technique rests largely on whether the energy stored in the ferrite is very much less, of the same order, or very much greater than the energy stored in the remainder of the microwave circuitry. For the general circuit of Fig. 2.8, this ratio is given by

$$\frac{W_f}{W_c} = \frac{Q_f R_f}{Q_0 Q_c} \quad . \tag{B.1}$$

We shall now go on to consider several specific circuit configurations.

1. Sample in a Reflection Cavity

This technique has been the one most commonly used in the past.[3] In a typical experiment one notes the variation of the Q and resonant frequency of a cavity containing a ferrite sample, as a function of the dc field. From these observations one can deduce the linewidth and, with some

assumptions about the nature of the coupling between sample and cavity, both the real and imaginary parts of the diagonal component of the tensor susceptibility.

To apply the present approach to this problem, we can specialize Fig. 2.8 to a reflection cavity by setting $n_2 = 0$. The linewidth is then to be deduced from impedance measurements made at the reference plane T_1 , as the dc field is varied. In general, the input impedance of the cavity is given, in the high-Q approximation, by

$$Z_{in} = \frac{1}{n_1^2}\left[R_c(1 + 2jQ_c\delta_c) + \frac{R_f}{1 + 4Q_f^2\delta_H^2} - \frac{2jR_fQ_f\delta_H}{1 + 4Q_f^2\delta_H^2}\right] , \qquad (B.2)$$

where $\delta_H \equiv (\omega - \omega_0)/\omega_0$ is the fractional deviation of the ferrite from resonance, and δ_c is the corresponding deviation for the cavity. With the ferrite far from resonance ($|\delta_H| \to \infty$) , and the cavity at resonance, the input impedance is given by

$$Z_{in_\infty} = \frac{R_c}{n_1^2} , \qquad (B.3)$$

whereas with both ferrite and cavity at resonance ($\delta_H = \delta_c = 0$) ,

$$Z_{in_{res}} = \frac{1}{n_1^2}(R_c + R_f) . \qquad (B.4)$$

With the dc field adjusted, according to the definition of ΔH , so that $|\delta_H| = 1/2Q_f$, but with cavity tuning and signal frequency unchanged so that $\delta_c = 0$, the input impedance is

$$Z_{in_{1/2}} = \frac{1}{n_1^2}\left(R_c + \frac{R_f}{1 + j}\right) . \qquad (B.5)$$

From Eqs. (B.3) to (B.5) it is evident that

$$\left|Z_{in_{1/2}}\right|^2 = \frac{Z_{in_\infty}^2 + Z_{in_{res}}^2}{2} , \qquad (B.6)$$

so that the linewidth could be determined as the dc field increment between points at which the absolute square of the input impedance is the mean of its value with the ferrite first far off and then on resonance. However, since impedances, as such, are relatively difficult to measure at microwave frequencies, the procedure outlined above, although very general, is of little more than academic interest. Rather, the use of a reflection cavity is usually restricted to the case where $W_f/W_c \ll 1$, for which a simple approximate technique exists, in which only the VSWR in the input line need be measured.

Thus, suppose both the ferrite and cavity to be initially on resonance. Then let the dc field be changed, so as to detune the ferrite by a fractional amount δH . Because of the ferrite-cavity coupling, this is equivalent to detuning the cavity by an amount

$$\delta_c \approx \frac{Q_f R_f}{Q_c R_c}\,\delta H = \frac{W_f}{W_c}\,\delta H \quad .$$

If the cavity is now brought back to resonance by a slight change in the signal frequency, the ferrite tuning parameter, δH , because it depends on frequency, will also change. If, however, $W_f \ll W_c$, so that $\delta_c \ll \delta_H$, this change in δ_H will be negligible, and we may assume that the entire change in δ_H arises from the variation of the dc field, even though ω is changed as H_{dc} varies, in order to keep the cavity at resonance. Thus, if we measure the input impedance at the ferrite half-power point, but with the frequency adjusted to bring the cavity back to resonance, we have

$$z'_{in_{1/2}} \approx \frac{1}{n_1^2}\left(R_c + \frac{R_f}{2}\right) \quad , \qquad \text{(B.7)}$$

the approximation being valid for $W_f/W_c = Q_f R_f/Q_c R_c < 1$. If the cavity is initially undercoupled, (i.e., $R_c > n_1^2 Z_0$) , the input impedance of the cavity at resonance, normalized to the wave impedance of the input guide, will always be numerically equal to the voltage standing-wave ratio, r , in the input line. Then from Eqs. (B.3), (B.4), and (B.7),

we find

$$r_{1/2} = \frac{1}{2}(r_\infty + r_{res}) \quad . \tag{B.8}$$

Thus, the linewidth of the material may be found by noting the dc field increment between the two points at which the VSWR is the average of its values with the dc field set first at resonance, and then far from resonance, the signal frequency being adjusted, in each case, so that the cavity is at resonance.

The foregoing procedure is the usual one discussed in the literature under the general heading of "cavity perturbation techniques."[3,38] Because the measurements are not made at constant frequency, however, the "linewidth" determined in this fashion will always be less than the actual linewidth,[(1)] unless the frequency change is a negligibly small fraction of the ferrite bandwidth, which, as we have seen, requires that $W_f \ll W_c$. In terms of the properties of the sample and cavity, we have

$$\frac{W_f}{W_c} = F \frac{\omega_M(\omega_H + N_y\omega_M)}{4(\eta_0 + \eta_0')^2} \quad , \tag{B.9}$$

as discussed in Chapter VIII, so that for low-loss samples, ($\eta_0 + \eta_0'$ small), the filling factor F must be kept very small if the linewidth is to be determined simply from VSWR measurements alone. For polished single crystals of garnet, having linewidths of 100 amps/meter or less, it is usually impossible to keep F adequately small, so that in a reflection cavity one must use the fixed frequency technique discussed earlier. An alternative procedure, often preferable, is to use a transmission cavity, as described in the next section.

2. Sample in a Transmission Cavity[45]

We define the transmission coefficient of a two-port microwave circuit as the ratio of the power delivered by the network to a matched load to the maximum power available from the generator. If, in the circuit of Fig. 2.8, the signal frequency is kept constant at the resonant frequency of the empty cavity, a straightforward circuit analysis, based on this

(1) This question has also been considered by Green (ref. 44)

definition, shows that

$$\frac{1}{T_{1/2}} = \frac{1}{2}\left(\frac{1}{T_\infty} + \frac{1}{T_{res}}\right) \quad , \tag{B.10}$$

where $T_{1/2}$, T_∞ and T_{res} are the transmission coefficients of the cavity with the dc field set, respectively, to the half power points of the ferrite response, far from resonance, and on resonance. Equation (B.10) is the analog of (B.6) for the reflection case, and holds exactly, with no restrictions on the relative magnitudes of W_f and W_c . It should be noted that if Eq. (B.10) is multiplied through by T_{res} , it can be recast in a convenient form,

$$\frac{T_{res}}{T_{1/2}} = \frac{1}{2}\left(1 + \frac{T_{res}}{T_\infty}\right) \quad , \tag{B.11}$$

which shows that it is not necessary to measure the absolute transmission coefficient. The linewidth of the sample may be determined by first noting the decrease in the transmission coefficient of the cavity caused by the losses in the ferrite at resonance (i.e., T_{res}/T_∞) , and then using Eq. (B.11) to compute the difference between the transmission coefficients on resonance, and at the ferrite half-power points. The dc field is then adjusted to obtain the calculated transmission coefficient, thus defining ΔH .

There is a practical limit on the "magnetic" size of sample to which the transmission cavity technique may be applied. With the sample at resonance, the transmission coefficient must not be so low that transmission via nonresonant modes accounts for an appreciable fraction of the total power transmitted by the cavity. Thus, the coupling coefficient between ferrite and cavity must not be too large, which implies, for low-loss materials, that the filling factor must be kept small. Although for a given sample size the filling factor can be made as small as desired by using a sufficiently large cavity, a large cavity implies that the frequency spacing between resonant modes is small, with the result that the smallest transmission coefficient on ferrimagnetic resonance that one can accept, before transmission in nonresonant modes becomes

important, is correspondingly increased. Nor is it usually feasible to place the sample in the cavity at a point where the h-field, and hence the coupling, is weak, for at such points the electric field is strong, resulting in large dielectric losses. Also, and more importantly for very narrow linewidth samples, the gradient of the magnetic field is large, giving rise to the possibility of exciting higher-order magnetostatic modes. Thus, for very narrow linewidth (high Q) materials, it is necessary to adopt a completely different approach, and, instead of considering the sample as a perturbation in a microwave circuit, consider it as a circuit element in its own right, as is done in the next section.

3. Measurements in Nonresonant Systems

If the losses in the ferrite are sufficiently low, it becomes quite feasible to measure its parameters using a circuit configuration in which both the energy stored and the losses in the microwave circuit are negligible compared to those of the ferrite. Such a microwave circuit might consist of a shorted section of uniform waveguide, or a reflection cavity very tightly coupled to its input waveguide, so as to have a very low external Q. In any case, the equivalent circuit of Fig. 2.9 applies. We may then treat the ferrite and its microwave coupling network as a one-port resonator, the parameters of which may be measured in a variety of standard ways. One method that has proved convenient in practice is to put a probe in the input line at the detuned short position,[35] i.e., at the reference plane T_1 of Fig. 2.9, and sweep the dc field. The 3-db points of the detected signal then define the loaded linewidth, ΔH_L, i.e., the linewidth as broadened by the radiation damping. In terms of the coupling coefficient[(1)] β, the unloaded linewidth is determined in the usual way as

$$\Delta H = \frac{\Delta H_L}{1 + \beta} \quad . \tag{B.12}$$

[(1)] When a microwave resonator is driven by an external generator, the coupling coefficient may be defined as the ratio of the power dissipated in the resonator to that dissipated in the rest of the circuit. As we defined the coupling coefficient for a ferrite resonator in Chapter IX, it was the reciprocal of this, or the ratio of the power dissipated in the external circuitry to that lost internally in the ferrite, when the rf magnetization was allowed to decay freely. When reciprocity holds, these two definitions are equivalent--and reciprocity does hold in the present discussion because we assume a linearly polarized driving field.

The coupling coefficient may be readily determined by measuring the voltage standing wave ratio, r, in the input arm. When the detuned short position is a voltage minimum, corresponding to the ferrite being undercoupled to the circuit, the coupling coefficient is just $1/r$. On the other hand, if the detuned short position is a voltage maximum, the ferrite is overcoupled, and the coupling coefficient is equal to r.

Another technique which can be used with the same configuration, in lieu of standing wave measurements, is to measure directly the relative power absorbed by the sample as a function of the dc field. It can then be shown that the unloaded linewidth is the dc field increment between points at which the power absorbed is given by[1]

$$P_{abs_{1/2}} = \frac{P_{abs_{res}}}{1 + \left(\frac{1}{1+\beta}\right)^2} \quad , \tag{B.13}$$

where β is the coupling coefficient previously defined.

4. Measurement of ΔH by Monitoring ΔM_z

There is another method of measuring ΔH, relying on the fact that in the small signal region ΔM_z is proportional to the power absorbed[2] by the sample, that does not fit into any of the categories previously discussed.

According to the fundamental definition, ΔH is the dc field increment between points where the power absorbed in the sample is one-half of that absorbed at resonance, the rf drive remaining constant. The fact that ΔM_z is proportional to P_{abs} then allows the linewidth to be measured

---

[1] Note that $P_{abs} \neq 1/2(P_{abs,res})$. The standard definition of ΔH in terms of P_{abs} implies that the driving field remains constant as the dc field is varied through resonance. If the sample absorbs an appreciable fraction of the incident power, such is not the case. Equation (B.13) then takes this into account.

[2] For the special case in which the uniform precession and all the spin modes have the same resonant frequency, and are circularly polarized, we have simply that

$$P_{abs} = \frac{2\eta_k \omega_0}{\gamma} \frac{(\eta_0 + \eta_0')}{(\eta_k + \eta_0')} \Delta M_z \quad ;$$

otherwise, the proportionality constant is quite complicated.

by monitoring ΔM_z , as we have done in our experiments, and by noting the value of dc field for which it has half of its maximum resonance value.[1] The linewidth obtained in this way is the loaded linewidth which, as we have seen in Part II, is the same as the unloaded linewidth, as ordinarily defined, only when the coupling coefficient is much less than unity.

The main feature of this technique is that it does not involve a microwave measurement -- one is not relying on the interaction between the sample and its microwave environment to provide any information. To realize this fundamental advantage, however, it is important that the coupling coefficient of the sample to the structure be kept small, so that radiation damping can be neglected. As we have seen in Part II, this implies, for a given size of sample, that the resonance susceptibility be not too high, and the rf structure be broadband. Thus, the method is particularly suited to the measurement of the linewidth as a function of frequency for polycrystalline samples, where the use of conventional cavity perturbation techniques becomes tedious because of the necessity of providing a resonant cavity for each frequency at which the linewidth is to be measured. With the ΔM_z technique, however, the sample can be placed in some broadband structure such as a coaxial line, or strip line, and measurements made over an almost unlimited range of frequencies. The only significant disadvantage of the technique which is immediately apparent is that in a broadband structure in which the radiation damping is negligible, a substantial amount of rf power, typically one watt peak, is required to produce an accurately measurable decline in M_z .

As an experimental demonstration of the technique, the linewidths obtained in this way were compared with those previously obtained by Seiden[57] using the cavity perturbation technique, for two samples each having a linewidth of about 4000 amps/m. We obtained a value about 1% higher in one case, and 10% lower in the other.

---

[1] Because of the presence, in the proportionality constant between P_{abs} and ΔM_z , of factors which depend on the dc field, this definition of ΔH will be equivalent to the usual one only when the line is not too broad. However, when the linewidth is large, it is not a useful, quantitative characterization of the loss anyway.

5. Summary

We have summarized the microwave measurement procedures for finding ΔH in Table B.I. The quantity χ''_0 which appears in the table is the resonance value of the particular diagonal component of the effective susceptibility tensor appropriate to the microwave field configuration; all of the remaining symbols have been defined elsewhere in the text. Included with each technique is a simplified sketch of the microwave equipment needed to make the measurements, which are to be ragarded as suggestive rather than definitive.

METHOD →	REFLECTION CAVITY	TRANSMISSION CAVITY	LESS CAVITY WITH LOW Q_{ext}	UNIFORM WAVEGUIDE	
				SHORTED	TERMINATED
Limitations of Validity	None	None	$F\tilde{\chi}_0^2 \gg 1$	Sample Placed in Transverse rf Field	
Range of Applicability	$F\tilde{\chi}_0^2 \ll 1$	$F\tilde{\chi}_0^2 \sim 1$	Cavity at Resonance	$(V_s/\lambda_c^3)\tilde{\chi}_0 > 1/10$	$1/100 < (V_s/\lambda_c^3)\tilde{\chi}_0 < 1/10$
Simplified Experimental Set-Up	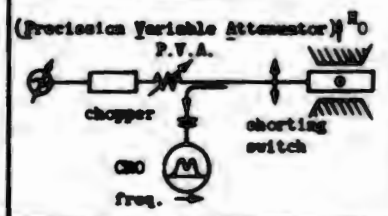		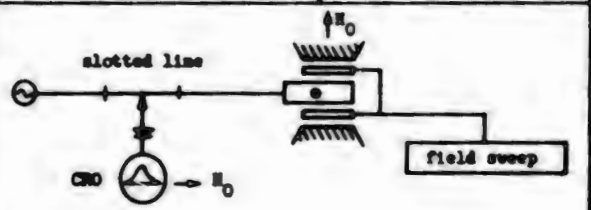		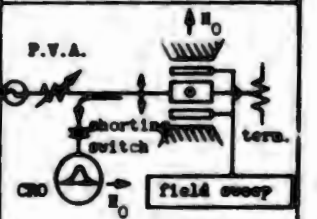
Generator Modulation	(i) frequency modulated through cavity resonance, and (ii) square wave amplitude modulated	Fixed Frequency square wave amplitude modulated	Fixed Frequency square wave amplitude modulated		
DC Field Modulation	Varied Manually		Swept Using Helmholtz Coils		
Approximate Equivalent Circuit	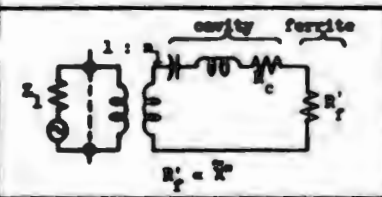	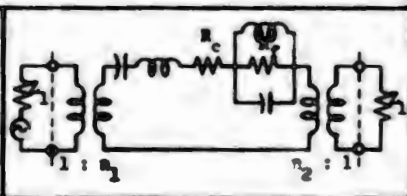	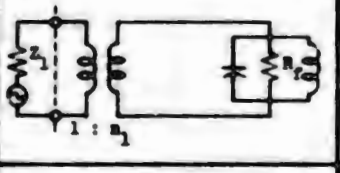	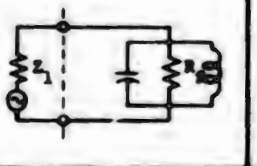	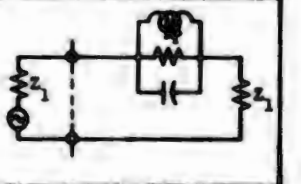
Coupling Coefficient β	$\beta = \frac{R_f}{R_c + n_1^2 Z_1}$	$\beta = \frac{R_f}{R_c + (n_1^2 + n_2^2)Z_1}$	$\beta = \frac{R_f}{n_1^2 Z_1}$	$\beta = \frac{R_f}{Z_1}$	$\beta = \frac{R_f}{2Z_1}$
Measurement of β	$\beta = \frac{1 - \Gamma_{res} - \frac{2Q_L}{Q_0}}{1 + \Gamma_{res}}$	$\beta = \left(\sqrt{\frac{\tau_\infty}{\tau_{res}}} - 1\right)\frac{Q_0}{Q_L}$	$\beta = \begin{cases} \Gamma_{res} & \text{- overcoupled} \\ \frac{1}{\Gamma_{res}} & \text{- undercoupled} \end{cases}$		$\beta = \frac{\Gamma_{res}}{1 - \Gamma_{res}}$
Calculation of β	$\beta = FQ_L\tilde{\chi}_0''$		$\beta = FQ_{ext}\tilde{\chi}_0''$	$\beta = \frac{2\pi}{\lambda_c} V_s \tilde{\chi}_0'' \frac{h^2}{\int_s h^2 ds}$	$\beta = \frac{\pi}{\lambda_c} V_s \tilde{\chi}_0'' \frac{h^2}{\int_s h^2 ds}$
Measurement of ΔH	Measure DC Field Increment Between Points Where:		Use $\Delta H = \frac{\Delta H_L}{1 + \beta}$, And Determine ΔH_L as DC Field Increment Between Points Where:		
	$\tau_{1/2} = \frac{1}{2}(\tau_{res} + \tau_\infty)$	$\frac{\tau_{1/2}}{\tau_{res}} = \frac{2}{1 + \frac{\tau_{res}}{\tau_\infty}}$	$V_{1/2}^2 = \frac{V_{res}^2}{2}$ V = voltage at detuned short position		$\|\Gamma\|_{1/2}^2 = \frac{\|\Gamma\|_{res}^2}{2}$

APPENDIX C

DESIGN OF THE ΔM_z DETECTION SYSTEM FOR OPTIMUM PERFORMANCE

As pointed out in the text, the most difficult problem connected with the relaxation measurements has been that of coupling to and displaying the z-component of magnetization. Since the configuration of the pick-up loop is largely determined by the requirement that its interaction with the transverse components of magnetization, and with the microwave driving field, be minimized, the problem reduces to that of optimally coupling the loop to the detection system. An equivalent circuit that we can use for the discussion is shown in Fig. C.1. We suppose for the moment that the loop consists of a single turn of inductance L_s and resistance R_s transformer coupled to an amplifier having a resistive input impedance R_{in} and a shunt capacity C_s. The problem is then to select the turns ratio n and the input resistance to achieve the optimum signal to noise ratio while maintaining a specified frequency response.

The rise time that can be tolerated in the detection system depends on the time constants of the relaxation processes to be investigated. For the single crystal garnets of prime interest to us, the most important time constant, that characterizing the intrinsic relaxation of the spin modes, was about 100 nanoseconds. In order to clearly separate this time constant from the much shorter one of the uniform mode, so as to allow an accurate determination of the spin mode relaxation rate and amplitude, it was decided that an overall system rise time of 10 nanoseconds was required, which in turn implied a time constant, L/R, for the input network (forgetting about C_s for the moment) of about 4 nanoseconds.

The inductance of the loop is determined both by the size of wire used and the diameter of the loop, primarily by the latter, and is fixed by various practical considerations. In order to minimize the interaction between the loop and the transverse magnetization, the wire should be as small as possible. The smallest wire available to us, that could still be easily handled, was insulated copper wire one mil in diameter. The diameter of the loop is determined by the size of the sample used, and should be about one and one-half times the diameter of the sample.[8]

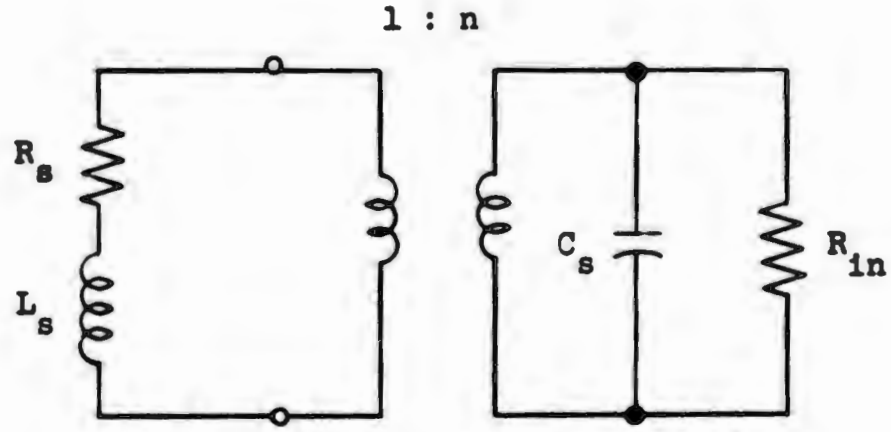

FIG. C.1--Circuit for discussion of the coupling between the pick-up loop and the amplifier.

If we assume, as will turn out to be the case, that the total inductance places a limit on the turns ratio n, it is evident that the sample should be as large as possible, since, if "a" is the radius of the sample, the voltage increases as na^2, while the inductance increases only slightly faster than n^2a. Accordingly, a sample about 35 mils in diameter, as large as could be tolerated without propagation effects becoming important, was used, thus fixing the loop diameter at 55 mils. A single turn of 1 mil wire, 55 mils in diameter, has a total low frequency inductance of about 4 nanohenries, with a resistance of about 0.1 ohms, so that it has an "intrinsic" time constant of some 40 nanoseconds. It is thus evident that we cannot simply match the source resistance of the loop into the input of the amplifier, but that in fact the actual source resistance is an almost negligible fraction of the total resistance required to obtain the desired time constant of 4 nanoseconds. Thus, we may assume that the transformer turns ratio and amplifier input resistance can be selected so that

$$\frac{n^2 L_s}{R_{in}} = 4 \times 10^{-9} \text{ seconds} \quad . \tag{C.1}$$

If it were not for the shunt capacity C_s, the optimum solution would be to use an amplifier having the highest possible input impedance, thus allowing the largest value of n, and hence providing the best signal. However, the inductance $n^2 L_s$ and the stray capacitance C_s from a shunt resonant circuit which will ring unless R_{in} is made sufficiently small. If we wish the circuit to be critically damped, we then have the additional requirement that

$$\sqrt{\frac{n^2 L_s}{C_s}} = R_{in} \quad . \tag{C.2}$$

If we assume that the shunt capacitance is about 20 pf, (this includes the input capacitance of the amplifier, shunt capacity of the input cable, etc.), Eqs. (C.1) and (C.2) may be solved for R_{in} and n, since L_s has been previously fixed at 4 nanohenries, with the result that $n = 14$, and $R_{in} = 200$ ohms.

In this analysis, we have said nothing of the noise properties of the amplifier or of the input circuit, but have chosen our parameters so as to obtain the largest signal voltage (i.e., largest n) consistent with adequate transient response. This is justified because our source resistance is so low, and because amplifiers whose input impedance is less than a few hundred ohms usually have an equivalent input noise voltage that is essentially independent of the source impedance in any case.

In the preceding discussion we assumed that the loop voltage was stepped up using a 1:n transformer. The same result could be achieved by using an n-turn loop, in place of the single turn, with the added advantage that the source resistance would then be only nR_s instead of n^2R_s, and hence truly negligible. The multi-turn loop and the step-up transformer both present practical difficulties. In the case of a multi-turn loop, the more turns that are added, the greater the difficulty in avoiding interaction with the transverse component of magnetization, and with the driving field. Also, if the coil is wound in the form of a spiral, as it must be to minimize these interactions, the peripheral turns become less and less effective as the total number of turns is increased. However, the design of a suitably wide-band step-up transformer is also difficult. Furthermore, the transformer must of necessity have a magnetic core, and hence must be placed outside the dc saturating field required for the resonance experiment, thus necessitating a length of low-impedance transmission line between the loop and the transformer input, with its attendant problems of stray pick-up.

After due consideration of these practical difficulties, together with the constructional facilities and know-how available to us, a final design was arrived at in which a 7-turn spiral loop was used with a transistorized amplifier having an input impedance of 100 ohms and a bandwidth of 30 Mc, resulting in an overall rise time of about 9 nanoseconds. This arrangement has provided adequate sensitivity for most of our work. Our experience indicated that the most promising approach to achieving greater sensitivity, while maintaining the same frequency response, would be to use a loop having more turns of finer wire, together with an amplifier having a higher input impedance. The substantial reduction in shunt capacity that would then be required could probably be effected by incorporating the preamplifier directly in the loop assembly.

APPENDIX D

DETERMINATION OF THE DRIVING FIELD FOR A FERRITE SAMPLE IN A LOSSLESS MICROWAVE CIRCUIT

When biased to resonance, a ferrite sample placed in any sort of one-port lossless[1] microwave structure can be represented by the equivalent circuit of Fig. D.1, in which the current i is proportional to the driving field at the ferrite, and the resistance R is proportional to the susceptibility χ''. In the general case, χ'' is a function of h, so that R is a function of i. From elementary considerations it is evident that if, in the absence of the ferrite ($R = 0$), a given signal source will produce at the ferrite a field h', in the presence of the ferrite the same generator will produce a field

$$h = \frac{h'}{1 + \beta} \quad , \tag{D.1}$$

where $\beta = R/n^2 Z_1$ is the coupling coefficient of the ferrite, which can be determined experimentally by straightforward microwave impedance measurements at the reference plane 1-1. If the sample is placed in a structure having a suitably simple geometry, h' can be calculated in terms of the incident power, and the problem is solved.

In many of our experiments, however, although the basic geometry was simple enough (e.g., a short-circuited rectangular waveguide), the sample itself was surrounded by a conducting loop, and imbedded in a block of polystyrene, the effect of which was to introduce a transformer, of unknown turns ratio, between the sample and the microwave structure proper, so that it became necessary to use a different approach. If we suppose that $h = Ki$, where K is some yet-to-be-determined constant, then for the circuit of Fig. D.1,

$$h^2 = \frac{K^2 V^2}{Z_1^2 (1 + \beta)^2} = \frac{8K^2}{Z_1} \frac{P_{inc}}{(1 + \beta)^2} \quad , \tag{D.2}$$

---

[1] In practice, of course, the losses in the structure need only be small compared with those in the ferrite.

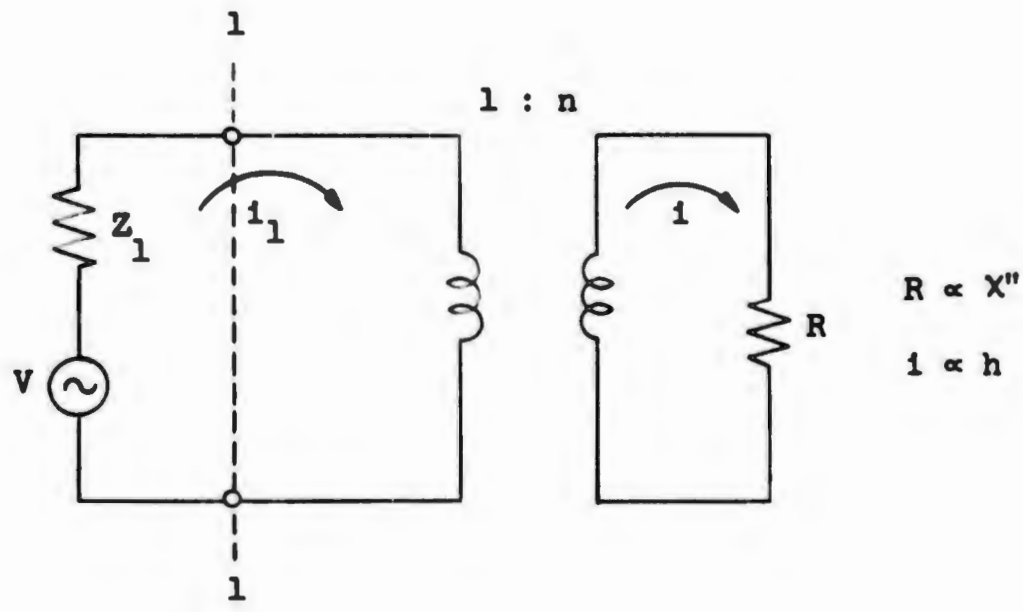

FIG. D.1--Circuit for the evaluation of the driving field for the ferrite.

where $P_{inc} = V^2/8Z_1$ is the incident power. To evaluate K, we use the fact that by definition,

$$P_{abs} = \frac{1}{2}\omega\mu_0\chi''h^2V_s \quad , \tag{D.3}$$

where P_{abs} is the power absorbed in the sample, given, in terms of the incident power by

$$P_{abs} = (1 - |\Gamma|)^2 P_{inc} = \frac{4\beta}{(1+\beta)^2} P_{inc} \quad . \tag{D.4}$$

In the small signal region, $\chi'' = \chi_0'' = M_s/\Delta H$, for which case Eq. (D.3) gives

$$h^2 = \frac{8\Delta H\beta_0}{\omega\mu_0 M_s(1+\beta_0)^2} P_{inc} \quad , \tag{D.5}$$

where β_0 is the small-signal coupling constant.

Making Eq. (D.5), which is valid under small signal conditions, consistent with Eq. (D.2), which is always true, allows us to eliminate K and obtain the general result

$$h^2 M_s = \frac{8\Delta H\beta_0}{\omega\mu_0 V_s} \frac{P_{inc}}{(1+\beta)^2} \quad , \tag{D.6}$$

relating the driving field to the incident power. Here ΔH is the small-signal linewidth, β_0 the small-signal coupling coefficient, and β the observed coupling coefficient at the actual power level for which h is desired.

APPENDIX E

INSTABILITIES AT HIGH POWER IN RADIATION DAMPED SYSTEMS

The possibility of instability must always be considered when nonlinear elements are incorporated into circuits. Microwave circuits containing ferrites fall into this category whenever they are operated in such a way that the susceptibility, for one reason or another, is a function of the rf drive. To show how instabilities can arise in a simple case of interest to us, consider the basic circuit of Fig. E.1, in which i is the analog of the magnetic field, h, and Z represents the nonlinear impedance of the ferrite, as seen at the terminals of a microwave structure, which we assume to be lossless and to store negligible energy. If, for simplicity, we take Z to be real, then

$$i = \frac{V}{Z_1 + Z} = \frac{V}{Z_1}\left(\frac{1}{1+\beta}\right) \quad , \tag{E.1}$$

where $\beta = Z/Z_1$ is the coupling coefficient of the ferrite. From Eq. (E.1) it is evident that a small change, $\delta\beta$, in β will produce a change $\delta i = \left[V/Z_1\right]\left[1/(1+\beta)^2\right]\delta\beta$, in the current. In the nonlinear region, β, being proportional to χ'', is a function of h and hence of i. A potential instability then exists whenever a small change in the drive produces a change in the susceptibility which in turn, through Eq. (E.1), produces a still larger change in the drive. Analytically, the instability condition required that

$$\frac{V}{Z_1}\,\frac{1}{(1+\beta)^2} > \frac{1}{\left|\frac{d\beta}{di}\right|} \quad . \tag{E.2}$$

For the circuit of Fig. E.1, V is related to the incident power, $V = \sqrt{8 Z_1 P_{inc}}$, and i to the driving field at the sample, $i = h/h_1$, h_1 being some proportionality constant.[1] The instability criterion

---

[1] For a microwave circuit made from a section of uniform waveguide propagating a single mode, h_1 is some appropriate component, or combination of components, of the eigenvectors defined in Part II, provided that we interpret Z_1 as the wave impedance of the mode.

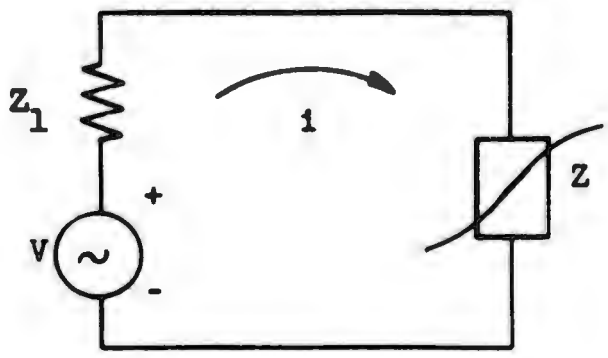

FIG. E.1--Circuit for discussion of large signal instabilities.

then becomes

$$P_{inc} > \frac{(1+\beta)^4}{8} \frac{Z_1}{\beta_0^2 h_1^2} \frac{1}{\left[\frac{d(\chi''/\chi_0'')}{dh}\right]^2} \quad , \qquad (E.3)$$

where β_0 is the small-signal coupling coefficient. Thus, instabilities can occur at a given power level, if the small-signal coupling is sufficiently great, the susceptibility changing sufficiently rapidly with drive, and the actual susceptibility at the operating point sufficiently small, so that β is small.

The dependence of χ'' on h can arise in a number of ways; thermal effects, spin wave excitation, anisotropy -- both geometrical and crystalline -- or simple saturation of the resonance, and will in general be quite complicated. A simple case that we can easily pursue further is the susceptibility decline produced by the nonlinear excitation of spin modes. In such a case, for sufficiently high powers, the susceptibility declines linearly with $1/h$. If we assume that the dependence of the susceptibility on the drive is given by $\chi''/\chi_0'' = C_1 + h_c/h$, where C_1 and h_c are constants, Eq. (E.2) predicts that instability can occur at a given power level provided that

$$\frac{\chi''}{\chi_0''} < 1 - \frac{1}{\beta_0} \quad , \qquad (E.4)$$

so that as a minimum requirement, the ferrite must be initially overcoupled ($\beta_0 > 1$) to the microwave circuit.

In the experimental configuration used to obtain some of the high-power data on sample MC-20, a cavity having an external Q of 20, providing a coupling coefficient of 3.6, was used, for which Eq. (E.4) predicts instabilities in the region of a $1/h$ dependence of the susceptibility whenever χ''/χ_0'' is less than 0.7 at the operating point. Experimentally, instabilities in the form of oscillations at a 5 to 10 Mc rate were observed on the reflected power for $\chi''/\chi_0'' < 0.5$. To avoid these effects, the susceptibility decline curves of Fig. 3.17 were obtained in a circuit for which $\beta_0 < 1$, so that the oscillations were not observed.

REFERENCES

1. N. Bloembergen, Proc. IRE 44, 1259 (1956).
2. D. Polder, Phil. Mag. 40, 99 (1949).
3. J. O. Artman and P. E. Tannenwald, J. Appl. Phys. 26, 1124 (1955).
4. H. B. Callen, J. Phys. Chem. Solids 4, 256 (1958).
5. M. Sparks and C. Kittel, Phys. Rev. Letters 4, 232 (1960).
6. E. Schloemann, Phys. Rev. 121, 1312 (1961).
7. T. Kasuya and R. C. LeCraw, Phys. Rev. Letters 6, 223 (1961).
8. R. C. Fletcher, R. C. LeCraw and E. G. Spencer, Phys. Rev. 117, 955 (1960).
9. M. Sparks, R. Louden and C. Kittel, Phys. Rev. 122, 791 (1961).
10. N. Bloembergen and S. Wang, Phys. Rev. 93, 72 (1953).
11. R. W. Damon, Revs. Mod. Phys. 25, 239 (1953).
12. R. T. Farrar, J. Appl. Phys. 29, 425 (1958).
13. H. Suhl, J. Phys. Chem. Solids 1, 209 (1957).
14. L. R. Walker, Phys. Rev. 105, 390 (1957).
15. J. Van Kranendlonk and J. H. Van Vleck, Revs. Mod. Phys. 30, 1 (1958).
16. A. M. Clogston, H. Suhl, L. R. Walker and P. W. Anderson, J. Phys. Chem. Solids 1, 129 (1956).
17. E. Schloemann, J. Phys. Chem Solids 6, 242 (1958).
18. A. M. Clogston, J. Appl. Phys. 29, 334 (1958).
19. H. Suhl and R. C. Fletcher, J. Appl. Phys. 32, 281 (1961).
20. H. Suhl, J. Appl. Phys. 30, 1961 (1959).
21. E. Schloemann, Raytheon Tech. Rep. R-48 (1[illegible]
22. T. Holstein and H. Primakov, Phys. Rev. 58, 10[illegible] (1940).
23. C. Kittel, Phys. Rev. 73, 155 (1948).
24. J. A. Osborn, Phys. Rev. 67, 251 (1945).
25. P. M. Richards, Microwave Laboratory Report 875, Stanford University (1962).
26. P. S. Epstein and A. D. Berk, J. Appl. Phys. 27, 1328 (1956).
27. A. A. Pistolkors, Radioteknika i Electronika 5, 3 (1960).
28. Siu Yan-Shen, Radioteknika i Electronika 5, 15 (1960).
29. V. V. Nikol'skii, Radio Engineering and Electronics 2, No. 7, 23 (1957).
30. W. Hauser, Quart. J. Mech. Appl. Math. 11, 427 (1958).
31. E. G. Spencer, L. A. Ault and R. C. LeCraw, Proc. IRE 44, 1311 (1956).

32. L. A. Steinert, J. Appl. Phys. 30, 1109 (1959).
33. N. Marcuvitz and J. Schwinger, J. Appl. Phys. 22, 806 (1951).
34. B. D. H. Tellegen, Philips Res. Repts. 3, 81 (1948).
35. E. L. Ginzton, Microwave Measurements, McGraw-Hill Book Company, New York (1957).
36. S. Ramo and J. R. Whinnery, Fields and Waves in Modern Radio, John Wiley and Sons, New York (1953).
37. C. G. Montgomery. R. H. Dicke and E. M. Purcell, Principles of Microwave Circuits, McGraw-Hill Book Company, New York (1948).
38. E. G. Spencer, R. C. LeCraw and L. A. Ault, J. Appl. Phys. 28, 130 (1957).
39. N. Bloembergen and R. V. Pounds, Phys, Rev. 95, 8 (1954).
40. S. Bloom, J. Appl. Phys. 28, 800 (1957).
41. G. Feher, J. P. Gordon, E. Buehler, E. A. Gere and C. P. Thurmond, Phys. Rev. 109, 221 (1958).
42. E. G. Spencer and R. C. LeCraw, J. Appl. Phys. 26, 250 (1955).
43. W. B. Nash and K. J. Standley, Proc. Phys. Soc., London 76, 99 (1960).
44. W. Hauser and L. Brown, Quart. J. Mech. Appl. Math. 13, pt. 3, 257 (1960).
45. J. J. Green, Tech. Rept. AFCRC-TN-60-367, Gordon McKay Laboratory of Applied Science, Harvard University.
46. J. I. Masters and R. W. Roberts, Jr., J. Appl. Phys. Suppl. 30, 179S (1959).
47. E. Schloemann, J. J. Green and U. Milano, J. Appl. Phys. Suppl. 31, 386S (1960).
48. B. J. Elliott, Doctoral Dissertation, Stanford University (1962).
49. M. A. Armistead, E. G. Spencer and R. D. Hatcher, Proc. IRE 44, 1875 (1956).
50. R. V. Garver, E. G. Spencer and R. C. LeCraw, J. Appl. Phys. 28, 1336 (1957).
51. R. V. Garver, E. G. Spencer and M. A. Harper, IRE Trans. PGMTT 6, 378 (1958).
52. P. E. Seiden, Compt, Rend. 250, 2530 (1960).
53. W. L. Bond, Rev. Sci. Inst. 22, 344 (1951).

54. J. A. Stratton, Electromagnetic Theory, McGraw-Hill Book Company, New York (1941).
55. E. G. Spencer, R. C. LeCraw and A. M. Clogston, Phys. Rev. Letters 3, 32 (1959).
56. A. W. Smith and A. Watanabe, J. Appl. Phys. Suppl. 32, 1555 (1961).
57. P. E. Seiden, Microwave Laboratory Report 657, Stanford University (1959).
58. M. T. Weiss, J. Appl. Phys. Suppl. 30, 146S (1959).
59. J. L. Carter, S. Dixon, Jr. and I. Reingold, IRE Trans. PGMTT 9, 195 (1961).
60. J. E. Kunzler, L. R. Walker and J. K. Galt, Phys. Rev. 119, 1609 (1960).
61. R. L. Comstock, Microwave Laboratory Report 850, Stanford University (1961).